

SOME ASPECTS OF DYNAMIC STRAIN AGING
IN THE NIOBIUM-OXYGEN SYSTEM

By

SOON CHUN PARK

A DISSERTATION PRESENTED TO THE GRADUATE SCHOOL
OF THE UNIVERSITY OF FLORIDA IN PARTIAL FULFILLMENT
OF THE REQUIREMENTS FOR THE DEGREE OF DOCTOR OF PHILOSOPHY

UNIVERSITY OF FLORIDA

1983

UNIVERSITY OF FLORIDA



3 1262 08552 3396

To my wife, Nam-He

ACKNOWLEDGEMENTS

I would like to thank a number of people for their contributions to this study. Foremost among them is Professor R. E. Reed-Hill, my advisor, whose intellectual stimulation, encouragement, ready assistance, and warm personal friendship have made my graduate work productive, rewarding and highly enjoyable.

I am also grateful to Dr. E. D. Verink, Jr., Dr. R. T. DeHoff, Dr. B. L. Adams and Dr. L. E. Malvern, for their valuable advice and helpful comments.

I would also like to acknowledge Miss Perrine for her fine typing work.

I would like to thank my wife, Nam-He, and my parents for their ever-present support and encouragement.

Finally, I do wish to acknowledge the financial support, partly by the Department of Energy under contract number DE-AS-05-76ER03262, and partly by the Engineering and Industrial Experimental Station(EIES), 1981 and 1982, University of Florida.

TABLE OF CONTENTS

	<u>Page</u>
ACKNOWLEDGEMENTS.....	iii
LIST OF TABLES.....	vi
LIST OF FIGURES.....	vii
ABSTRACT.....	xii
CHAPTER	
I INTRODUCTION.....	1
II PRINCIPLE OF STRAIN AGING.....	5
2.1 Introduction.....	5
2.2 Mechanisms of Strain Aging.....	8
2.3 Theories of Dynamic Strain Aging.....	11
2.3.1 The Cottrell Theory.....	11
2.3.2 The McCormick Theory.....	14
2.3.3 The van den Beukel Theory.....	16
2.3.4 The Reed-Hill Theory.....	19
III PREVIOUS INVESTIGATIONS.....	23
3.1 Portevin-Le Chatelier Effect.....	23
3.1.1 Effect of Strain Rate and Temperature.....	26
3.1.2 Effect of Strain.....	27
3.1.3 Effect of Solute Concentration.....	29
3.2 Strain Rate Sensitivity (SRS).....	32
3.2.1 SRS at Low Temperature Where Dynamic Strain Aging is Not Important.....	35
3.2.2 SRS at Temperature Ranges Where Dynamic Strain Aging Becomes Significant.....	35
3.2.2.1 Effect of Temperature.....	35
3.2.2.2 Effect of Strain.....	37
3.2.2.3 Effect of Base Strain Rate.....	39
3.2.2.4 Effect of Magnitude of Strain Rate Change.....	40
3.3 Strain Aging Under Stress.....	40
3.3.1 Introduction.....	40
3.3.2 Effect of Aging Under Stress on the Yield Point Return.....	41
3.3.3 Effect of Prestrain on the Yield Point Return...	44
3.3.4 Two Stages of Strain Aging Kinetics Curve.....	45

CHAPTER		Page
IV	EXPERIMENTAL PROCEDURE.....	47
	4.1 Materials and Materials Preparation.....	47
	4.2 Tensile Testing.....	51
V	EXPERIMENTAL RESULTS.....	55
	5.1 Portevin-Le Chatelier Effect Due to Snoek Dynamic Strain Aging.....	55
	5.1.1 Tensile Tests.....	55
	5.1.2 The Ratio of the Strain Rate to the Diffusion Coefficient.....	58
	5.1.3 Kinetics of the Snoek Ordering.....	60
	5.1.4 Strain Dependence of Serrated Flows.....	60
	5.2 Strain Rate Sensitivity of the Flow Stress.....	66
	5.2.1 Effect of Temperature.....	66
	5.2.2 Effect of Oxygen Concentration.....	69
	5.2.3 Effect of Base Strain Rate.....	77
	5.2.4 Effect of Magnitude of Strain Rate Change.....	80
	5.2.5 Effect of Prestrain.....	83
	5.3 Work Hardening Parameter.....	86
	5.4 Strain Aging Under Stress.....	90
	5.4.1 Effect of Aging Stress, Prestrain on the Yield Point Return.....	90
	5.4.2 Average Strain Rate During Aging Under Stress.....	94
VI	DISCUSSION.....	100
	6.1 Strain Rate Sensitivity of the Flow Stress.....	100
	6.1.1 Two Strain Rate Sensitivity Minima.....	100
	6.1.1.1 Effect of Oxygen Concentration.....	106
	6.1.1.2 Effect of Base Strain Rate.....	111
	6.1.1.3 Effect of Prestrain.....	113
	6.1.1.4 Comments on the Relationship Between Serrations and SRS.....	117
	6.1.2 Strain Rate Sensitivity Peak Above the Cottrell SRS Minimum Temperature.....	121
	6.2 Work Hardening.....	132
	6.3 Strain Aging Under Stress.....	135
VII	CONCLUSIONS.....	138
	REFERENCES.....	140
	BIOGRAPHICAL SKETCH.....	145

LIST OF TABLES

<u>Table</u>		<u>Page</u>
4.1	Chemical Analysis of Marz-Nb-VP-Nb and WC-Nb, ppm	48
6.1	Values of the Parameters Used in Equation (6.2)	102

LIST OF FIGURES

<u>Figure</u>	<u>Page</u>
2.1 Schematic representation showing the various stages in static strain aging. a) No aging period between unloading and reloading. b) Short aging period. c) Long aging period.	6
2.2 Logarithm of the aging stress versus logarithm of the average strain rate over a 35-minute aging period for V-0 aged at 373 K.	9
3.1 Two typical forms of serrated flow. a) Type A serrations are associated with Lüders bands that can travel the length of the gage section. b) Type B serrations involve bands that do not propagate.	24
4.1 Specimen dimensions used in this investigation.	49
4.2 Illustration of the extrapolations used for the calculation of the strain rate sensitivity on various stress strain curves.	52
4.3 Schematic representation showing the method used to measure the yield point return when a specimen was aged at a fixed load.	53
5.1 Stress-strain curve of Nb-0.75 at.% oxygen specimens for temperatures between 335 K and 422 K.	56
5.2 Details of the serrated curves.	57
5.3 A plot of the maximum serration height observed during a tensile test as a function of the $(\dot{\epsilon}/D)$ ratio, Nb-0.75 at.% oxygen.	59
5.4 A comparison of the average time between serrations with the jump time of an oxygen atom.	61
5.5 A plot of the critical strain, ϵ_C , for the onset of serrations as a function of temperature between 340 and 422 K. Nb-0.75 at.% oxygen.	63
5.6 The strain between successive periodic serrations, ϵ_S , at $T = 381$ K.	64

Figure		Page
5.7	Variation of the strain rate sensitivity, S , with strain at 346 K. Nb-0.75 at.% oxygen, $\dot{\epsilon}_L = 8.8 \times 10^{-5} \text{ s}^{-1}$ $\dot{\epsilon}_H = 4.4 \times 10^{-4} \text{ s}^{-1}$.	65
5.8	Variation of the strain rate sensitivity, $\Delta\sigma/\Delta\ln\dot{\epsilon}$, with temperature. VP Nb specimens, $\dot{\epsilon}_L = 8.8 \times 10^{-5} \text{ s}^{-1}$ $(\dot{\epsilon}_H/\dot{\epsilon}_L) = 5$.	67
5.9	Variation of the strain rate sensitivity, $\Delta\ln\sigma/\Delta\ln\dot{\epsilon}$, with temperature. VP Nb specimens, $\dot{\epsilon}_L = 8.8 \times 10^{-5} \text{ s}^{-1}$ $(\dot{\epsilon}_H/\dot{\epsilon}_L) = 5$.	68
5.10	Variation of the strain rate sensitivity, $\Delta\sigma/\Delta\ln\dot{\epsilon}$, with temperature. Nb-0.24 at.% O specimens. $\dot{\epsilon}_L = 8.8 \times 10^{-5} \text{ s}^{-1}$ $(\dot{\epsilon}_H/\dot{\epsilon}_L) = 5$.	71
5.11	Variation of the strain rate sensitivity, $\Delta\ln\sigma/\Delta\ln\dot{\epsilon}$, with temperature. Nb-0.95 at.% O specimens. $\dot{\epsilon}_L = 8.8 \times 10^{-5} \text{ s}^{-1}$ $(\dot{\epsilon}_H/\dot{\epsilon}_L) = 5$.	72
5.12	Variation of the strain rate sensitivity, $\Delta\sigma/\Delta\ln\dot{\epsilon}$, with temperature. Nb-0.95 at.% O specimens, $\dot{\epsilon}_L = 8.8 \times 10^{-5} \text{ s}^{-1}$ $(\dot{\epsilon}_H/\dot{\epsilon}_L) = 5$.	73
5.13	Variation of the strain rate sensitivity, $\Delta\ln\sigma/\Delta\ln\dot{\epsilon}$, with temperature. Nb-0.95 at.% O specimens, $\dot{\epsilon}_L = 8.8 \times 10^{-5} \text{ s}^{-1}$ $(\dot{\epsilon}_H/\dot{\epsilon}_L) = 5$.	74
5.14	Variation of the strain rate sensitivity, $\Delta\sigma/\Delta\ln\dot{\epsilon}$, with temperature for specimens containing three levels of oxygen. $\dot{\epsilon}_L = 8.8 \times 10^{-5} \text{ s}^{-1}$, $(\dot{\epsilon}_H/\dot{\epsilon}_L) = 5$.	75
5.15	The effect of the base strain rate on a plot of $(\Delta\sigma/\Delta\ln\dot{\epsilon})$ versus temperature, VP=Nb specimen.	78
5.16	The effect of the base strain rate on a plot of $(\Delta\ln\sigma/\Delta\ln\dot{\epsilon})$ versus temperature.	79
5.17	The effect of the magnitude of the strain rate change on a plot of $(\Delta\sigma/\Delta\ln\dot{\epsilon})$ versus temperature. $\dot{\epsilon}_L = 8.8 \times 10^{-5} \text{ s}^{-1}$.	81
5.18	The effect of the magnitude of the strain rate change on a plot of $(\Delta\ln\sigma/\Delta\ln\dot{\epsilon})$ versus temperature. $\dot{\epsilon}_L = 8.8 \times 10^{-5} \text{ s}^{-1}$.	82
5.19	The effect of strain on a plot of $(\Delta\sigma/\Delta\ln\dot{\epsilon})$ versus temperature. $\dot{\epsilon}_L = 8.8 \times 10^{-5} \text{ s}^{-1}$ $(\dot{\epsilon}_H/\dot{\epsilon}_L) = 25$.	84

Figure		Page
5.20	The effect of strain on a plot of $(\Delta \ln \sigma / \Delta \ln \dot{\epsilon})$ versus temperature. $\dot{\epsilon}_L = 8.8 \times 10^{-5} \text{ s}^{-1}$ ($\dot{\epsilon}_H / \dot{\epsilon}_L$) = 25.	85
5.21	Variation of the work hardening as a function of the temperature for three different strain rates. VP-Nb specimens.	87
5.22	The logarithm of the strain rate as a function of the reciprocal peak temperature for each work hardening maximum. VP-Nb specimens.	89
5.23	The effect of oxygen concentration on the variation of the work hardening as a function of temperature. $\dot{\epsilon} = 8.8 \times 10^{-5} \text{ s}^{-1}$.	91
5.24	Variation of the work hardening peak as a function of the oxygen concentration. $\dot{\epsilon} = 8.8 \times 10^{-5} \text{ s}^{-1}$.	92
5.25	The effect of aging stress on the yield point return. VP-Nb aged at 371 K for 35 minutes. $\epsilon = 5\%$.	93
5.26	Effect of strain on the yield point return. VP-Nb aged at 371 K for 35 minutes. $\sigma_a = 96\% \sigma_f$.	95
5.27	Logarithm of the aging stress versus the logarithm of the average strain rate over a 35-minute aging period. VP-Nb aged at 371 K. Data obtained from V-0 are also shown.	97
5.28	Variation of the average aging strain rate with aging time at two aging stresses, 98% and 100% σ_f . T = 371 K. VP-Nb specimen.	99
6.1	The calculated strain rate sensitivity, S as a function of temperature. a) Curve of S for the dynamic strain aging independent part of the stress. b) Curve of S for Snoek strain aging. c) Curve of S for Cottrell dynamic strain aging.	103
6.2	The calculated strain rate sensitivity as a function of temperature. Experimental data obtained from Nb-0.24 at.% O specimens are also shown. $\dot{\epsilon}_L = 8.8 \times 10^{-5} \text{ s}^{-1}$, $\dot{\epsilon}_H = 4.4 \times 10^{-4} \text{ s}^{-1}$.	104
6.3	A plot of the strain aging kinetics curve showing the effect of the prestrain strain rate (or waiting time) on the magnitude of the yield point return increment.	107

<u>Figure</u>		<u>Page</u>
6.4	Analytical curves of strain rate sensitivity versus temperature for two relaxation times. $\tau_2 = 2\tau_1$.	110
6.5	Analytical curves of strain rate sensitivity versus temperature for three base strain rates. $\dot{\epsilon}_1 = 8.8 \times 10^{-5} \text{ s}^{-1}$, $\dot{\epsilon}_2 = 5 \dot{\epsilon}_1$, $\dot{\epsilon}_3 = 25 \dot{\epsilon}_1$.	112
6.6	Logarithms of the strain rate as a function of the reciprocal temperature corresponding to the Snoek SRS minimum and the Cottrell SRS minimum.	114
6.7	Analytical curves of strain rate sensitivity versus temperature at three prestrains versus temperature at three prestrains between 1% and 4.5%. The values of t_w at the various strains were determined by the equation $t_w = 2.63 (\epsilon/4.5)^\beta$ with β equal to 1.2.	116
6.8	Variation of the strain rate sensitivity with strain for three temperatures, 395 K, 425 K and 600 K. $\dot{\epsilon}_L = 8.8 \times 10^{-5} \text{ s}^{-1}$ ($\dot{\epsilon}_H/\dot{\epsilon}_L$) = 25. VP-Nb specimens.	118
6.9	a) A schematic diagram showing the effect of two base strain rates on the SRS versus temperature relation. This diagram may predict the variation of the stress strain curve at two strain rates. b) Variation of the stress-strain curves at two strain rates. $T = 470 \text{ K}$, 488 K and 520 K . Nb-0.24 at.% O.	119
6.10	The effect of oxygen concentration on the strain rate sensitivity peak at 600 K. $\dot{\epsilon}_L = 8.8 \times 10^{-5} \text{ s}^{-1}$ ($\dot{\epsilon}_H/\dot{\epsilon}_L$) = 5.	122
6.11	A schematic diagram of the drag stress as a function of tensile strain rate. The calculated value of critical strain rate at $T = 600 \text{ K}$ is $2.02 \times 10^{-4} \text{ s}^{-1}$.	125
6.12	A schematic diagram showing the effect of concentration on a plot of the drag stress versus tensile strain rate.	127
6.13	Variation of the stress strain curves upon increasing the strain rate from $\dot{\epsilon}_L = 8.8 \times 10^{-5} \text{ s}^{-1}$ to $\dot{\epsilon}_H = 4.4 \times 10^{-4} \text{ s}^{-1}$ at several temperatures. Nb-0.95 at.% oxygen.	128
6.14	a) Variation of the flow stresses with temperature at two strain rates, $\dot{\epsilon}_L = 8.8 \times 10^{-5} \text{ s}^{-1}$ and $\dot{\epsilon}_H = 4.4 \times 10^{-4} \text{ s}^{-1}$. Nb-0.07 at.% O. $\epsilon = 4.5\%$.	131

FigurePage

- 6.15 Superimposed are the variations of work hardening and strain rate sensitivity with temperature. An arrow points to the temperature range over which serrations were observed. $\dot{\epsilon}_L = 8.8 \times 10^{-5} \text{ s}^{-1}$ ($\dot{\epsilon}_H/\dot{\epsilon}_L = 5$). VP-Nb specimens. 134
- 6.16 Variation of $(\dot{\epsilon}_a/\dot{\epsilon}_p)$ with (σ_a/σ_f) . $T = 371 \text{ K}$. $\dot{\epsilon}_p = 8.8 \times 10^{-5} \text{ s}^{-1}$. $t_a = 35 \text{ minutes}$. VP-Nb specimens. 137

Abstract of Dissertation Presented to the Graduate School
of the University of Florida in Partial Fulfillment of the
Requirements for the Degree of Doctor of Philosophy

SOME ASPECTS OF DYNAMIC STRAIN AGING
IN THE NIOBIUM-OXYGEN SYSTEM

by

Soon Chun Park

December, 1983

Chairman: Dr. R. E. Reed-Hill

Major Department: Materials Science and Engineering

Some important aspects of dynamic strain aging (DSA) in niobium containing oxygen between 0.01 and 0.95 at.% were investigated between 77 K and 971 K. These aspects include negative strain rate sensitivity, occurrence of the serrations on a stress strain curve and high work hardening rate.

The strain rate sensitivity (SRS) of the flow stress was measured as a function of temperature by changing the strain rate. It was observed that there were two temperature intervals within which the SRS becomes negative. These occurred near 390 K and 500 K for Nb-0.01 at.% oxygen specimens prestrained 4.5% when a (5:1) strain rate change and a base strain rate of $8.8 \times 10^{-5} \text{ s}^{-1}$ was used. It was found that the SRS minimum temperature is a function of the base strain rate, the magnitude of the strain rate change, the prestrain and the oxygen concentration.

The first two cause the SRS versus T curve to shift towards higher temperatures whereas the other two have an opposite effect. The two SRS minima were explained by using the phenomenological theory. They were found to be due to Snoek and Cottrell DSA.

It is proposed that the serrated flow observed in a higher oxygen specimen in the low temperature range, between 355 and 422 K, is due to Snoek dynamic strain aging. This is supported by 1) the occurrence of the serrations at much lower temperatures than those normally associated with Cottrell dynamic strain aging, 2) the observation that the time between the Type A serrations equals the jump time of an oxygen atom, and 3) the observation of a negative strain rate sensitivity in this region.

The Cottrell SRS minimum was observed to be closely related to the work hardening peak for Nb-0.01 at.% oxygen specimen.

Above the region of the Cottrell SRS minimum, the SRS passes through a sharp maximum. This peak increases sharply in height with increasing oxygen concentration. It was deduced that this peak is probably associated with the viscous dragging of solute atoms by dislocations.

CHAPTER I INTRODUCTION

It is well known that the mechanical properties of bcc metals are extremely sensitive to the presence of interstitial solute atoms in solid solution. One of the best examples is strain aging. The strain aging phenomena in the bcc metals containing interstitials such as oxygen, carbon and nitrogen, are due to the interactions between dislocations and interstitial solute atoms.

The strain aging may take place after or during plastic deformation. The case of aging after straining is the more normal one and is referred to as "static strain aging." If the aging takes place during plastic straining it is called "dynamic strain aging." The best known aspect of dynamic strain aging is the so-called "blue brittle" effect in iron or low carbon steel strained in tension in the range of 150-200°C. Other examples of dynamic strain aging are well documented in the literature [1]: these are serrated yielding (Portevin-Le Chatelier Effect), abnormally high work hardening rates, a low (or negative) strain rate sensitivity, yield stress plateaus in a plot of yield stress versus temperature and flow stress transients on changes in strain rates.

Among the features of the dynamic strain aging, the most visible is the appearance of serrated flow in stress-strain curves. Serrated yielding has been widely investigated in both bcc alloys [2-7] and fcc alloys [8-12]. Most of the investigations in substitutional alloys have been concerned with rationalizing the onset of serrations through

the enhanced diffusion of solute atoms due to vacancies produced by plastic deformation. In the case of bcc interstitial alloys, it is considered that the dynamic strain aging may take place when the dislocations are pinned by the interstitial solute atoms during deformation.

It is generally agreed that there are two forms of dislocation pinning processes in bcc interstitial alloys. The first is due to "Snoek ordering" of the interstitial atoms in the stress fields of the dislocations. This was analyzed originally by Cochardt et al. [13] and later in more detail by Schoeck and Seeger [14]. It has also been treated more recently by Evans and Douthwaith [15] and by Reed-Hill [16]. The second form of pinning process of the dislocations involves the long range drift of interstitial solute atoms to form solute atmospheres at the dislocations. These are called "Cottrell atmospheres." This area was originally treated by Cottrell and Bilby [17] who derived a kinetics law for the time dependence of the arrival of the solute at the dislocations.

A study by Bradford and Carlson [2] on dynamic strain aging in the vanadium-oxygen system is interesting because serrations were observed in two different temperature ranges when specimens were deformed at the same strain rate. A strong effect of oxygen concentration was also noted. Thus, for specimens containing between 47 and 265 ppm of oxygen, well defined serrations were observed only between 623 and 723 K.

However, specimens containing higher oxygen concentrations, i.e., 955 and 1800 ppm, also showed serrations in a lower temperature range between 423 and 448 K, with the largest serrations appearing in the

specimens with the higher oxygen concentration. They interpreted the high temperature serrations as being due to Cottrell dynamic strain aging by using the relationship, $\dot{\epsilon}/D = 10^9$, which was obtained by Cottrell [18], using Manjoine's experimental data [19] for the condition of the onset of serrations. However, they were not able to explain which mechanism was responsible for the low temperature serrations. It is now believed that the low temperature serrations are due to Snoek dynamic strain aging [20-23]. The results of Bradford and Carlson also suggest that a high solute concentration is needed to make the Snoek serrations apparent.

There is a good correlation between the appearance of serrated yielding and the strain rate sensitivity of the flow stress; i.e., a negative value of the strain rate sensitivity of the flow stress is necessary for the occurrence of serrated yielding [24-26].

In the present study, work on Snoek and Cottrell dynamic strain aging has been extensively done in the niobium-oxygen system. It was again shown that the low temperature serrations are associated with Snoek dynamic strain aging by using different approaches. These include

- 1) Measurement of the average time between serrations on the stress-strain curve,
- 2) a plot of the maximum serration height of low temperature serrations as a function of the $(\dot{\epsilon}/D)$ ratio, and
- 3) measurements of the strain rate sensitivity as a function of temperature.

Since no strain rate sensitivity data, as a function of temperature, including both Snoek and Cottrell dynamic strain aging are available, an extensive study of the effects of the experimental parameters on the plot of strain rate sensitivity versus temperature were made and analyzed by using the phenomenological theory developed recently [27-29]. An attempt was also made to relate the strain rate sensitivity to the work hardening.

The material employed was niobium containing between 0.01 and 0.95 at.% oxygen. A study of Snoek dynamic strain aging was largely made with Nb-0.75 at.% O. Niobium is an ideal bcc metal to use in a dynamic strain aging study since the solubility limits of interstitial atoms, such as oxygen and nitrogen, are very high [30].

CHAPTER II PRINCIPLE OF STRAIN AGING

2.1 Introduction

Strain aging is a phenomenon involving strengthening or hardening due to aging after some plastic deformation. This can occur either in the static or dynamic mode.

In static strain aging, as illustrated in Figure 2.1, the specimen is first prestrained to a point X on the stress-strain curve. It is then unloaded and allowed to age for some period of time. At the end of the aging period, the specimen is again deformed. If the aging time is very short, the restraining curve will rise up to the flow stress at point X and then follow the same stress-strain path as that of an unaged specimen. This is indicated by curve (a) in Figure 2.1. Aging for an intermediate time will result in the appearance of a small yield point upon reloading. This indicates that a higher stress level is needed to initiate yielding. However, after the yield point the stress-strain curve again follows the path of a specimen that was not subjected to the aging. This is indicated by the curve marked (b). If the specimen is allowed to age for a long period of time, not only the magnitude of the yield point but also the level of the stress-strain curve will be raised, as may be seen in curve (c). Thus, the primary results of static strain aging are twofold. First there is a return of the yield point and then at long aging times there may be a basic strengthening of the material.

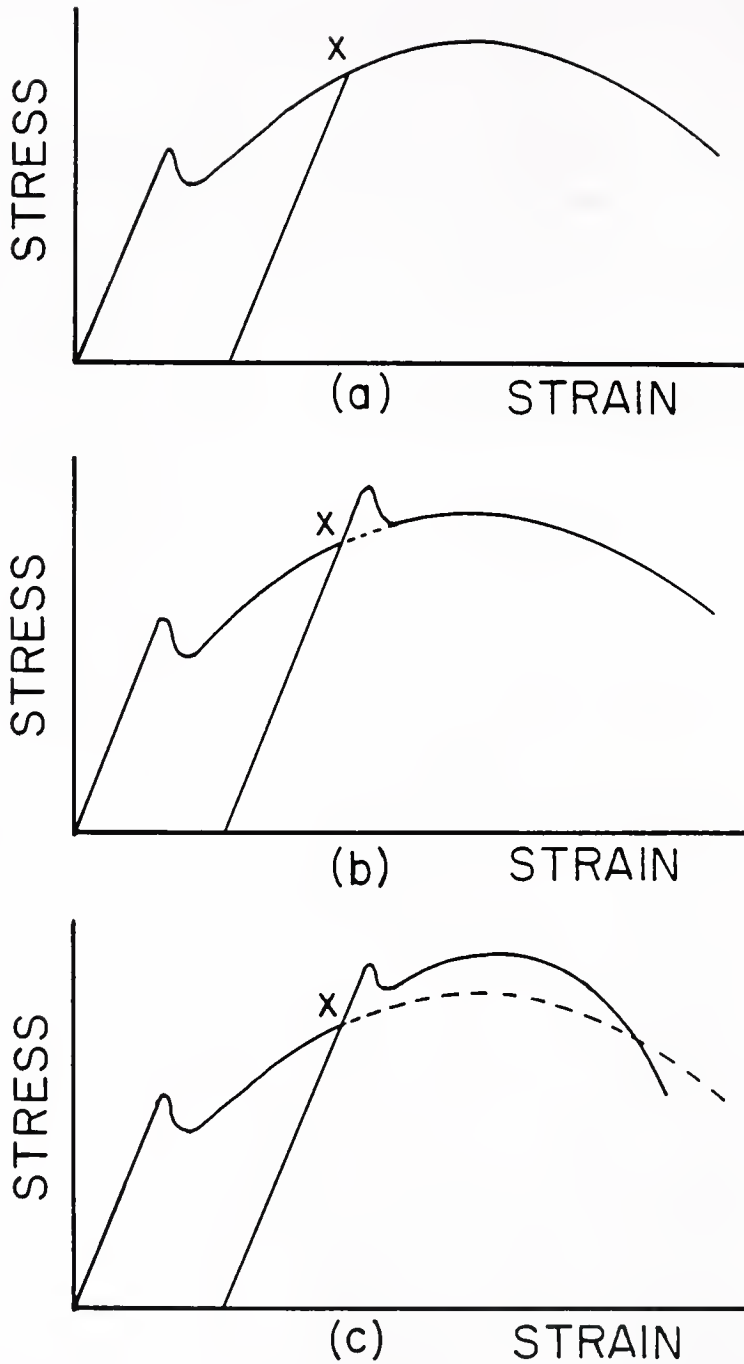


Figure 2.1. Schematic representation showing the various stages in static strain aging. a) No aging period between unloading and reloading. b) Short aging period. c) Long aging period. After Beckerman [23].

In static strain aging, since the aging occurs while the specimen is unloaded, the dislocation can be considered to be effectively at rest while they are being aged. However, in the case of dynamic strain aging, the interaction between the mobile solute atoms and the dislocations occurs with dislocations that are not at rest but that are moving. However, if the concepts of thermally activated dislocation motion are assumed, then the dislocations are periodically immobilized as they move. Sleswyk [31] was the first to propose that during this arrest time the dislocations could be subject to strain aging. Thus, during the waiting time both reordering of the interstitials and the formation of Cottrell atmospheres could occur. Therefore, it can be considered that two factors determine the degree of dynamic strain aging. These are

- 1) How long does it take for a dislocation to wait at an obstacle for thermal activation?
- 2) How fast do solute atoms diffuse to the dislocations while they dwell at the obstacles?

In this regard it can be argued that the waiting time should be inversely related to the strain rate; the faster the strain rate, the shorter the aging time. On the other hand, the mobility of the solute should vary directly as the diffusion coefficient of the solute. Thus, the solute mobility should increase rapidly with increasing temperature. From this it can be concluded that dynamic strain aging phenomena should exhibit a strong interrelationship between the strain rate and the temperature.

Bolling [32] pointed out that during a strain aging under stress experiment the specimen usually deforms plastically as it is aged.

Recently, Beckerman and Reed-Hill [23,33] have measured, as a function of the applied aging stress, the average strain rate over a fixed aging period of 35 minutes using vanadium specimens. Thus, in Figure 2.2 data [23,33] corresponding to the average strain rate in a 35-minute aging period are plotted as a function of the fraction of the pre-strain stress that was applied during the aging period. It may be seen from the figure that the strain rates in typical strain aging under stress experiments are not significantly different from those in slow tensile tests and in fast creep tests. In other words, the strain aging under stress experiments allows the strain aging process in a metal to be observed under conditions approaching those existing during dynamic strain aging.

2.2 Mechanisms of Strain Aging

It is generally agreed that there are two primary mechanisms involving interactions between the interstitial solute of atoms and dislocations in bcc metals. The first of these merely involves the re-ordering of the interstitial solute atoms around the dislocations. This can be explained in terms of the Snoek effect [34]. An interstitial atom in bcc lattice will produce a local tetragonal distortion.

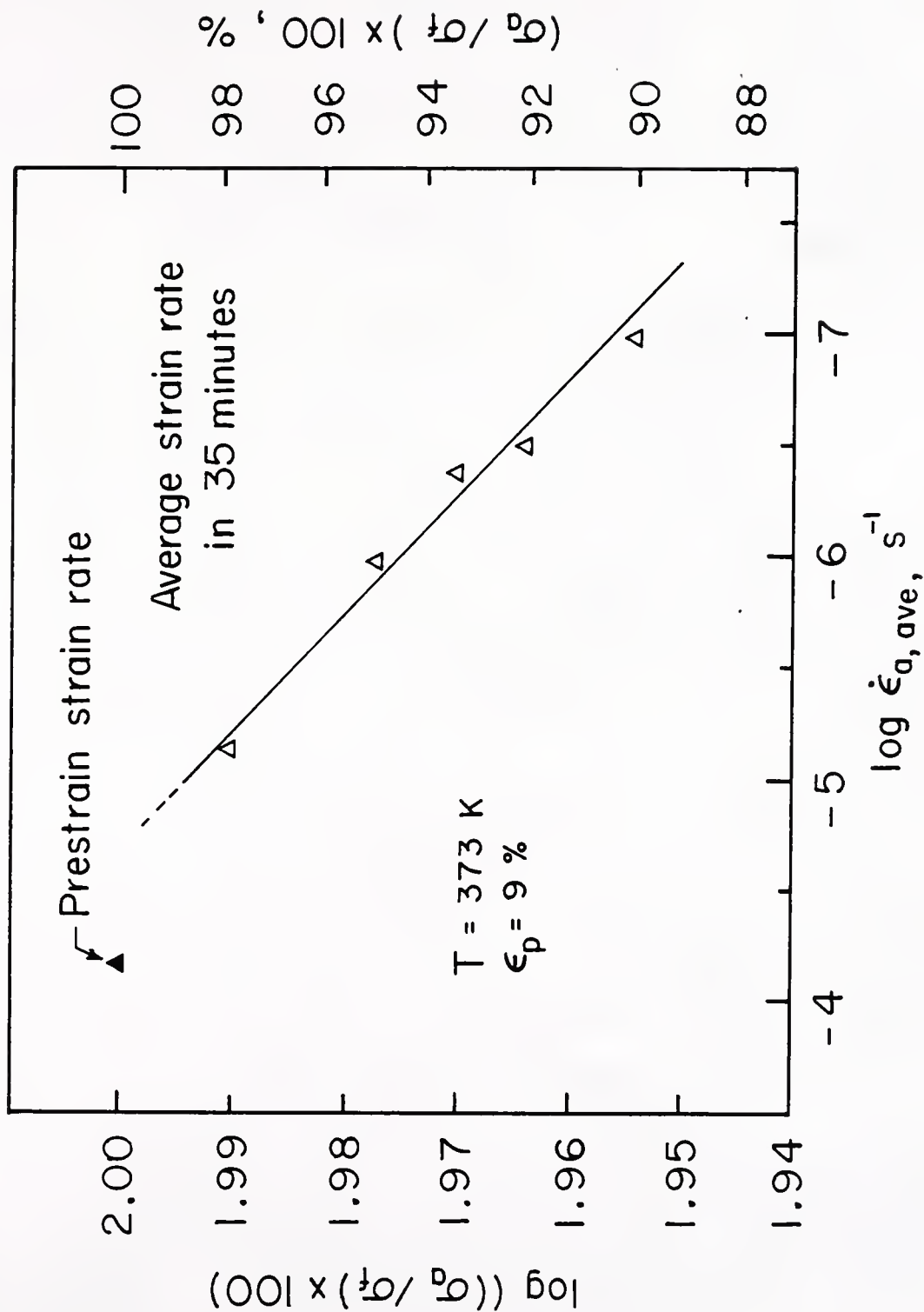


Figure 2.2 Logarithm of the aging stress versus logarithm of the average strain rate over a 35-minute aging period for V-O aged at 373 K. Prestrain strain rate, $6.7 \times 10^{-5} \text{ s}^{-1}$. (Ref. [23].)

There are three types of interstitial sites in a bcc unit cell so that the tetragonal distortion can occur in three mutually perpendicular directions. In the absence of an applied stress, each of the three kinds of site will be occupied by the same fraction of interstitial atoms and there will be no overall tetragonality. However, when a stress is applied, some sites are preferred since the interaction energy between the stress and the interstitial will depend on the direction of the tetragonal distortion. If the interstitials can diffuse they will tend to move preferentially to those sites with the lower energy. The diffusion distance will be less than one atomic spacing and therefore no long range diffusion is required.

A similar redistribution will occur in the stress field of a dislocation and will produce a lowering of the energy of the system. As a result, an additional stress will be required to move the dislocation. This is called Snoek aging and has been critically analyzed by Schoeck and Seeger [14]. Since no long range diffusion is required this reordering can occur very rapidly and is normally essentially completed in about the time required for an average interstitial atom to make one jump.

The second form of strain aging is called Cottrell aging and was originally treated in detail by Cottrell and Bilby [17]. It involves the slow drift of the interstitial atoms to the dislocations so as to form atmospheres of the solute around the dislocations. This process is much slower than that of Snoek aging since it involves a long range migration of the interstitials requiring many atomic jumps. Both the Snoek and the Cottrell form of aging result in lowering of the energy

of the system. This effectively locks the dislocations in the sites which they occupy while they are being aged. Consequently an increase in the stress is required in order to move dislocations after they are aged.

2.3 Theories of Dynamic Strain Aging [27]

2.3.1. The Cottrell Theory [35,36]

Cottrell's model of dynamic strain aging for the onset of the Portevin-Le Chatelier effect (or serrated yielding) suggests that solute atmospheres form about, and are dragged along, by dislocations moving at less than a critical velocity, v_c , given by [35,36]

$$v_c \approx \frac{4D}{\ell} \quad (2.1)$$

where D is the solute diffusion coefficient and ℓ is the effective radius of the atmosphere. The radius ℓ is equal to A/kT where A is a parameter that depends on the elastic constants, the volume change caused by the solute atom, and the strength of the dislocation. Since at this velocity the stress to move a dislocation decreases as the velocity increases, it is logical to conclude that v_c also represents a critical condition for the appearance of serrations on a stress-strain curve.

If it is now assumed that the Orowan equation is valid, we have

$$\dot{\epsilon} = \rho_m b v_c \quad (2.2)$$

or

$$\dot{\epsilon} = \rho_m b \frac{4D}{\ell} \quad (2.3)$$

where $\dot{\epsilon}$ is the applied strain rate, ρ_m is the mobile dislocation density, b the Burgers vector, D the solute diffusion coefficient, and ℓ the radius of the dislocation atmosphere. The dislocation density is normally considered to be a function of the strain, ϵ , so that we can write

$$\rho_m = N\epsilon^\beta \quad (2.4)$$

where N and β are constants. In addition, in the case of substitutional alloys, the diffusion occurs by vacancy motion and the diffusion coefficient is given by

$$D = D_0 \exp \left[-\left(\frac{Q_m + Q_f}{kT} \right) \right] \quad (2.5)$$

where Q_m is activation energy for the movement of vacancies and Q_f is the work to form a vacancy. The diffusion equation may also be written

$$D = D_0 C_v^* \exp \left(-\frac{Q_m}{kT} \right) \quad (2.6)$$

where $C_v^* = \exp \left(-\frac{Q_f}{kT} \right)$ is the thermal equilibrium concentration of vacancies. During plastic deformation vacancies are formed at a rapid rate and it is generally agreed that the vacancy concentration increases with strain according to the empirical relation

$$C_v = K\epsilon^m \quad (2.7)$$

where C_v is the vacancy concentration and K and m are constants.

The vacancy concentration created by the plastic deformation normally exceeds the thermal equilibrium concentration by many orders of magnitude so that the diffusion equation becomes

$$D = D_0 C_v \exp\left(-\frac{Q_m}{kT}\right) \quad (2.8)$$

or

$$D = D_0 K \epsilon^m \exp\left(-\frac{Q_m}{kT}\right) \quad (2.9)$$

With the aid of equations (2.4) and (2.9) we may now write the Orowan equation as

$$\dot{\epsilon} = \frac{4b}{\ell} N \epsilon^\beta K \epsilon^m D_0 \exp\left(-\frac{Q_m}{kT}\right) \quad (2.10)$$

or

$$\dot{\epsilon} = \frac{4b}{\ell} N K D_0 \epsilon^{(\beta+m)} \exp\left(-\frac{Q_m}{kT}\right) \quad (2.11)$$

Solving for the strain term gives

$$\epsilon_c^{(\beta+m)} = \frac{\ell \dot{\epsilon} \exp\left(\frac{Q_m}{kT}\right)}{4bNKD_0} \quad (2.12)$$

where ϵ_c is the critical strain for the start of serrations on the stress-strain curve of a substitutional alloy. Equation (2.12) suggests experiments for the determination of the parameters $(\beta+m)$ and Q_m .

While the Cottrell theory is able to predict both the strain rate and the temperature dependence of the critical strain, it fails when it comes to predicting the critical strain itself [37].

2.3.2 The McCormick Theory

An alternative model for the Portevin-Le Chatelier effect in substitutional alloys has been proposed [37-39]. McCormick's model is based on the assumption that dislocation motion is a discontinuous process. For such a process the average dislocation velocity may be expressed in terms of an arrest or waiting time at the obstacles, t_w , and a time of flight time through the lattice to the next obstacle, t_f , as

$$\bar{v} = \frac{L}{t_w + t_f} \quad (2.13)$$

where L is the average distance between arresting obstacles. In most instances, the average dislocation velocity is determined primarily by the arrest time, so that we may write

$$\bar{v} = \frac{L}{t_w} \quad (2.14)$$

McCormick uses a suggestion originally due to Sleswyk [31] that during the time when a dislocation waits in front of an obstacle, mobile solute atoms could be drawn to it and result in strain aging. Thus he proposed that the initiation of serrations on the stress-strain curve occurs when the time required to age or lock a moving dislocation, t_a , becomes equal to the time that the dislocation has to wait at an obstacle for a thermally activated event that will allow it to pass through the obstacle; i.e., $t_w \approx t_a$. If t_w is less than t_a at the start of plastic deformation dislocations arrested at obstacles will not be locked and the stress-strain curve will be continuous. However, during straining, t_a will

decrease due to vacancy production while t_w increases as a result of dislocation multiplication so that at the critical strain, ϵ_c , t_a becomes equal to t_w . At ϵ_c the few remaining unlocked dislocations will multiply rapidly, causing the formation of a Luders front and the start of serrated yielding.

The arrest time, t_w , may be expressed in terms of the strain rate and dislocation density as

$$t_w = \frac{\rho_m b L}{\dot{\epsilon}} \quad (2.15)$$

where it is assumed that $t_w \gg t_f$. The time required to age or pin an arrested dislocation, for elastic solute-dislocation interactions is given by, for short aging times, by [17]

$$t_a \approx \left(\frac{C_1}{\Omega C_0} \right)^{3/2} \frac{k T b^2}{3 D U_m} \quad (2.16)$$

where C_1 is the solute concentration at the dislocation line which is required to lock it, C_0 is the solute concentration of the alloy ($C_1 \gg C_0$), U_m the binding energy between the solute and the dislocation, Ω is a constant equal to about 3 and D is the solute diffusion coefficient.

On the assumption that both the dislocation density, ρ_m , and the vacancy concentration are functions of the strain as expressed in equations (2.4) and (2.7), McCormick arrives at a critical strain equation for strain aging involving a substitutional solute of the form

$$\epsilon_c^{m+\beta} = \left(\frac{C_1}{\Omega C_0} \right)^{3/2} \frac{\dot{\epsilon} K T b \exp(Q_m/kT)}{N K U_m D_0 L} \quad (2.17)$$

In bcc interstitial alloy systems diffusion occurs by a mechanism involving the jumping of interstitial atoms from one interstitial site to another. Since this form of diffusion is independent of the vacancy concentration, the equation for the critical strain in bcc interstitial alloy systems becomes

$$\epsilon_c^\beta = \left(\frac{C_1}{\Omega C_0}\right)^{3/2} \frac{\dot{\epsilon} k T b \exp(Q/kT)}{N L U_m D_0} \quad (2.18)$$

where D_0 is the interstitial diffusion frequency factor and Q is the activation energy for the diffusion of interstitial solute atoms.

2.3.3 The van den Beukel Theory

While the Cottrell and McCormick models are specific to the conditions controlling the start of serrations on a stress-strain curve, the van den Beukel's theory [40] is more general and tries to treat most of the well recognized aspects of dynamic strain aging [1].

The van den Beukel's theory is based on the idea that the moving dislocations "see" a solute concentration which depends on the waiting time and the solute diffusion coefficient. In effect, he assumes that the activation enthalpy H in the thermally activated strain rate equation is modified by the concentration variation due to dynamic strain aging. Thus, he starts with the equation

$$\dot{\epsilon} = \dot{\epsilon}_0 \exp(-H/kT) \quad (2.19)$$

and the assumption that

$$H = H(\sigma^*, C) \quad (2.20)$$

were σ^* is the effective stress and C is the solute concentration that it "sees." The value of C will be a function of the time that a dislocation waits at an obstacle, that is t_w , and the rate at which the solute diffuses to the dislocation. Thus, he writes

$$C = C(Dt_w) \quad (2.21)$$

He shows further that the quantity Dt_w is a function of strain, strain rate and temperature as follows.

$$Dt_w \sim \frac{\epsilon^{(m+\beta)}}{\dot{\epsilon}} \exp\left[-\frac{Q_m}{kT}\right] \quad (2.22)$$

where m and β are constants, and Q_m is the migration energy of vacancies. For small values of Dt_w , he uses a $t^{2/3}$ relation between the concentration and the time formulated by Friedel [41].

$$C - C_0 = K(Dt_w)^{2/3} \quad (2.23)$$

where C_0 is the nominal solute concentration of the alloy, and K is given by

$$K = \frac{3U_m}{b^2 kT} (\pi C_0)^{3/2} \quad (2.24)$$

and U_m is the solute atom-dislocation binding energy.

By considering H to be a function of both the local concentration of the solute at the dislocation, as well as of the effective stress, he obtains some very significant relationships as follows.

First of all, the activation enthalpy equation he obtains has the form of

$$H = -TV \frac{\partial \sigma^*}{\partial T} + T \frac{\partial H}{\partial C} \frac{dC}{dT} \quad (2.25)$$

where V is the activation volume. Equation (2.25) shows that the activation enthalpy can be expressed as the sum of two terms, the first of which represents the Conrad-Wiedersich relationship [42] for the activation enthalpy, which assumes that a single thermally activated mechanism controls the flow stress. This term is considered to give the activation enthalpy in the presence of dynamic strain aging. The second term on the right hand side of the above equation is considered to represent the component of the activation enthalpy associated with dynamic strain aging.

Second, he shows the strain rate dependence of flow stress,

$$\frac{\partial \sigma}{\partial \dot{\epsilon}} = \frac{kT}{\dot{\epsilon}V} - \frac{1}{\dot{\epsilon}V} \frac{\partial H}{\partial C} D t_w \frac{dC}{d(D t_w)} \quad (2.26)$$

The first term on the right hand side is again the normal one in the absence of diffusion; the second is due to dynamic strain aging.

Third, he also obtains the relationship of the strain rate sensitivity by assuming that, when the strain rate is changed from $\dot{\epsilon}_L$ to $\dot{\epsilon}_H$ at a constant strain, the change of activation enthalpy is given by

$$\Delta H = - kT \ln \frac{\dot{\epsilon}_H}{\dot{\epsilon}_L} \quad (2.27)$$

Thus, he writes

$$\left(\frac{\Delta \sigma}{\Delta \ln \dot{\epsilon}} \right)^{-1} = \frac{kT}{V} + \frac{1}{V} \frac{\partial H}{\partial C} \frac{dC}{d \ln \dot{\epsilon}} \quad (2.28)$$

The first term on the right, $\frac{kT}{V}$, corresponds to the strain-rate sensitivity in the absence of dynamic strain aging, and the second term is considered to be due to dynamic strain aging.

¹ $\left(\frac{\Delta \sigma}{\Delta \ln \dot{\epsilon}} \right)$ should read $\left(\frac{\Delta \sigma}{\Delta (\ln \dot{\epsilon})} \right)$ throughout the text.

Van den Beukel extends further his investigation and shows that the temperature dependence of the flow stress as well as the work hardening can be expressed by two terms; one of these is that which would exist in the absence of dynamic strain aging. The other is the part due to dynamic strain aging.

2.3.4 The Reed-Hill Theory [27-29]

The more general theory of van den Beukel obviously represents a major advance over the earlier theories of Cottrell and McCormick. However, the theory of van den Beukel does have some shortcomings. The most important of these are

- 1) Quantitative predictions of the theory depend largely upon a knowledge of just how the activation enthalpy H varies with changes in the solute concentration near the dislocation. Data to evaluate this subject are not generally available.
- 2) With the theory, it is difficult to visualize the simple physics of dynamic strain aging due to its basically mathematical approach.
- 3) The theory deals only with the long range diffusion of solute to dislocation. It is thus specific to Cottrell form of strain aging. However, in bcc interstitial alloys, Snoek dynamic strain aging is significant [14,16,20,23,33].

All of the shortcomings led Reed-Hill to propose a phenomenological theory of dynamic strain aging.

It is assumed in the phenomenological model that the total flow stress, σ_t , consists of two parts. The first being the stress σ that

would exist in the absence of dynamic strain aging and the second σ_D that is due to dynamic strain aging. Thus

$$\sigma_t = \sigma + \sigma_D \quad (2.29)$$

It is also shown that the dynamic strain aging independent part of the flow stress σ has two parts, the internal stress σ_E and the effective stress σ^* . Thus it becomes

$$\sigma_t = \sigma_E + \sigma^* + \sigma_D \quad (2.30)$$

He developed a new technique [28] to evaluate the internal stress. He also demonstrated that in commercial purity niobium the effective stress can be approximately by a power law of the form

$$\sigma^* = \sigma_0^* \left(\frac{\dot{\epsilon}}{\dot{\epsilon}_0} \right)^{kT/H^0} \quad (2.31)$$

where σ^* is the effective stress, σ_0^* is the effective stress at 0 K, $\dot{\epsilon}$ is the nominal strain rate, $\dot{\epsilon}_0$ and H^0 are constants, and k and T have their usual significance.

At the same time the dynamic strain aging component of flow stress, σ_D , can be represented by an equation deduced from the strain aging under stress studies of Delobelle, Oytana and Varchon [43]. In this equation, which follows, the first term on the right hand side represents the contribution of Snoek aging and the second term that is due to Cottrell aging.

$$\sigma_D = \sigma_{S_{\max}} \left\{ 1 - \exp\left[-\left(\frac{t_w}{\tau_S}\right)\right] \right\} + \sigma_{C_{\max}} \left\{ 1 - \exp\left[-\left(\frac{t_w}{\tau_C}\right)^{2/3}\right] \right\} \quad (2.32)$$

where $\sigma_{S_{\max}}$ and $\sigma_{C_{\max}}$ are the isothermal maximum obtainable magnitudes of the Snoek and Cottrell contributions of the flow stress, respectively, t_w is the waiting time of a dislocation at an obstacle, and τ_S and τ_C are empirical relaxation times for Snoek and Cottrell aging, respectively. These parameters are strongly temperature dependent and can normally be expressed by

$$\begin{aligned} \tau_S &= \tau_{S_0} \exp(Q/RT) \\ \tau_C &= \tau_{C_0} \exp(Q/RT) \end{aligned} \quad (2.33)$$

where Q is the activation energy for the diffusion of the solute atom, and τ_{S_0} and τ_{C_0} are constants that can be determined experimentally. The parameters $\sigma_{S_{\max}}$ and $\sigma_{C_{\max}}$ are expected to be temperature dependent and to decrease with temperature due to an increase in dynamic recovery with increasing temperature. Thus,

$$\begin{aligned} \sigma_{S_{\max}} &= \sigma_{S_{\max}}^0 \exp[-\alpha(T-300)] \\ \sigma_{C_{\max}} &= \sigma_{C_{\max}}^0 \exp[-\alpha(T-300)] \end{aligned} \quad (2.34)$$

where $\sigma_{S_{\max}}^0$ and $\sigma_{C_{\max}}^0$ are the maximum amplitudes of the dynamic strain aging stress components at 300 K, and α is a dynamic recovery parameter. Thus, the total stress may be written

$$\begin{aligned}
 \sigma_t = & \sigma_E + \sigma_0^* \left(\frac{\dot{\epsilon}}{\dot{\epsilon}_0} \right)^{kT/H^0} + \{ \exp[-\alpha(T-300)] \} \\
 & \cdot \left\langle \sigma_{S_{\max}}^0 \left\{ 1 - \exp\left[-\left(\frac{t_w}{\tau_S}\right)\right] \right\} \right. \\
 & \left. + \sigma_{C_{\max}}^0 \left\{ 1 - \exp\left[-\left(\frac{t_w}{\tau_C}\right)^{2/3}\right] \right\} \right\rangle
 \end{aligned} \tag{2.35}$$

If the above equation is differentiated with respect to $\ln \dot{\epsilon}$, one obtains the following equation for the strain rate sensitivity of the flow stress.

$$\begin{aligned}
 \frac{d\sigma_t}{d \ln \dot{\epsilon}} = & \frac{\sigma_0^* kT}{H^0} \left(\frac{\dot{\epsilon}}{\dot{\epsilon}_0} \right)^{kT/H^0} - \exp[-\alpha(T-300)] \\
 & \cdot \left\langle \sigma_{S_{\max}}^0 \left(\frac{t_w}{\tau_S} \right) \exp\left[-\left(\frac{t_w}{\tau_S}\right)\right] \right. \\
 & \left. + \frac{2}{3} \sigma_{C_{\max}}^0 \left(\frac{t_w}{\tau_C} \right)^{2/3} \exp\left[-\left(\frac{t_w}{\tau_C}\right)^{2/3}\right] \right\rangle
 \end{aligned} \tag{2.36}$$

It has been shown that the phenomenological theory can model the temperature dependence of the flow stress and the strain rate sensitivity of niobium-oxygen specimens [27] as well as those of a substitutional solid solution of Cu-3.1 at.%Sn [29]. It has also been demonstrated that the theory can model both the temperature as well as the strain dependence of the strain aging under stress kinetics curve of niobium specimens containing oxygen in solid solution [44].

CHAPTER III PREVIOUS INVESTIGATIONS

3.1 Portevin-LeChatelier Effect

Probably the best known aspect of dynamic strain aging is serrated yielding which is commonly called the Portevin-LeChatelier effect because in 1924 these authors reported [45] stress-strain curves showing serrations.

Serrated flow can take a number of forms or shapes. The two most important forms were shown by Reed-Hill [1] and reproduced in Figure 3.1. In both of the cases the yield point associated with a serration is related to the formation of a Lüders band. In the Type A bands shown in Figure 3.1a the Lüders band nucleates at one end of the gage section and then moves progressively along the gage section to its other end. When the Lüders band front has completely crossed the gage section, plastic deformation effectively stops and the load rises elastically until another band is formed. This new band then forms at the same end as where the previous band was formed. Its formation causes the load to drop. Note that the load rises as the Lüders band front traverses the gage section. The rise in load is a result of a strain gradient along the gage section which developed as the first band began to form. The Lüders bands thus propagate into material that is progressively harder and harder.

Type B bands, as illustrated in Figure 3.1b, are Lüders bands that form but do not propagate [8]. Both Type A and B bands can form in the same specimen. Type B bands are normally observed at higher temperatures

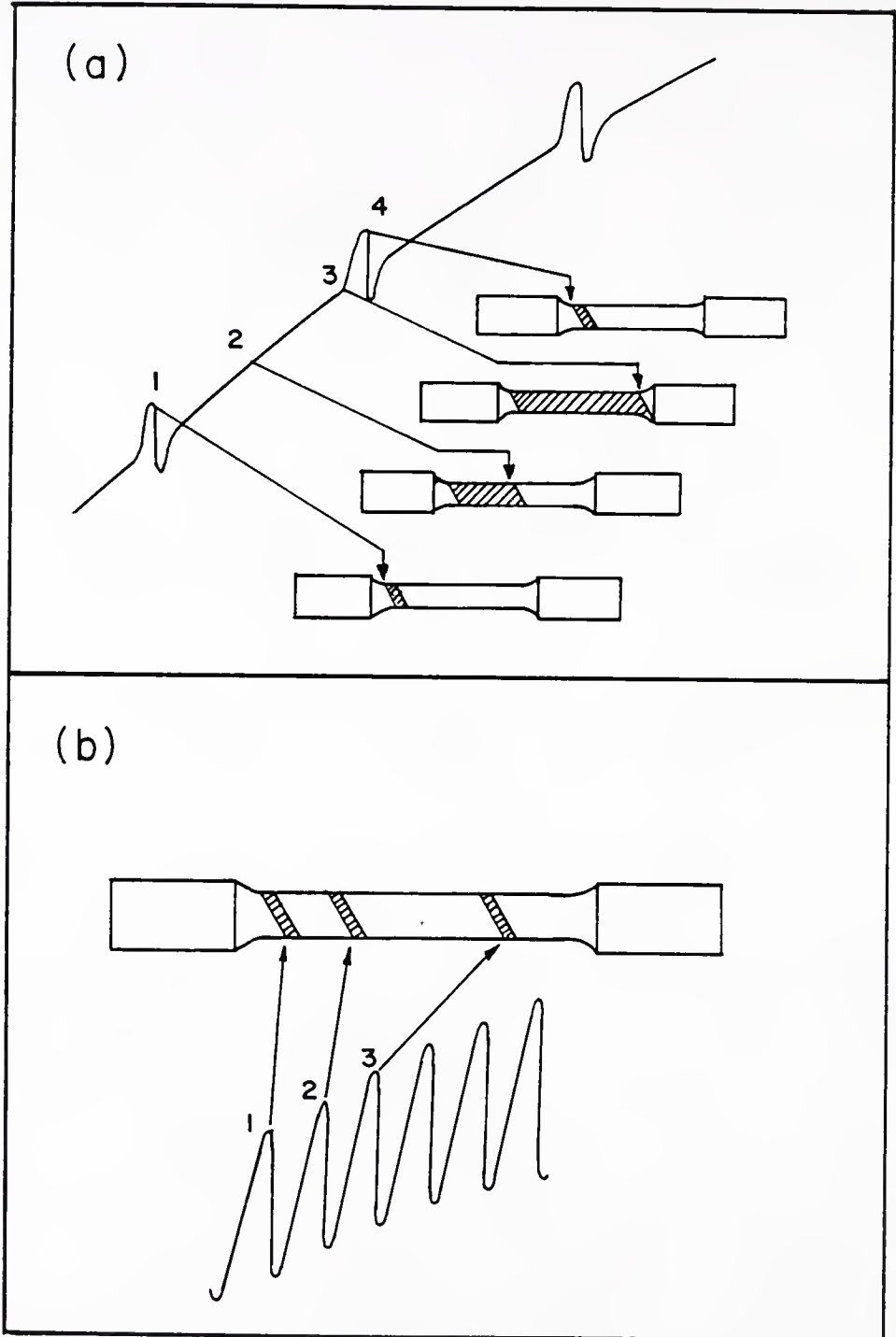


Figure 3.1 Two typical forms of serrated flow. a) Type A serrations are associated with Lüders bands that can travel the length of the gage section. b) Type B serrations involve bands that do not propagate. (After Reed-Hill [1].)

or slower strain rates than are required for Type A bands; thus they occur where the diffusion rate of the solute atoms is higher. In this case, the dislocations in the bands become pinned at the bottom of the load drops. Succeeding Lüders bands may form sequentially next to each other.

The Portevin-LeChatelier effect [45] or serrated yielding has been observed in a large number of alloy systems, including steels [3,5,6], vanadium [2,46], aluminum alloys [8,11,12,45], Ni alloys [24,47] and titanium alloys [48].

The effect can therefore operate in bcc, fcc and hexagonal crystal structures. It is generally attributed to a dynamic strain aging process which occurs when solute atoms are diffusing sufficiently rapidly to dislocation. If the solutes are interstitials, for example C, N, O, etc. in bcc metals, serrated yielding may be observed at two temperature intervals: one being due to Snoek dynamic strain aging while the other due to Cottrell dynamic strain aging. Thus, in this system, it may be possible to observe serrations even at temperatures close to room temperature. For substitutional alloy systems, on the other hand, since the Snoek dynamic strain aging effect does not operate, the Portevin-Le Chatelier effect is normally seen only at elevated temperatures, unless diffusion has been intentionally accelerated, for example; by quenching from a high temperature to retain excess vacancies or generating vacancies during plastic deformation, or by radiation damage.

In the following sections, the effects of strain rate, temperature, strain and solute concentration on the Portevin-Le Chatelier effect will be briefly reviewed.

3.1.1 Effect of Strain Rate and Temperature

The Portevin-Le Chatelier effect is usually observed in certain strain rate-temperature regions. Thus, a large number of authors, including Keh et al. [5], Nakada and Keh [47], Pink and Griberg [3], Mulford and Kocks [24], Kinoshita et al. [49] and Dadras [50], show plot of the strain rate-temperature domains for serrated flow.

On the basis of Manjoine's results [19], Cottrell [18] related the strain rate and temperature corresponding to the onset of serrations due to Cottrell dynamic strain aging by the relation

$$\frac{\dot{\epsilon}}{D} = 10^9 \quad (3.1)$$

This relation has been conformed by a number of investigators 2,20,23 .

A study by Bradford and Carlson [2] of dynamic strain aging in the vanadium-oxygen system shows that there are two temperature different ranges at the same strain rate. The specimens were deformed at a strain rate of $1.67 \times 10^{-4} \text{ s}^{-1}$ between room temperature and 773 K. Five alloy compositions were used containing 47, 150, 265, 955 and 1800 ppm oxygen. For specimens containing 47, 150 and 265 ppm oxygen, serrations were observed between 623 K and 773 K. The specimens containing 955 and 1800 ppm oxygen showed serrations in the temperature range 423 K to 448 K. They interpreted the high temperature serrations as being due to Cottrell dynamic strain aging by solving Cottrell's relation $\dot{\epsilon}/D = 10^9$ for their data. The low temperature serrations were not identified at that time.

Beckerman [23] solved for the ratio $\dot{\epsilon}/D$ corresponding to the low temperature serrations, and obtained a value of $\dot{\epsilon}/D$ in the tange of 3.11×10^{12} to 2.3×10^{14} with a value of $\dot{\epsilon}/D = 1.54 \times 10^{13}$ corresponding

to the maximum height of the serrations observed. On the basis of these values, Beckerman concluded that these low temperature serrations could be due to Snoek dynamic strain aging. Evans and Douthwaite [15] calculated the strain rate corresponding to the maximum drag force exerted on a moving dislocation by a Snoek atmosphere. They compared this with a similar calculation for the maximum drag force exerted on a moving dislocation by a dynamic Cottrell atmosphere and determined that Snoek ordering should occur at a strain rate three orders of magnitude faster. Baird [20], in his review article on strain aging, also suggests that these low temperature serrations are due to Snoek dynamic strain aging.

It can be concluded from the above published results that serrations may be observed in two temperature ranges in bcc interstitial alloys when a single strain rate is used; one being due to Snoek dynamic strain aging, the other due to Cottrell dynamic strain aging.

3.1.2 Effect of Strain

It has been reported in the literature by many authors that there is a critical strain, ϵ_c , at which serrated flow begins to appear. It is often emphasized that the critical strain increases with strain rate and reciprocal temperature. McCormick [8] found in an Al-Mg-Si alloy that at higher strain rates, $1.7 \times 10^{-3} \text{ s}^{-1}$, the critical strain increases with decreasing temperature. MacEwen and Ramaswami [11] demonstrated in both single crystal and polycrystal of an Al-Mg alloy, that the critical strain decreases as strain rate decreases when tested at 295 K.

However, the critical strain decreased in both single and polycrystal specimens with increasing temperature when deformed at a rate of $\sim 10^{-5} \text{ s}^{-1}$. They had, however, some difficulties in defining the critical strain. For single crystals, the small irregularities in the stress-strain curve prior to the development of a regular background made the precise definition of critical strain impossible. However, there was no ambiguity in defining the critical strain in polycrystalline specimens.

Pink and Grinberg [3] reported that they could not distinguish between the onset of Type A and onset of Type B serrations. They plotted the critical strains for different types of serrations as a function of the reciprocal temperature at several strain rates. The results show that, for pure Type A serrations, the slope is positive, while for combined Type (A + B) serrations it is positive or zero. At higher temperatures, and especially when Type C serrations appear, the slope is negative.

Recently, Jovanovic, Djuric and Drobnjak [51] observed several types of serrations in a Cu-Be-Co alloy. They distinguished the critical strain for the onset of Type A, $\epsilon_c(A)$ from that for Type B serrations, $\epsilon_c(B)$. They plotted both critical strains, $\epsilon_c(A)$ and $\epsilon_c(B)$ as a function of strain rate at several temperatures. It was found that at 150 C and 180 C, $\epsilon_c(A)$ decreases initially with increasing strain rate down to the critical strain rate, about $1 \times 10^{-4} \text{ s}^{-1}$ and $5 \times 10^{-4} \text{ s}^{-1}$ for 150 C and 180 C, respectively, and then an inverse behavior was observed; i.e., $\epsilon_c(A)$ increases with further increase in strain rate. At lower temperatures, 90 C and 120 C, the critical strain, $\epsilon_c(A)$ increases with decreasing

temperature for all strain rates employed. However, at slightly higher temperature tests, 150 C and 180 C, the strain rate dependence of critical strain, $\epsilon_c(A)$ becomes more complicated. $\epsilon_c(A)$ at 150 C becomes smaller than that at 180 C at slower strain rates. However, as the strain rate increases, the situation becomes reverse: $\epsilon_c(A)$ at 150 C is larger than that at 180 C. In contrast to the case of Type A serrations, $\epsilon_c(B)$ has a linear dependence of strain rate. It was also observed that at all test temperatures $\epsilon_c(B)$ becomes smaller as the temperature increases.

A recent study made by Qian and Reed-Hill [29] in Cu-3.1 at.% Sn also shows that the critical strain is a function of temperature as well as strain rate. Thus, they reported a plot of critical strain versus temperature at three different strain rates, 1×10^{-5} , 4×10^{-4} and $4 \times 10^{-3} \text{ s}^{-1}$. They observed that the critical strain decreases rapidly as temperature increases from about 320 K to 650 K for all strain rates. The critical strain at higher strain rates was always greater than that at slower strain rates. From the plot of ϵ_c versus T at several strain rates, they were able to evaluate the activation energy by plotting the strain rate needed to obtain a fixed critical strain versus the reciprocal temperature.

3.1.3 The Effect of Solute Concentration

In order to study the effect of carbon content on several serrations, Nakada and Keh [47] used Ni-C specimens with six different carbon concentrations at various strain rate-temperature combinations. The critical

strain for initiation of serrations was used to classify the degree of serrations; the smaller the critical strain, the more pronounced are the serrations. They plotted the critical strain versus $\frac{1}{T}$ and also versus strain rate for specimens containing six different carbon concentrations, between 0.022 and 0.2 at.%. It was concluded that the critical strain at a given temperature decreases with increasing carbon content. It is thus shown in Figure 4 in Nakada and Keh's paper [47] that at 273 K the critical strain observed at 0.048 at.% C was approximately 1%, which should be compared with 0.6% ϵ for a specimen containing 0.16 at.% carbon.

Bradford and Carlson [2] observed serrated yielding at two temperature ranges in vanadium alloys containing different levels of oxygen between 47 ppm and 1800 ppm. At the lower temperature (~ 423 K), the frequency and height of the serrations increases with increasing oxygen content. In the higher temperature range (623 to 673 K), however, the serrations diminish in frequency as well as magnitude with increasing oxygen concentrations and virtually disappear at the higher oxygen contents. In other words, increased amounts oxygen tend to diminish the intensity of the serrations and do not give the expected increase in the size of the maximum in the Cottrell dynamic strain aging temperature range. A high interstitial content is necessary for the observation of serrations due to Snoek dynamic strain aging.

Roberts and Owen [52] investigated the serrated flow in martensite and ferrite with various concentrations of carbon. The martensitic specimens were Fe-21% Ni-C alloys with different carbon concentrations between 0.015 and 0.12%. They observed two types of unstable flow at

constant strain rate tests of ferrite iron-carbon alloys; jerky flow due to Snoek dynamic strain aging and serrated flow due to Cottrell dynamic strain aging. At any strain-rate and carbon concentration, jerky flow occurs at a lower temperature than serrated flow. However, in martensitic alloys, only the higher temperature serration was observed. In both cases of plastic flow, an increasing carbon concentration decreases the temperature at which unstable flows are observed. It can be said that the purer the specimen, the higher the temperature required to get the same degree of serrations. This has also been pointed out by other authors [5,20,53,54].

Russell [10] obtained in Cu-Sn alloys the relationship between the critical strain and the Sn contents as $\epsilon_c \propto C_{Sn}^{-1/2}$ by assuming that the strain aging is due to the movement of a Sn atom to a dislocation by a vacancy mechanism.

McCormick [37] also showed the concentration dependence of the critical strain for the onset of serration, $\epsilon_c \propto C_0^{-3/2(m+\beta)}$, assuming the obstacle spacing is independent of solute concentration. The above relationship was shown in section (2.3.2) in Chapter II. If solute atoms act as the controlling obstacles, however, then the average distance between obstacles would be expected to decrease with increasing solute concentration, thus decreasing the concentration dependence of ϵ_c .

It was reported in carbon steel [55,56] that the presence of substitutional solute suppresses the serrations in the stress-strain curve. Bratina et al. [56] found in Fe-C steel that adding 0.95% Mn in Fe-0.095 C alloys suppressed the serrations at room temperature in tests made at a rate of $7 \times 10^{-5} \text{ s}^{-1}$. However, serrations became pronounced at elevated

temperatures, 360 K. It was concluded that manganese is responsible for the delay of the serrated flow by either reducing the amount of interstitials in solution by forming carbide or impeding the motion towards dislocations.

3.2 Strain Rate Sensitivity (SRS)

The strain rate sensitivity is a useful parameter for studying different aspects of deformation. First, since the strain rate sensitivity is related to the thermal component of the stress, it can be a tool for studying the thermally activated deformation mechanism [57,58]. Second, the variation of the strain rate sensitivity with strain can determine the validity of Cottrell-Stokes law [59] in a metal. According to Cottrell-Stokes law, $\Delta\sigma/\sigma = \text{constant}$, where $\Delta\sigma$ is the change in the flow stress upon changing the strain rate or temperature. Third, there is a considerable amount of evidence in the literature [24,27,40] involving many metals showing a strain rate sensitivity-temperature diagram with a minimum in the dynamic strain aging temperature interval. Therefore, the temperature variation of the strain rate sensitivity can be used to detect regions where dynamic strain aging is significant.

There are two forms of parameters in common use to evaluate the dependence of the flow stress upon the strain rate. The first of these is

$$n = \frac{d \ln \sigma}{d \ln \dot{\epsilon}} \quad (3.2)$$

where n is known as the strain rate sensitivity, σ is the flow stress and

$\dot{\epsilon}$ is the strain rate. It is often possible to write a power law to express the stress in terms of the strain rate; i.e.,

$$\sigma = \sigma_0 (\dot{\epsilon})^n \quad (3.3)$$

where σ_0 is a constant. Note that in this case, n , the strain rate sensitivity, is the exponent in the power law equation. Under the assumptions that 1) the Orowan equation holds, 2) that the thermally activated component dominates the flow stress, and 3) that the mobile dislocation density does not change during a strain rate change, n defined in this manner is equal to the reciprocal of the dislocation velocity-stress exponent m , defined by the Johnston-Gilman empirical relationship [60]

$$\frac{v_1}{v_2} = \left(\frac{\sigma_1}{\sigma_2}\right)^m \quad (3.4)$$

The second form of the strain rate sensitivity parameter, S , is

$$S = \left(\frac{d\sigma}{d\ln\dot{\epsilon}}\right) \quad (3.5)$$

This is based on the assumption that the deformation can be described by an equation

$$\dot{\epsilon} = \dot{\epsilon}_0 \exp(-H/kT) \quad (3.6)$$

where $\dot{\epsilon}$ is the strain rate, $\dot{\epsilon}_0$ is a constant, H is the activation enthalpy, and k and T have their usual meanings.

The parameter S is normally preferred to be used because it is primarily easy to measure from the strain rate change test and it can also be related directly to the activation volume.

3.2.1 Strain Rate Sensitivity at Low Temperatures Where Dynamic Strain Aging is Not Important

In the low-temperature region where deformation is thermally activated, it has been observed that the strain rate sensitivity (SRS) passes through a maximum at a certain temperature, T_m [29,58,61-65]. The magnitude of the maximum in SRS varies with material and other experimental parameters, such as base strain rate, grain size and concentration of the alloying elements.

Michalak [65] investigated the influence of temperature on the development of long range internal stress during the plastic deformation of high purity iron. Differential strain rate tests were performed during the tensile deformation of single crystal and polycrystalline specimens of two zone-refined irons in the temperature range 78-300 K. He observed that below about 175 K the strain rate sensitivity of iron was independent of strain. The magnitude of the SRS maximum for the single crystal was smaller than that of polycrystalline irons. It was also found that the SRS maximum temperature, T_m , shifted to higher temperature for the polycrystalline specimens; the maximum temperature falls at about 190 and 225 K for the single crystal and polycrystalline specimens, respectively.

Ravi and Gibala [61] reported that the addition of small amounts of oxygen to niobium resulted in alloy softening and an increase in the strain rate sensitivity peak temperature. An inverse effect of impurity content was observed Tseng and Tangri [64] on iron specimens with different impurity levels. They found that T_m increases with decreasing impurity content. However, their results [64] of the magnitude of the

strain rate sensitivity maximum agree with the data in the literature: SRS increases with increasing impurity content.

Christian and Masters [58] have reported data on strain rate sensitivity of the flow stress for polycrystalline niobium, vanadium and tantalum over the temperature range 4.2 to 373 K. They found that the SRS peak temperatures fall at about 90 K, 75 K and 220 K for niobium, vanadium and tantalum, respectively. It was also observed that, above 90 K, the strain rate sensitivity was dependent on the purity of the niobium; the higher the purity content, the higher the magnitude of the strain rate sensitivity. However, at 90 K and below, this dependence disappeared.

The SRS peak temperature, T_m , the magnitude of the strain rate sensitivity maximum and the flow stress at T_m appear to be very useful experimental data in order to estimate the internal stress. This technique has been recently uniquely developed by Reed-Hill and Qian [28]. The internal stress at 0 K, σ_{E_0} , is evaluated with the aid of the equation

$$\sigma_{E_0} = \frac{\sigma_0 - e\sigma_m}{1 - eE_m/E_0} \quad (3.7)$$

where σ_0 is the flow stress at 0 K, e is the base of the natural logarithms and E_m and E_0 are Young's modulus at T_m and 0 K, respectively. This technique has been successfully tested in Nb-0 [28] and Cu-3.1 at.% Sn [29].

3.2.2. Strain Rate Sensitivity at Temperature Ranges Where Dynamic Strain Aging Becomes Significant

3.2.2.1 Effect of Temperature. It is well documented that in a number of materials in the intermediate temperature regions the strain

rate sensitivity becomes abnormally low or negative due to dynamic strain aging. Bradford and Carlson [2] showed a plot of strain rate sensitivity, n , as a function of temperature for a vanadium specimen containing 265 ppm O. They found that strain rate sensitivity decreases gradually as temperature increase and has a minimum value of -0.023 at about 610 K. At this temperature, the intensity of the serration and the yield stress curve reached a maximum. Negative values of the strain rate sensitivity were observed in the temperature range between 408 K and 698 K. At that time, they were not able to explain the significance of this negative strain rate sensitivity. A close examination of Figure 6 in the paper of Bradford and Carlson [2] reveals that there is another minimum in strain rate sensitivity at around 408 K, which is close to the temperature of the serration peak observed in the higher oxygen specimens. This minimum is due to Snoek dynamic strain aging. They ignored this low temperature minimum because they did not realize that in bcc metals Snoek dynamic strain aging also contributes negatively to the strain rate sensitivity of the flow stress.

Thompson and Carlson [46] made a similar study of nitrogen in vanadium. They plotted the strain rate sensitivity, n , as a function of temperature for vanadium specimens containing 210 ppm of oxygen. They observed that the strain rate sensitivity was negative between 538 K and 753 K and reached a value of -0.012 at the minimum. The strain rate sensitivity minimum occurs at about 673 K, which is approximately 60 K higher than in the vanadium-oxygen specimens.

The strain rate sensitivity minimum has also been recently reported by Qian and Reed-Hill [29] in Cu-3.1 at.% Sn alloy. $\Delta\sigma/\Delta\ln\dot{\epsilon}$ was measured at a fixed strain, 2%, using a tenfold change in strain rate at temperatures between 77 and 800 K. The base strain rate was $4 \times 10^{-4} \text{ s}^{-1}$. They observed that the strain rate sensitivity becomes negative between 390 and 620 K with a minimum at about 500 K.

3.2.2.2 Effect of Strain. The strain rate sensitivity (SRS) of the flow stress plays a crucial role in determining macroscopic behavior. Any solute mobility makes a negative contribution to the total rate sensitivity and this contribution increases with strain [27,37,43,44,66]. When the total rate sensitivity becomes negative, plastic flow becomes unstable in the characteristic form of serrated flow [26,66-69]. This assumption has been supported by the experimental observation [24,26]; a negative strain rate dependence of the flow stress is a necessary condition for the occurrence of serrated flow.

The strain dependence of the SRS has been reported by a number of authors [24-27,44,67]. Van den Brink et al. [26] investigated the effects of strain and composition on the strain rate sensitivity of Au-Cu alloys. For alloys containing more than 1% Cu, $\Delta\sigma/\Delta\ln\dot{\epsilon}$ decreased with increasing strain, becoming negative at sufficiently large strains. The strain ϵ_0 , at which $\Delta\sigma/\Delta\ln\dot{\epsilon} = 0$, decreased with increasing composition and serrated yielding was observed to initiate at somewhat larger strains in the negative strain rate sensitivity region.

Mulford and Kocks [24] noted that the SRS in normal alloys is more appropriately described in terms of the flow stress than the strain. Thus, they measured the strain rate sensitivity of Inconel 600 as a function of

flow stress at several different temperatures. At 300 K or lower, $\Delta\sigma/\Delta\ln\dot{\epsilon}$ increases with increasing flow stress. At 400 K, however, the behavior is anomalous: $\Delta\sigma/\Delta\ln\dot{\epsilon}$ decreases linearly with increasing flow stress but still remains positive. At higher temperature (e.g., 700 K), $\Delta\sigma/\Delta\ln\dot{\epsilon}$ decreases rapidly with flow stress and as the deformation continues a negative strain rate sensitivity is observed. When the deformation is continued into the region of negative strain rate sensitivity, the $\Delta\sigma/\Delta\ln\dot{\epsilon}$ versus flow stress plots are no longer linear.

At 960 K, it was observed that there is a rapid drop of $\Delta\sigma/\Delta\ln\dot{\epsilon}$ through zero, followed by a subsequent increase to positive values again. Serrated flow was observed during the portions of the stress-strain curves where the rate sensitivity was negative.

Recently, Reed-Hill documented [27,44] the effect of the dynamic strain aging. He showed that dynamic strain aging phenomena are basically functions of the quotient of the waiting time of dislocation at an obstacle, t_w , and a temperature dependent relaxation time, τ . The waiting time is actually a function of both mobile dislocation density, ρ_m , and strain rate, $\dot{\epsilon}$: i.e.,

$$t_w = (\rho_m bL)/\dot{\epsilon} \quad (3.8)$$

Accordingly, as ρ_m grows with increasing strain, t_w must also increase. Thus, for a given condition such as the onset of serrations, an increase in t_w can be compensated by a corresponding increasing in the relaxation time; i.e., a decrease in the temperature. Therefore, the increase in ρ_m with strain may be expected to expand the lower temperature boundary of the temperature range in which serrations are observed.

3.2.2.3 Effect of Base Strain Rate. As equation (3.8) indicates, since t_w is inversely proportional to the strain rate, increasing the base strain rate should decrease the waiting time. Therefore, it is expected that changing the base strain rate will modify the temperature or strain dependence of the strain rate sensitivity.

Van den Brink et al. [26] made a measurement of SRS versus strain at four different base strain rates in Au-4.5% Cu alloy at 20 C. They observed that SRS decreases with increasing strain at all base strain rates used. Decreasing base strain rate causes $\Delta\sigma/\Delta\ln\epsilon$ to be negative at much smaller strains. At a strain rate of $4 \times 10^{-4} \text{ s}^{-1}$, $\Delta\sigma/\Delta\ln\epsilon$ remains positive up to about 9% of strain. However, it becomes negative at only 4% when tested at $4 \times 10^{-5} \text{ s}^{-1}$.

The effect of base strain rate on the SRS has also been observed by Mulford and Kocks [24] in an Al-1% Mg alloy. They made a strain rate sensitivity measurement at 250 K at three base strain rates, 1×10^{-5} , 5×10^{-5} and $1 \times 10^{-4} \text{ s}^{-1}$, and plotted the $\Delta\sigma/\Delta\ln\epsilon$ versus flow stress data. They observed that, for all three base strain rates, $\Delta\sigma/\Delta\ln\epsilon$ decreased as the flow stress increases and increases with a further increasing flow stress. The strain rate sensitivity, S , at a higher strain rate, is always greater at all flow stresses than that at a slower strain rate.

McCormick [25] also studied the effect of base strain rate on the strain rate sensitivity in low carbon steel at 353 K. He plotted $\Delta\sigma/\Delta\ln\epsilon$ versus strain for four strain rates. Measurements of $\Delta\sigma/\Delta\ln\epsilon$ were found to decrease with increasing strain for all strain rates. The rate of decreasing of the strain rate sensitivity increased with decreasing base strain rate.

3.2.2.4 Effect of Magnitude of Strain Rate Change. Van den Brink et al. [26] studied the effect of the magnitude of a strain rate change on the strain rate sensitivity at a temperature of 293 K in a Au-4.5 at. % Cu. alloy. The base strain rate was $8.33 \times 10^{-5} \text{ s}^{-1}$ and three different strain rate ratios were used ($\dot{\epsilon}_H/\dot{\epsilon}_L = 5, 10 \text{ and } 20$). The strain rate sensitivity decreases with increasing strain for all strain rate change ratios. It was found that increasing the ratio at constant base strain rate resulted in an increase in the strain, ϵ_0 , where $\Delta\sigma/\Delta\ln\dot{\epsilon} = 0$. The values of ϵ_0 were found to be approximately 4.6%, 5.2% and 5.9% for the ratios of 5, 10 and 20, respectively. Except at small strains, less than 1.5%, where $\Delta\sigma/\Delta\ln\dot{\epsilon}$ was independent of $\Delta\ln\dot{\epsilon}$, the strain rate sensitivity increases with increasing the magnitude of the strain rate change.

3.3 Strain Aging Under Stress

3.3.1 Introduction

Strain aging under stress is known to enhance the strain aging process. This effect is commonly observed when strain aging monitored by observing the return of the yield point. When a specimen is aged under an applied stress, a greater yield point return is obtained than when it is aged in a stress-free condition. Most of the strain aging under stress experiments were conducted under the condition of relaxation of the specimen; i.e., aging was carried out by merely stopping the testing machine for a period of time and then continuing the deformation. Alternatively, the specimen may be unloaded from the flow stress to desired aging

stress and then aged. In both cases, the specimen is allowed to relax during aging. Since the stress changes continuously it cannot be said that the specimen is aged at a constant stress. This problem was largely eliminated by Beckerman and Reed-Hill [23,33] by utilizing an electronically controlled feedback loop between the Instron strip chart and cross-head. The advantages of this method are twofold. The first is that it is possible to maintain a nearly constant stress during aging. The second is that the amount of strain as well as the average strain rate during aging can be measured.

Beckerman and Reed-Hill [23,33] found that the strain rate during aging was a maximum when aging occurred at stress levels approaching the prestrain flow stress, and decreases as the aging stress level decreased. Thus, the average strain rate in a 35-minute aging period at 92% σ_f in the V-0 system, where σ_f is the prestrain flow stress, was found to be only about 2.5 orders of magnitude slower than the prestrain strain rate. This strongly suggests that a material deforms with a finite strain rate during strain aging under stress.

3.3.2 Effect of Aging Under Stress on the Yield Point Return

The effect of the aging under stress on the yield point return has been investigated by a number of authors. Wilson and Russell [70] observed that aging a low carbon steel under stress resulted in a greater yield point return than aging in an unstressed condition.

Mura and Brittain [71] studied the effect of the application of stress during aging on the yield point return of ingot iron. They aged a set of specimens for a constant time of 2800 seconds and observed the

development of heterogeneous yielding as the aging stress was increased from 0 to 212 Mpa. Their results indicated that the yield point became more fully developed.

Almond and Hull [72] studied the effect of applying a tensile stress during the strain aging of iron, niobium and tantalum. They observed that the upper yield stress, the lower yield stress and the yield point elongation are all increased when tensile specimens are aged under stress.

Duval and Dickson [73] investigated the influence of the aging stress on the yield point phenomena in very low carbon steel. Specimens were prestrained at a nominal strain rate of $6.6 \times 10^{-4} \text{ s}^{-1}$ and unloaded to the desired aging stress, whereupon the crosshead was stopped, allowing the stress to relax for the desired aging time; after this the specimen was reloaded at the nominal strain rate. The procedure was repeated at intervals of 1 or 2% of the strain.

One set of specimens was prestrained 2%, 6% and 14%, and aged at 266 K and 300 K for 30 seconds at several stress levels. For specimens aged at 300 K after prestraining 6%, the magnitude of the yield point return was observed to initially decrease with increasing aging stress to 40% of the prestrain flow stress. Upon aging at stress levels greater than 40%, the magnitude of the yield point return increased until it attained a maximum value at 60% σ_f . Aging at stress levels above 60% σ_f caused the magnitude of the yield point return to decrease until a minimum was attained at 90% σ_f . A further increase in the aging stress caused the magnitude of the yield point return to increase to a value at 100% of the flow stress, about equal to that obtained at 60% σ_f .

Only a minor difference was observed in the manner by which the yield point return varied with aging stress when the specimens were prestrained 2% and 4% instead of 6%.

On the other hand, for specimens aged at 266 K, raising the aging stress increased the magnitude of the yield point return up to a maximum value at an aging stress level approximately 70% of the prestrain flow stress. A further increase in aging stress up to 80% of the prestrain flow stress caused the yield point return to decrease and a value about equal to that obtained upon aging at 60% σ_f was found. Upon increasing the aging stress up to 100% σ_f , the magnitude of the yield point return continuously increased.

The most extensive study of the dependence of the yield point return on aging stress was performed by Beckerman and Reed-Hill [23,33]. A number of vanadium specimens were prestrained to 9% at a rate of $6.7 \times 10^{-5} \text{ s}^{-1}$ and aged for 35 minutes at 353 K, 363 K and 373 K at several stress levels between 27% σ_f and 98% σ_f . They observed that raising the level of the aging stress caused the yield point return to increase continuously up to a maximum value at 92% σ_f . At this aging stress level, the magnitude of the yield point return is approximately three times that obtained at the lowest stress level (27%). Aging above 92% σ_f results in the magnitude of the yield point return dropping off rapidly. At 98% σ_f , it approaches or falls below the value obtained upon aging at 27% σ_f . It was also observed that the effect of raising the test temperature is to increase the magnitude of the yield point return at all aging stresses.

They also showed the aging stress dependence of the yield point return in tantalum. Tantalum specimens were prestrained 9% at 378 K using a strain rate of $6.7 \times 10^{-5} \text{ s}^{-1}$ and then aged for 25 minutes at a number of stress levels between 20% σ_f and 95% σ_f . Their results indicated that the effect of raising the aging stress level was to increase the magnitude of the yield point return continuously up to a maximum at 85% σ_f . Upon aging at stress levels above 85% σ_f , the magnitude of the yield point return decreased slightly. The yield point return obtained by aging at 85% σ_f was approximately four times greater than that obtained upon aging at 20% σ_f .

3.3.3 Effect of Prestrain on the Yield Point Return

The results of Szkopiak and Derby [74] who strain aged commercially pure niobium for 10 hours at 350 C show that the magnitude of the yield point return increases rather rapidly as prestrain increases to 6%. With further increase in prestrain, the magnitude of yield point return gradually falls off.

In contrast are the results of Rosinger et al. [75] for strain aging of annealed Ferrovac E iron strain aged at 21 C and 40 C for aging times from 5 to 3600 seconds at various strain intervals. They observed that the yield point return remained essentially independent of strain up to 300 sec at 21 C and up to 30 sec at 40 C. For longer aging periods, 1800 and 3600 sec, the magnitude of yield point return decreased slightly with strain.

Duval and Dickson [73] reported the influence of the strain on the magnitude of yield point return in low carbon steel aged at various

temperatures for 30 seconds. It was found that for a small homogeneous strain ($< 1\%$), the yield point return increased rapidly with strain. However, for greater strains, it decreased slowly with increasing strain.

The prestrain dependence of the yield point return was also investigated by Delobelle, Oytana and Varchon [43] for the niobium-oxygen system. They determined the variation of the magnitude of the yield point return with time at 344 K, 371 K and 398 K at different amounts of prestrain, 2%, 4%, 8% and 12%. At all test temperatures the magnitude of yield point return increases with prestrain.

Beckerman [23] also reported the effect of prestrain on the yield point return for vanadium specimens prestrained to 2.8% and 9% at a rate of $6.7 \times 10^{-5} \text{ s}^{-1}$ and aged at 363 K for 35 minutes at different levels of aging stress. It was found that different amounts of prestrain did not significantly affect the magnitude of the yield point return at all aging stress levels.

3.3.4 Two Stages of the Strain Aging Kinetics Curve

When a strain aging experiment is performed in a bcc interstitial alloy at a proper temperature for a reasonable period of time, one normally observes two plateaus in a plot of the magnitude of the yield point return versus aging time. The magnitude of the first plateau appearing at shorter aging time is much smaller than that of the other plateau at longer aging times. It was pointed out by Wilson and Russell [70] for the Fe-C system, later by Carpenter and Baker [76] for the Ta-O system and Nakada and Keh [21] for the Fe-N system, that the first stage aging

occurs too quickly for long range diffusion of interstitial atoms to take place. Nakada and Keh [21] compared the time to reach the first plateau to the interstitial atom jump time and concluded that the first aging stage is the result of Snoek ordering of nitrogen atoms in the Fe-N system. This was supported by Owen and Roberts [22], who studied the deformation kinetics and the effects produced by aging iron-nickel-carbon martensite during relaxation under stress. They also found that the time to reach the first plateau value agrees reasonably well with the time for a single jump of a carbon atom in ferrite.

Rosinger et al. [75] plotted the magnitude of the yield point return versus time to the $2/3$ power for Ferrovac E iron. For each test temperature, they observed that the data appeared to define two stages: each stage being linear with $t^{2/3}$, but having a different slope. They then assumed that the first stage corresponds to Snoek strain aging, and the second to Cottrell strain aging. They further assumed that the time corresponding to the inflection between the two stages represented the time required for a carbon atom to undergo a single jump. They checked this assumption by plotting the logarithm of the inflection time versus the reciprocal of the absolute temperature. This curve was then compared to a plot of the logarithm of the carbon atom jump time versus $1/T$, and they concluded that the agreement was good.

It is generally accepted that the second stage of the strain aging is due to Cottrell strain aging. It involves the long range diffusion of solute atoms to form so-called "Cottrell atmospheres."

CHAPTER IV EXPERIMENTAL PROCEDURE

4.1 Materials and Materials Preparation

The two purity grades of niobium used in this study were initially obtained from the Materials Research Corporation in the form of 6.35 mm diameter annealed rods and are designated as Marz Nb and VP Nb in Table 4.1. The two grades of niobium were used for a survey of the tensile properties of low oxygen niobium. The rods were swaged directly to a diameter of 3.18 mm and then machined into tensile specimens having dimensions shown in Figure 4.1. These tensile specimens were annealed in groups of 10, in a "Precision Scientific Minivac" vacuum furnace under a dynamic vacuum of 10^{-4} Torr at 1073 K for 1 hour. The finished specimen had a mean linear grain intercept of 65 μm . The tensile specimens were measured using an optical comparater for average gage section diameter and gage section length.

VP grade niobium rods were also used as a base material for producing the higher oxygen specimens. The rods were first swaged to a diameter of 3.18 mm. Then niobium alloys containing 0.24, 0.75 and 0.95 at.% oxygen were prepared in the following manner. First, the rods were cut into 3.5 cm lengths. Sets of four of these sections were then inserted, along with 6 gm of a 325 mesh Nb_2O_5 powder, into the open end of a 1.59 OD thin walled niobium tube whose other end had been crimped and welded closed. Following this, the open end was crimped and welded to form a totally enclosed packet. These enclosed

TABLE 4.1
 CHEMICAL ANALYSIS OF Marz Nb, VP Nb and WC Nb, ppm

	<u>Marz Nb</u>	<u>VP Nb</u>	<u>WC Nb</u>
C	25	40	35
O	15	20	120
N	< 5	< 5	50
H	< 1	< 1	< 5
Fe	3.4	20	<50
Si	17	25	<50
Ta	200	250	750
Ni	1	<30	<20
Cr	1.8	30	--

All dimensions in mm

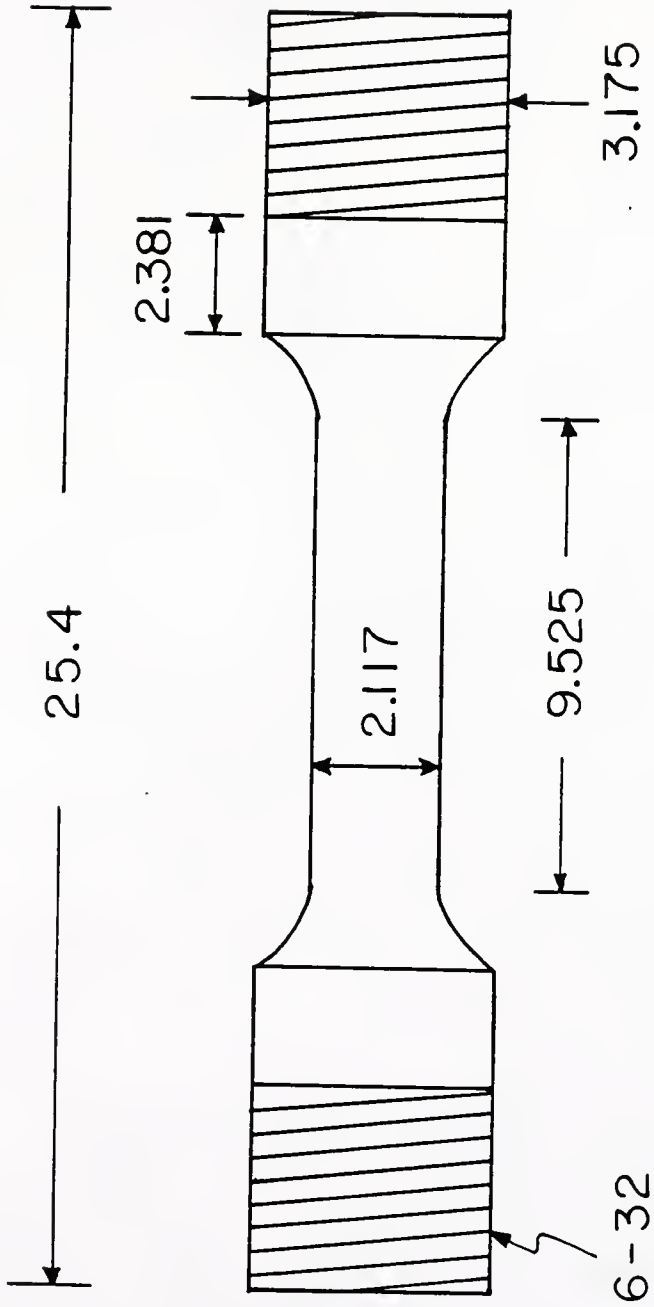


Figure 4.1 Specimen dimensions used in this investigation.

packets were next heated in a tube furnace under a flowing argon atmosphere for 4.5 hours at 1173 K to produce the 0.24 atomic percent composition and for 10 and 12 hours, respectively, at 1273 K to yield the 0.75 and 0.95 atomic percent alloys. The packets containing the oxidized specimens were allowed to cool in the furnace. The specimens were then removed from the packets and lightly etched in a 30% HF-70% HNO₃ solution to remove a thin surface scale left from the oxidizing step. After de-scaling they were given a homogenizing anneal in a vacuum furnace under a dynamic vacuum of 10^{-4} Torr at 1273 K for 18 hours.

Some of the sections were then mounted, polished, and etched to provide a suitable surface for a microhardness survey. All microhardness measurements were made on a Kentron microhardness tester using a DPH indenter and were correlated with published DPH versus oxygen concentration surveys [77]. It was possible to maintain microhardness values over all tensile specimens of this composition to ± 4 DPH units, which corresponds to a variation of oxygen concentration of approximately ± 0.04 at.%. Each rod section was then machined into cylindrical threaded tensile specimens, with the dimensions given before.

Initially, the research plans called for the work to be done with VP grade Nb as a base material. As testing proceeded, and the VP niobium stock neared depletion, another batch of niobium was obtained from the Wah-Chang Corporation. This will be designated by WC Nb. The major impurity concentrations of this niobium are also listed in Table 4.1. The oxygen concentration is about six times larger than that of VP niobium. The Wah-Chang niobium was directly used for the measurement of the tensile properties. Tensile specimens were prepared in the same manner as for the VP niobium.

4.2 Tensile Testing

Tensile tests were performed in an Instron Testing Instrument Model 1125 which allows the recorder chart to be driven in conjunction with crosshead commands. Tensile tests were conducted over the temperature range between 77 K and 971 K. For the tests up to 473 K, specimens were tested by using an inverted tensile fixture suspended in temperature controlling baths. Below room temperature, the specimens were tested in conventional cryogenic baths. Tests between room temperature and 473 K were carried out in an agitated silicon oil bath. For the temperatures above 473 K, the tests were performed in a vertical resistance furnace under a flowing high purity (99.99%) argon atmosphere. During the test period the temperature was controlled to within ± 1 K at each test temperature.

The strain rate sensitivity was determined by changing the strain rate at a fixed strain and measuring the change in flow stress. The extrapolation technique was used to measure the flow stress difference, as defined in Figure 4.2. When jerky flow was present, the extrapolations were drawn tangent to the stress peaks. Most of the strain rate sensitivity measurements were made by changing the strain rate by five times with a base strain rate of $8.8 \times 10^{-5} \text{ s}^{-1}$.

VP grade Nb was used to investigate the strain aging at a constant stress. A technique [23,33] for aging under load is shown in Figure 4.3. Here the specimen is unloaded to some fraction of the flow stress developed during the prestrain. This is accomplished by holding the

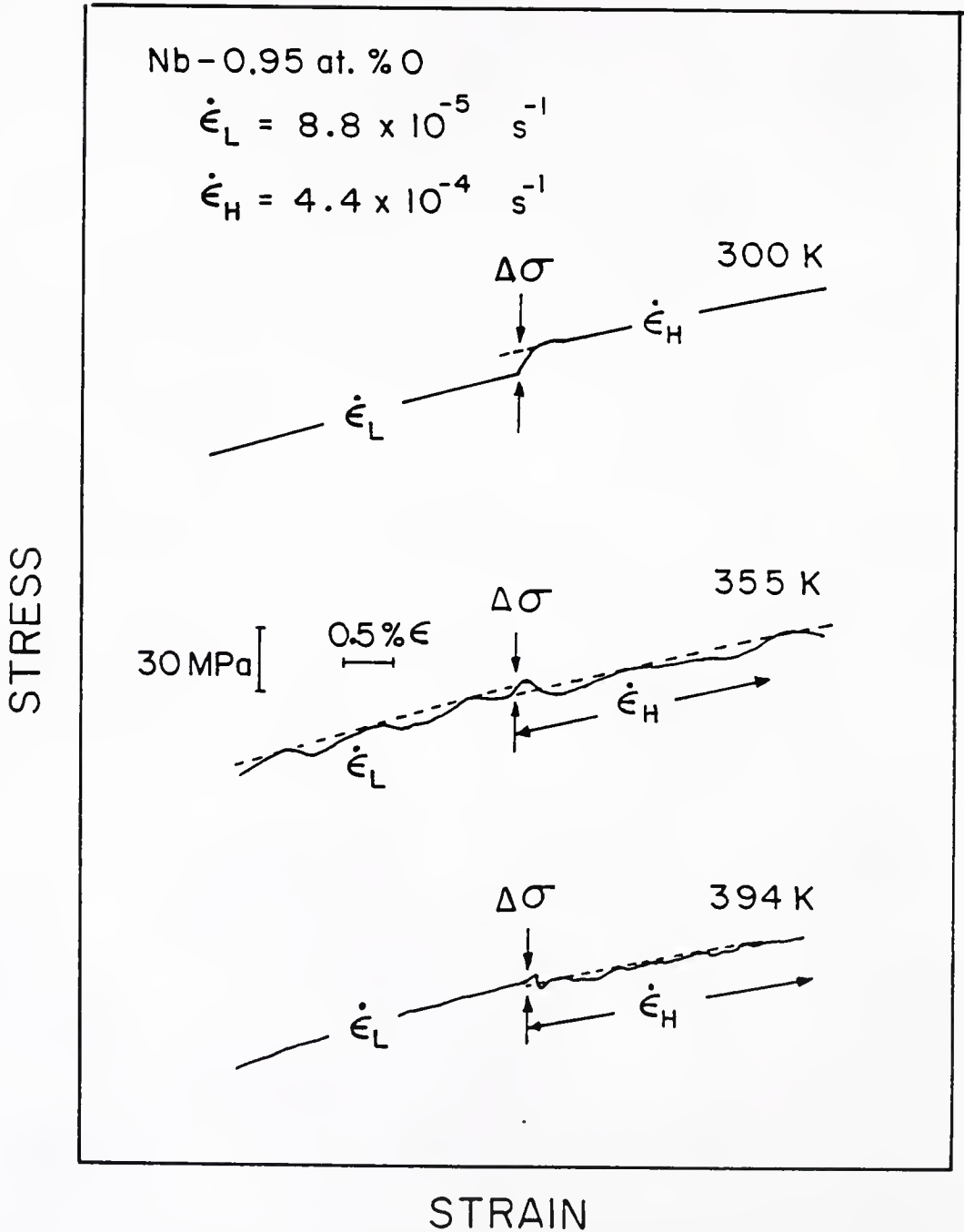
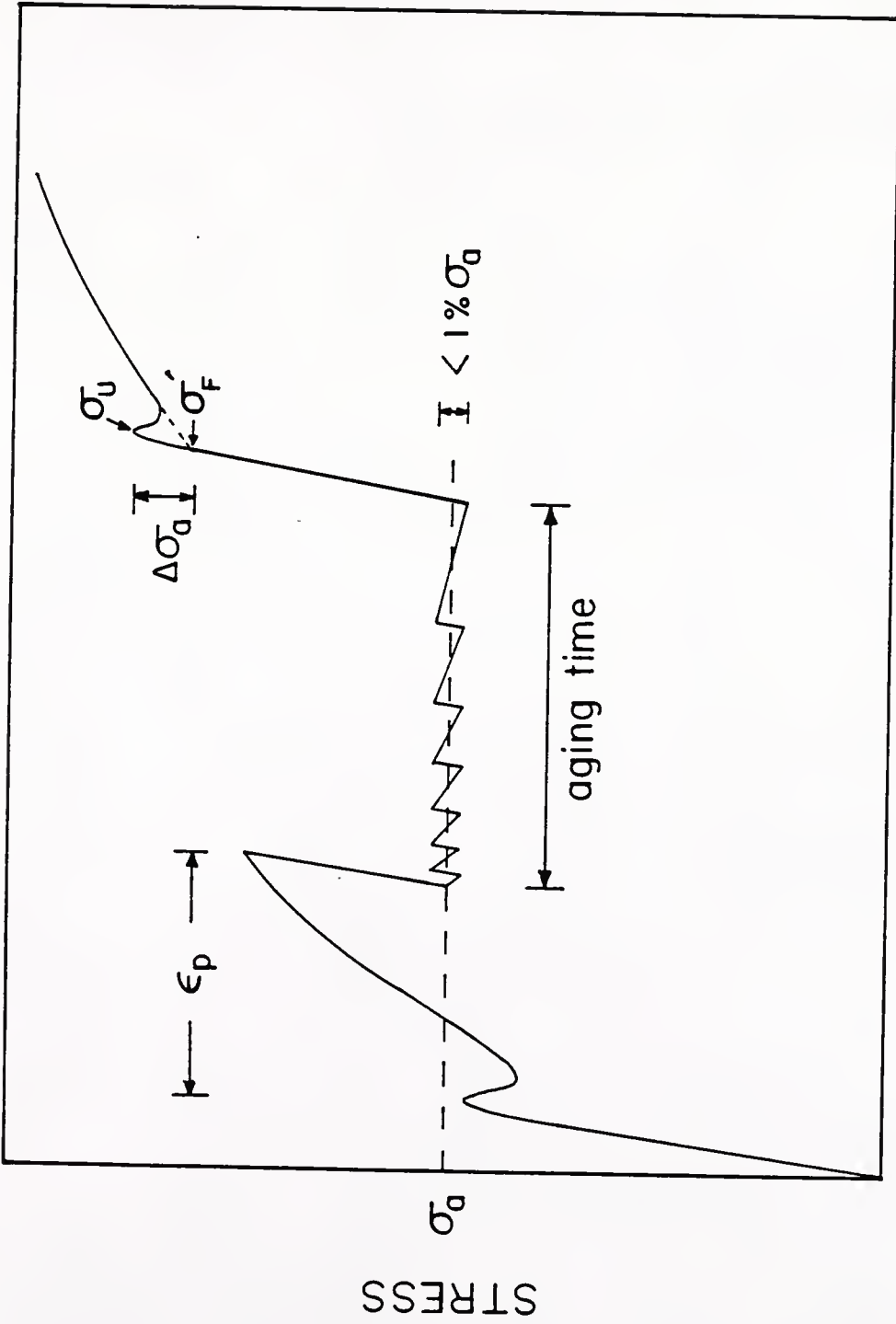


Figure 4.2 Illustration of the extrapolations used for the calculation of the strain rate sensitivity on various stress strain curves.



STRAIN

Figure 4.3 Schematic representation showing the method used to measure the yield point return when a specimen was aged at a fixed load.

specimen between two closely spaced load limits. Within these load limits the specimen undergoes a number of small relaxation and reloading cycles. Thus, as it deforms plastically during the load relaxation part of a cycle the load falls until the lower load limit is reached, then the machine is turned on. The load then rises to the upper load limit at which point the machine is again turned off and the cycle is repeated. Figure 4.3 also shows the manner in which the yield point return data were measured in a strain aging test. In this method, the yield point return, $\Delta\sigma_a$, is defined as the stress difference between the upper yield point and the point σ_f' , at which the flow curve obtained after yielding extrapolates back to the elastic part of the stress-strain curve.

The average strain rate during an aging period was measured at each test.

CHAPTER V EXPERIMENTAL RESULTS

5.1 Portevin-Le Chatelier Effect Due to Snoek Dynamic Strain Aging

5.1.1 Tensile Tests

Figure 5.1 shows a set of stress strain curves for specimens with 0.75 at.% oxygen deformed at a strain rate of $8.8 \times 10^{-5} \text{ s}^{-1}$ between 335 K and 422 K. The pertinent details of these stress strain curves are reproduced in Figure 5.2. Serrations were observed on these curves as described in the following. Note these serrations occur at temperatures too low to be identified as the usual Cottrell type of serrations. Serrations of this type have not been previously reported except in a very few cases [2,15,56]. At 335 K (curve 1), no serrations were observed. At 340 K (curve 2), on the other hand, a single serration appeared on the stress-strain curve near the point of maximum load. With increasing temperature the number of serrations increased. At 355 K (curve 4) periodic embryo Type A serrations appeared. Definition of this type of serrations has been reviewed in section 3.1. With further increase in temperature the number of serrations increased while the magnitude of the serrations decreased. In curves 6 and 7 in Figure 5.2, it can be seen that between 381 K and 394 K smaller irregular serrations appeared between the regular larger Type A serrations. These smaller serrations are probably associated with nucleation of secondary Lüders bands. At a still higher temperature, 409 K, curve 8 in Figure 5.2, both the Type A serrations and the closely spaced irregular intermediate serrations disappeared while Type B serrations began to appear just before the maximum

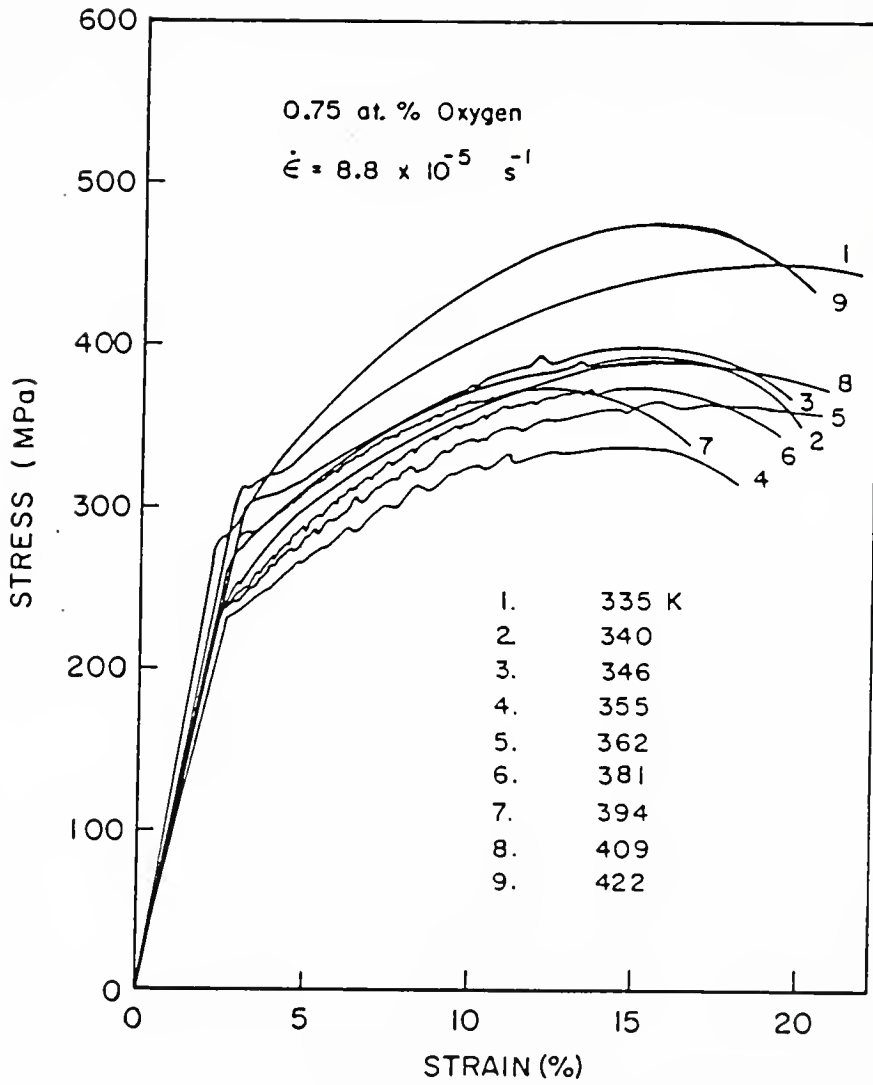


Figure 5.1 Stress-strain curve of Nb-0.75 at.% oxygen specimens for temperatures between 335 K and 422 K.

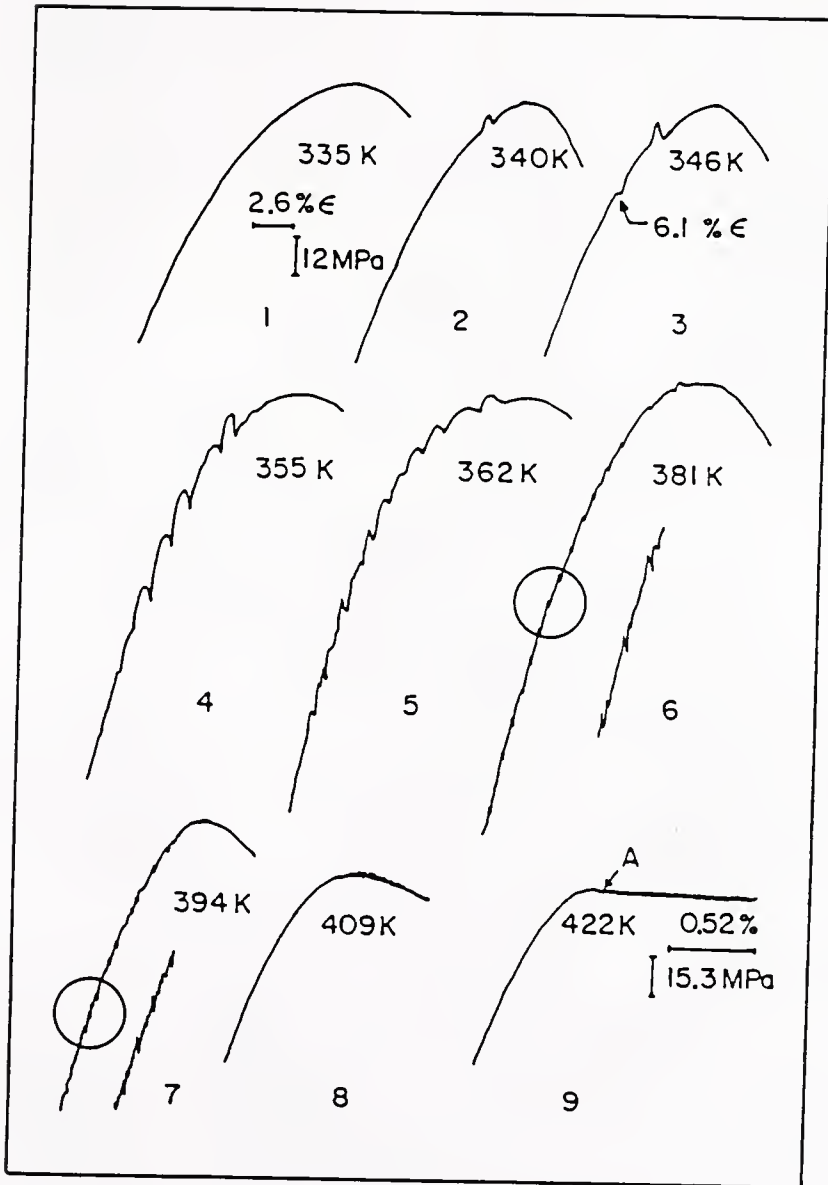


Figure 5.2 Details of the serrated curves shown in Figure 5.1.

load was attained. These serrations reached a maximum size just after necking began and then decreased in size and disappeared. Note that, at point A in curve 9 in Figure 5.2, the chart speed was increased by a factor of 10.

5.1.2 The Ratio of the Strain Rate to the Diffusion Coefficient ($\dot{\epsilon}/D$)

Cottrell [18] was the first to propose that the ratio of the strain rate to the diffusion coefficient, $\dot{\epsilon}/D$ could be used as an index for the conditions controlling the start of the serrations on a stress-strain curve. On the basis of Manjoine's data for mild steel [19], he proposed that the $\dot{\epsilon}/D$ should be about 10^9 for serrations associated with Cottrell dynamic strain aging. Beckerman [23] has also used the $\dot{\epsilon}/D$ ratio to characterize the range of strain rates and corresponding temperatures where dynamic strain aging due to the Snoek effect is expected to occur. She showed that, for the onset of serrations due to Snoek dynamic strain aging, the $\dot{\epsilon}/D$ ratio should lie between 10^{12} and 10^{14} . This is generally three orders of magnitude greater than that for Cottrell dynamic strain aging.

A plot of the magnitude of the largest serrations observed on the stress-strain curves of the Nb-0.75 at.% O specimens between 335 and 422 K is given as a function of the $\dot{\epsilon}/D$ ratio in Figure 5.3. The $\dot{\epsilon}/D$ ratios were calculated using the diffusion coefficient for oxygen in niobium as determined by Boratto and Reed-Hill [78]. Figure 5.3 shows that these serrations were observed at $\dot{\epsilon}/D$ ratios between 10^{11} and 10^{15} with the largest serrations appearing at an $\dot{\epsilon}/D$ equal to 10^{14} .

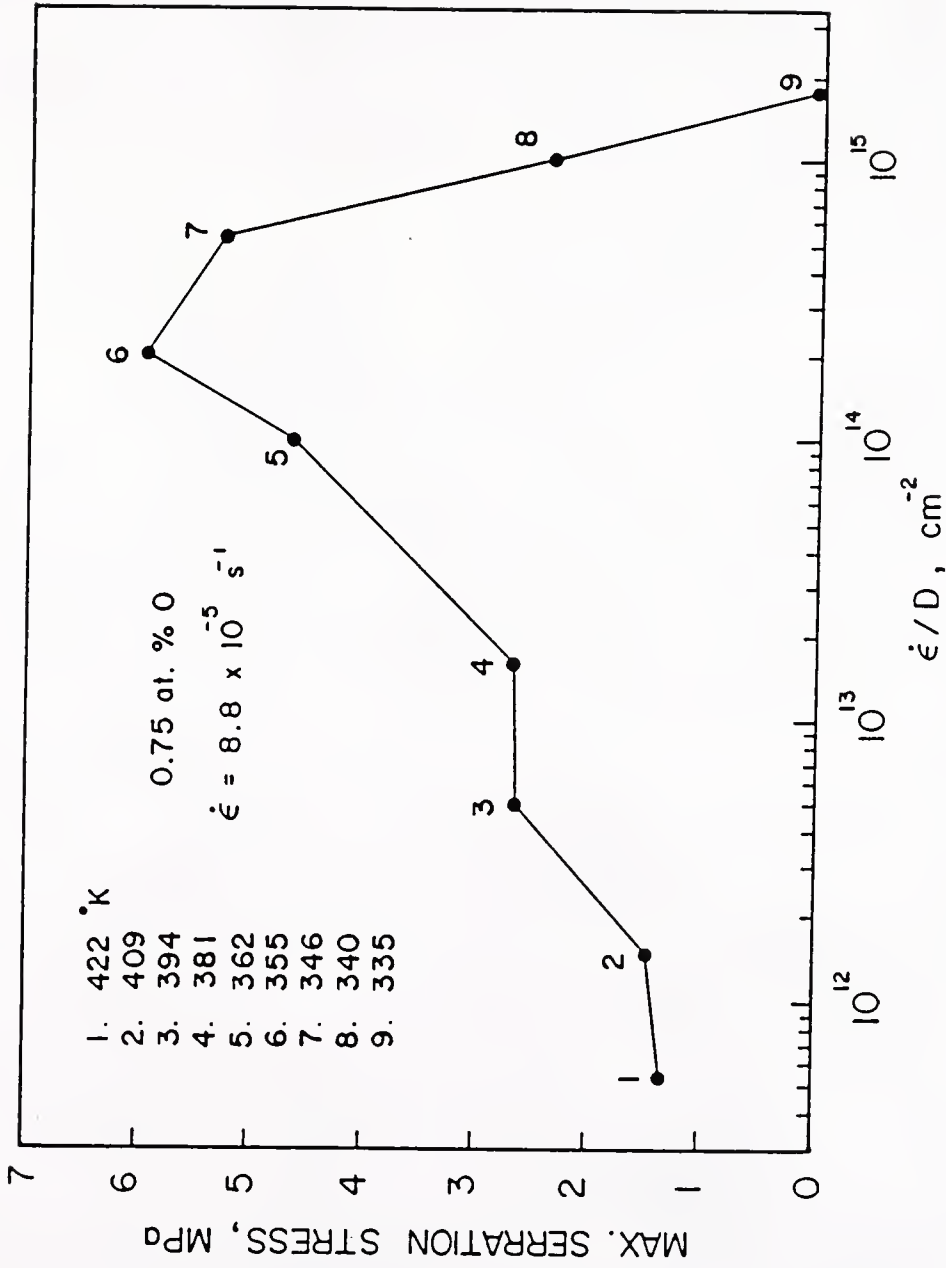


Figure 5.3 A plot of the maximum serration height observed during a tensile test as a function of the $(\dot{\epsilon}/D)$ ratio for 0.75 at.% oxygen.

5.1.3 Kinetics of the Snoek Ordering

Since in this temperature interval the serrations are most likely to be related to Snoek aging, it was felt that the period between successively larger peaks on the stress-strain curve might be related to the jump time of the oxygen atoms.

The average time between Type A serrations was determined for each test temperature between 346 and 394 K. The solid line in Figure 5.4 shows this average time when plotted against the test temperature. The dashed line in this figure gives the jump time of the oxygen atom versus the temperature as determined by the equation below [79].

$$\tau = \frac{a^2}{24D} \quad (5.1)$$

where τ is the mean time of stay of an oxygen atom in an interstitial position, a is the lattice constant of the niobium crystal, and D is the diffusion coefficient for oxygen in niobium. Figure 5.4 shows that between 346 and 381 K, where relatively periodic Type A serrations appear, the experimentally determined average time between serrations agrees well with the jump time of the oxygen atom.

5.1.4 Strain Dependence of Serrated Flows

In addition to the magnitude of the serrations and the number of serrations, three other parameters are also used to characterize these low temperature serrations; the critical strain, ϵ_c , for the onset of the serrations, and the strain occurring between successive serrations, ϵ_s , and the strain rate sensitivity, S .

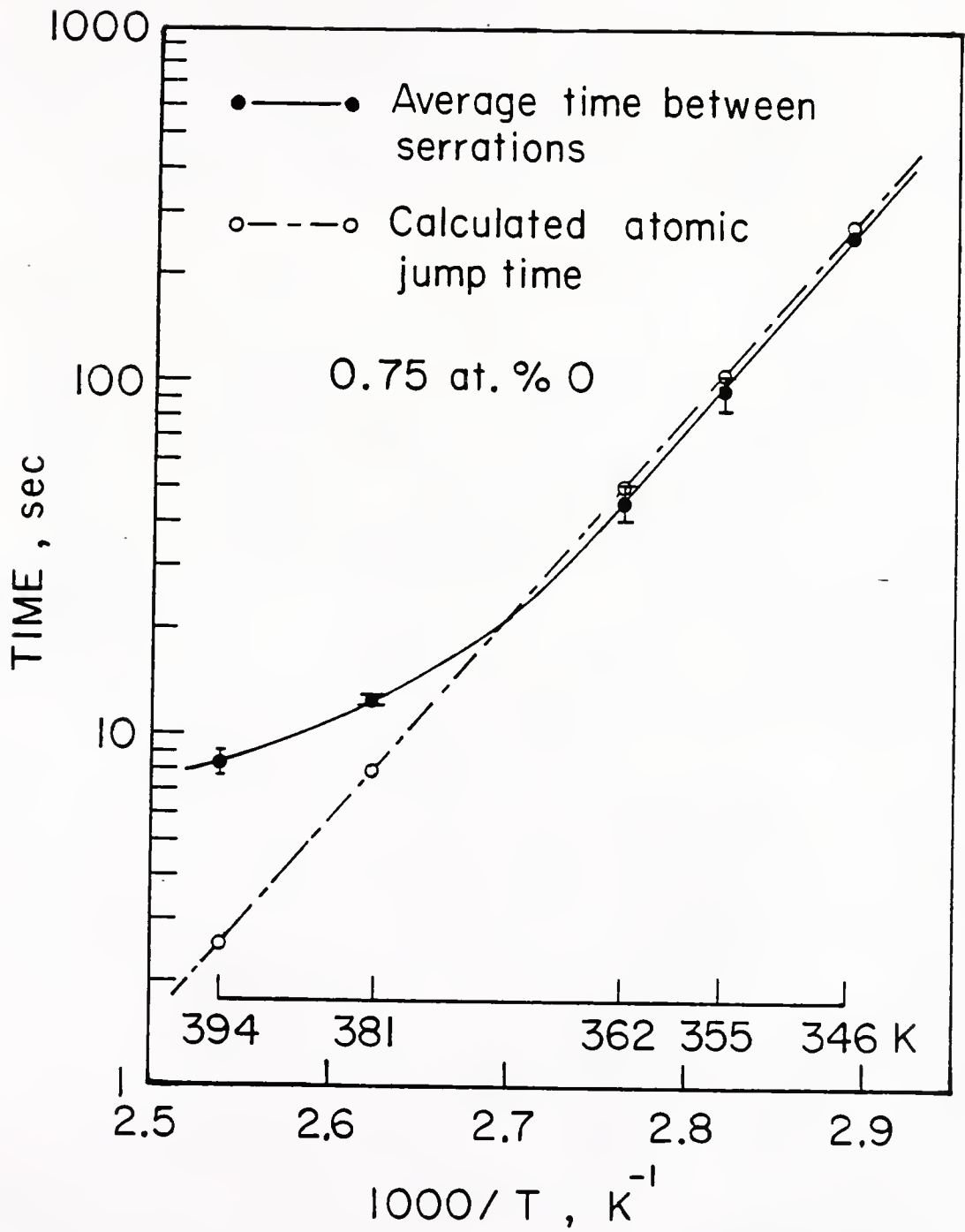


Figure 5.4 A comparison of the average time between serrations with the jump time of an oxygen atom.

The critical strain, ϵ_c , for the onset of serration, is plotted in Figure 5.5 as a function of temperature. The critical strain falls sharply from about 8.8% to 1% as temperature increases from 340 K to 355 K. At the intermediate temperature range, between 355 and 394 K, the critical strain becomes small and relatively constant, i.e., the serrations at this temperature range begin to appear as early as the deformation proceeds $\sim 1\%$ strain. With further increase in temperature, the serrations appear near the maximum load and the value of the critical strain increases rapidly. In other words, no visible serrations were observed during uniform plastic deformation.

The strain between successive serrations, ϵ_s , was measured from a stress-strain curve obtained at 381 K. It appears that at this temperature serrations become regular and consistent. Figure 5.6 is a plot of ϵ_s as a function of strain. It can be seen that ϵ_s increases linearly with increasing strain. A definition of ϵ_s is shown in this figure.

The strain dependence of the strain rate sensitivity at this low temperature range where the Portevin-Le Chatelier effect is observed was studied. As may be seen in Figure 5.2, the stress-strain curve at 346 K shows only two well defined Type A serrations, the first appearing at about $6.1\% \epsilon$. Just below or at this strain homogeneous deformation breaks down into discontinuous plastic flow. Thus, 346 K appeared to be an ideal temperature for studying the interrelationship between the strain, the strain rate sensitivity, and the initiation of the Portevin-Le Chatelier effect. The results of the strain rate sensitivity measurements made on a 0.75 at.% oxygen specimen as a function of the strain

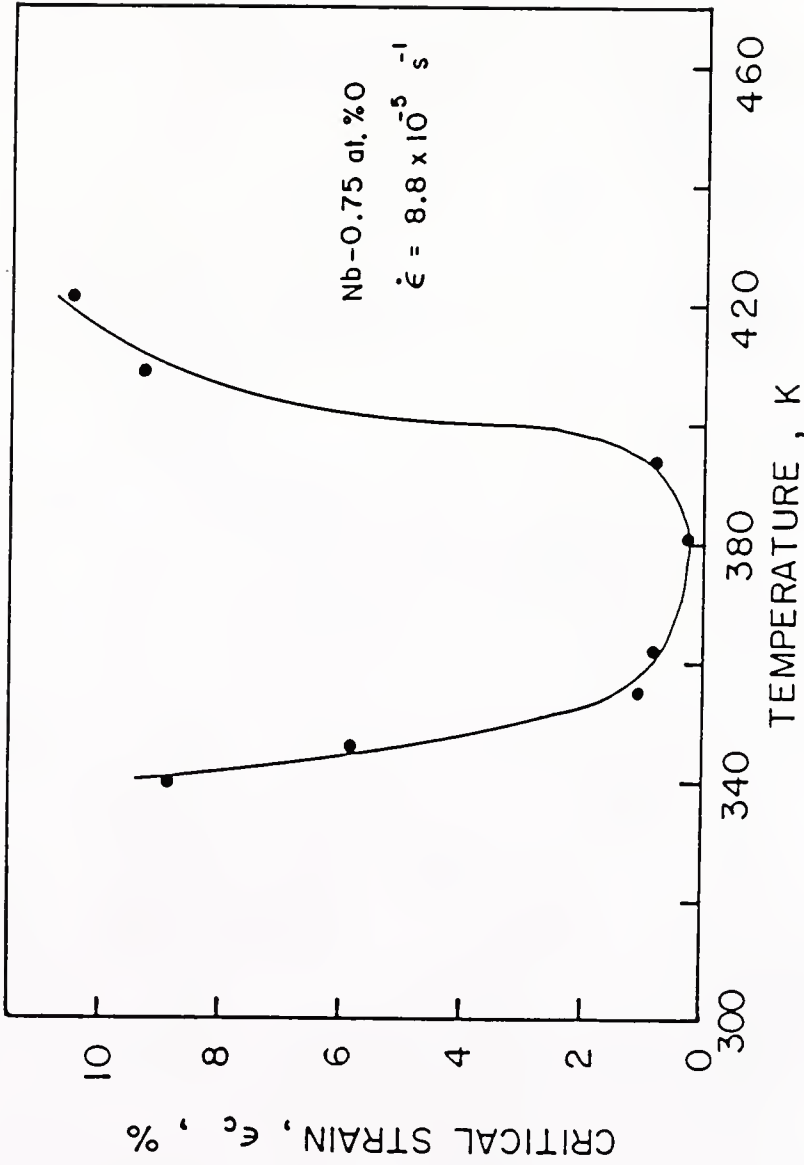


Figure 5.5 A plot of the critical strain, ϵ_c , for the onset of serrations as a function of temperature between 340 and 422 K. Nb-0.75 at.% oxygen.

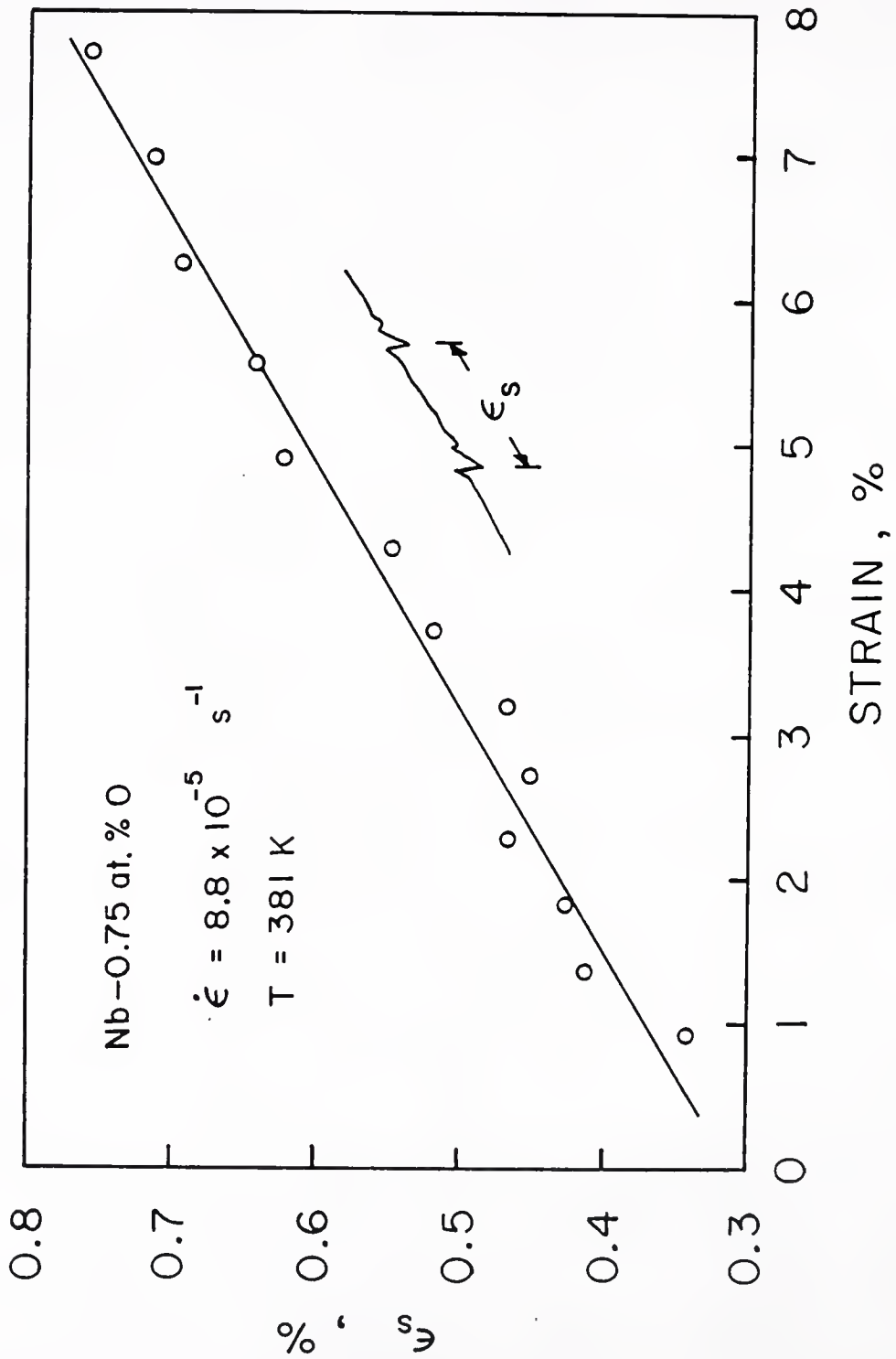


Figure 5.6 The strain between successive periodic serrations ϵ_s , at $T = 381 \text{ K}$.

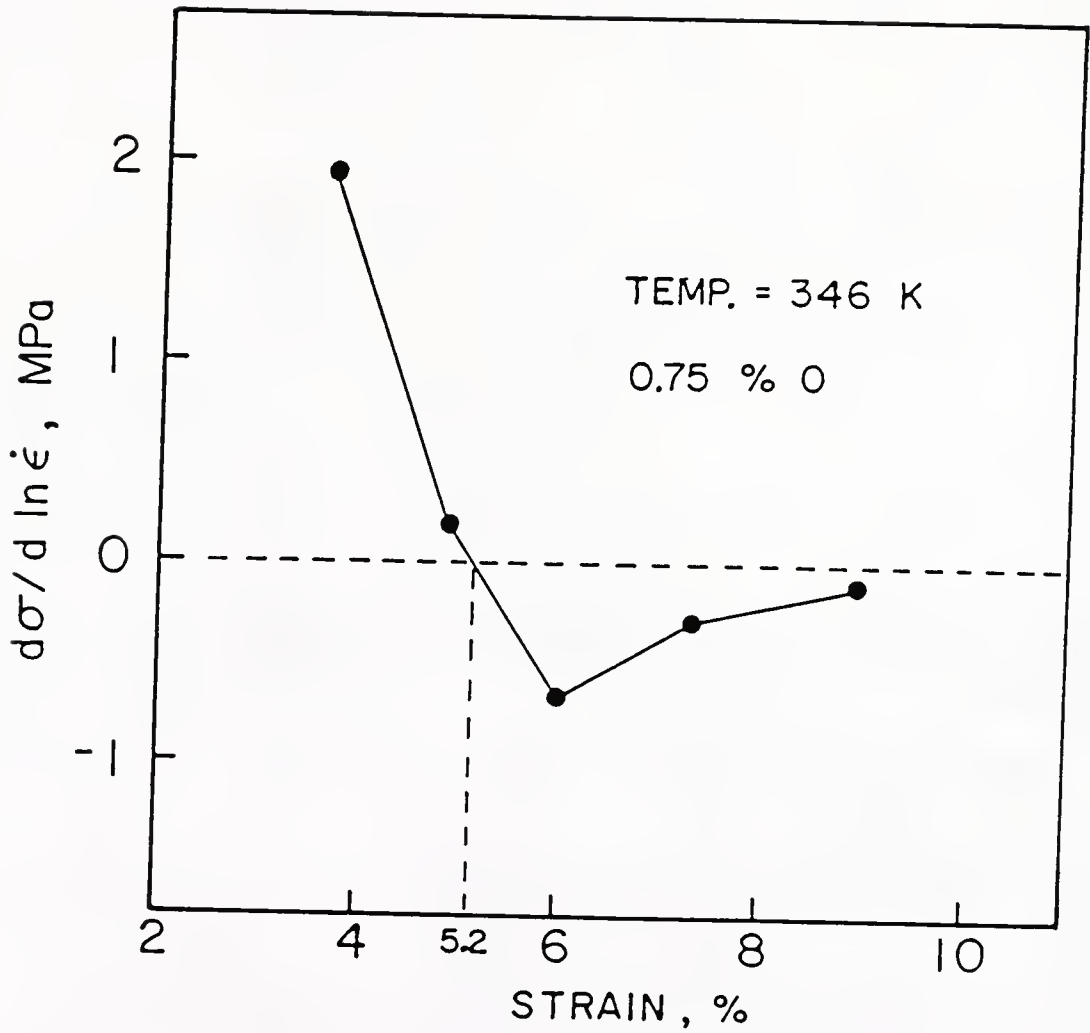


Figure 5.7 Variation of the strain rate sensitivity, S , with strain at 346 K. Nb-0.75 at.% oxygen
 $\dot{\epsilon}_L = 2.8 \times 10^{-5} \text{ s}^{-1}$, $\dot{\epsilon}_H = 4.4 \times 10^{-4} \text{ s}^{-1}$.

at 346 K are shown in Figure 5.7. The strain rate sensitivity parameter that was used in this figure is

$$S = \left(\frac{\Delta \sigma}{\Delta \ln \dot{\epsilon}} \right)_T \quad (5.2)$$

where σ is the flow stress and $\dot{\epsilon}$ the strain rate. The strain rate sensitivity was measured using the extrapolated steady state change of stress rather than the initial transient stress peak, as defined in Figure 4.2. As may be seen in Figure 5.7, the strain rate sensitivity, S , is positive up to $\epsilon \sim 5.2\%$. Above this strain S becomes negative. A minimum occurs at about 6.1% strain followed by a gradual increase with further deformation. The effect of strain on the strain rate sensitivity will be discussed in detail in the discussion chapter.

5.2 Strain Rate Sensitivity of the Flow Stress

5.2.1 Effect of Temperature

The strain rate sensitivities, S and n , are plotted against temperatures between 77 K and 773 K for VP Nb in Figures 5.8 and 5.9. The specimen was deformed to 4.5% strain at a strain rate ($\dot{\epsilon}_L$) of $8.8 \times 10^{-5} \text{ s}^{-1}$ and then the rate change to $\dot{\epsilon}_H$, where $\dot{\epsilon}_H = 5 \dot{\epsilon}_L$, was made. The difference in flow stresses at two strain rates was measured. Note that a horizontal dotted line indicates zero strain rate sensitivity. The results show that the strain rate sensitivity is strongly dependent on the temperature. At the temperatures below 200 K, there is a very high peak in the strain rate sensitivity. Although the experimental data are limited, it is seen that the peak appears at around 150 K and that the magnitude of the peak is

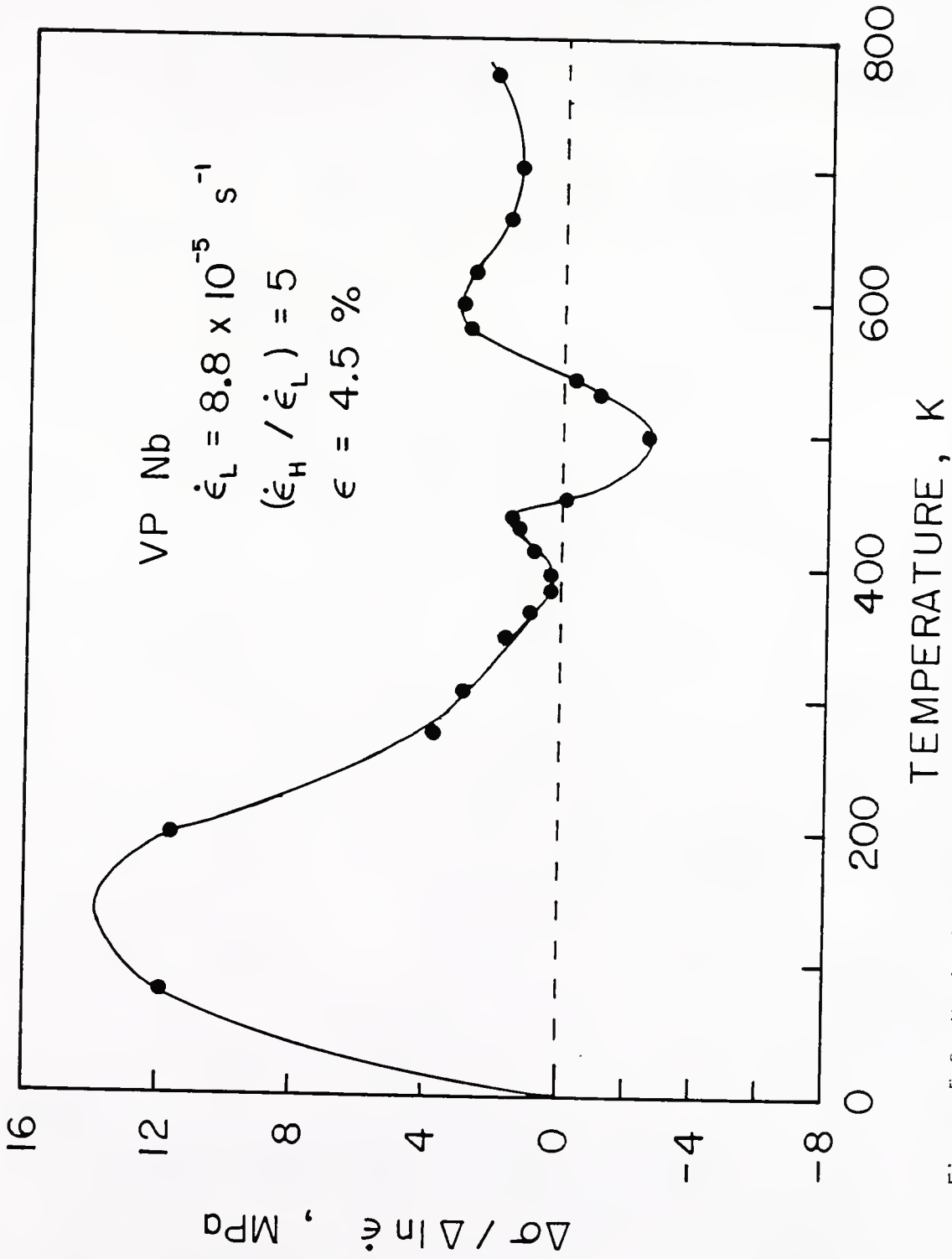


Figure 5.8 Variation of the strain rate sensitivity, $\Delta \sigma / \Delta \ln \dot{\epsilon}$, with temperature. VP-Nb specimens, $\dot{\epsilon}_L = 8.8 \times 10^{-5} \text{ s}^{-1}$, $(\dot{\epsilon}_H / \dot{\epsilon}_L) = 5$.

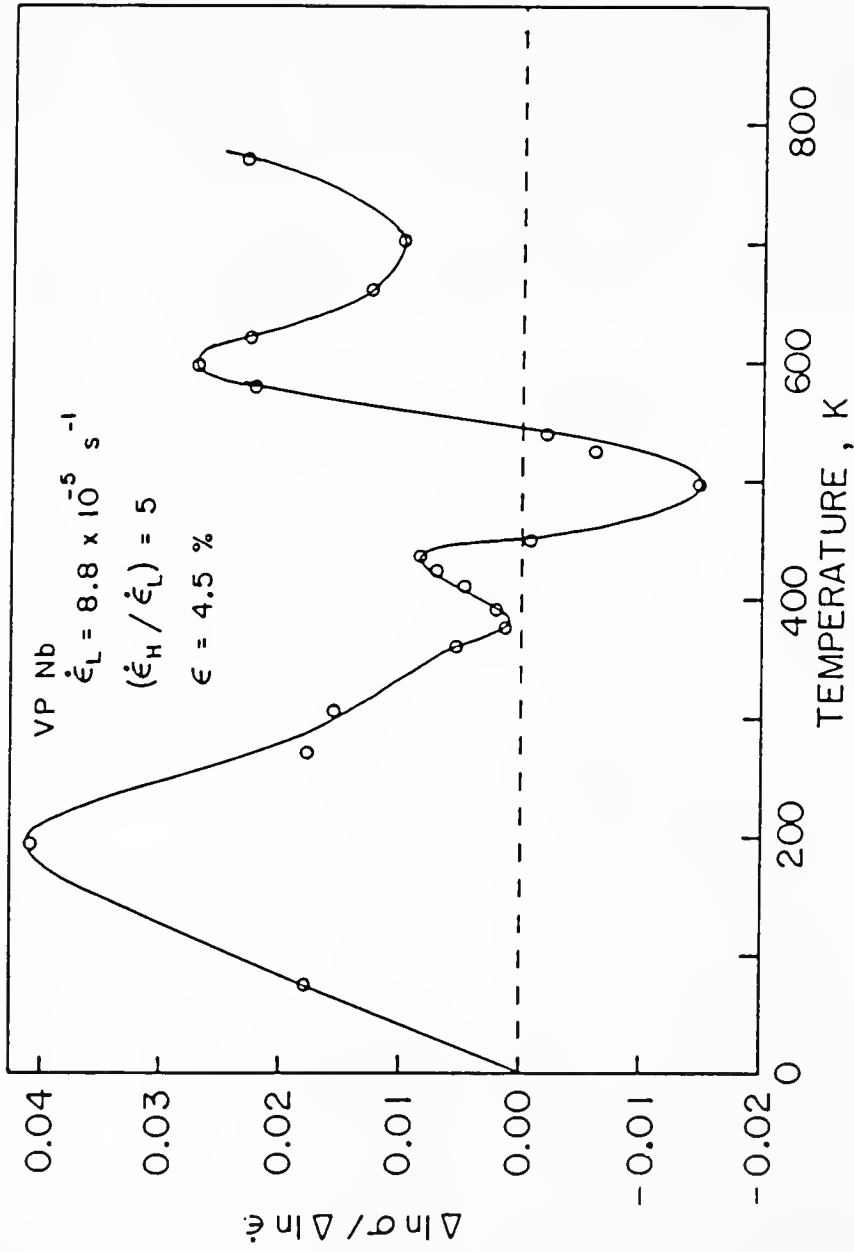


Figure 5.9 Variation of the strain rate sensitivity, $\Delta \ln \sigma / \Delta \ln \dot{\epsilon}$, with temperature. VP-Nb specimens, $\dot{\epsilon}_L = 8.8 \times 10^{-5} \text{ s}^{-1}$, $(\dot{\epsilon}_H / \dot{\epsilon}_L) = 5$.

about 14 Mpa. As the temperature increases, the strain rate sensitivity drops sharply and shows a minimum at $T \approx 370$ K. At this temperature, the $\Delta\sigma/\Delta\ln\dot{\epsilon} \approx 0$. As the temperature increases further, the strain rate sensitivity increases and reaches a small peak at around 440 K with the value of approximately 1.5 Mpa, followed by a sharp drop as temperature rises. As the temperature passes around 455 K, the strain rate sensitivity becomes negative again. The negative character of the strain rate sensitivity grows with further increasing temperature. When the temperature reaches ~ 500 K the strain rate sensitivity has a deep minimum with a value of approximately - 2.5 Mpa. With further increase in temperature, the strain rate sensitivity increases but it still has a negative value. At temperatures around 550 K, the strain rate sensitivity again passes the dotted horizontal line, where $\Delta\sigma/\Delta\ln\dot{\epsilon} = 0$, followed by another sharp peak at $T \approx 600$ K. At the temperatures above 600 K, the strain rate sensitivity decreases gradually as the temperature increases and the values remain positive. In summary, there are two temperature intervals within which the strain rate sensitivity is a minimum. One is centered near 370 K, the other around 500 K. At the higher temperature minimum, the strain rate sensitivity becomes negative. Following the high temperature minimum, the strain rate sensitivity passes a sharp positive peak at about 600 K. This will be discussed in detail in the discussion chapter.

5.2.2 Effect of Oxygen Concentration

The measurements of the strain rate sensitivity for specimens containing higher oxygen concentrations are shown in Figures 5.10 through

5.14. Here again the higher oxygen specimens were deformed to a pre-strain of 4.5% and the strain rate sensitivity was measured by varying the strain rate between $8.8 \times 10^{-5} \text{ s}^{-1}$ ($\dot{\epsilon}_L$) and $4.4 \times 10^{-4} \text{ s}^{-1}$ ($\dot{\epsilon}_H$).

Figures 5.10 and 5.11 are plots of the strain rate sensitivity S and n , for niobium specimens containing 0.24 at.% oxygen. The overall picture of the strain rate sensitivity versus temperature for 0.24 at.% oxygen specimens are not much different from that of the VP grade specimen; i.e., for 0.24 at.% oxygen specimen, there are also two temperature intervals within which the strain rate sensitivity becomes a minimum and a sharp positive peak at $T \approx 600 \text{ K}$. Even for the higher oxygen specimen, 0.95 at.% oxygen, the temperature dependence of the strain rate sensitivity remains basically unchanged. Plots of the strain rate sensitivity, S and n , versus temperature for 0.95 at.% oxygen specimens are shown in Figures 5.12 and 5.13. In these figures, a dotted horizontal line again indicates zero strain rate sensitivity.

Effect of oxygen concentration on the strain rate sensitivity-temperature curve are clearly seen in Figure 5.14 in which Figures 5.8, 5.10 and 5.12 are superimposed. It may be seen from Figure 5.14 that increasing oxygen concentration from 0.01 to 0.95 at.% does not change the basic plot of strain rate sensitivity versus temperature. In other words, for all three composition specimens, there exists a low temperature peak, two minima at two different temperature intervals and another peak at high temperature around 600 K.

Even though the data are limited it can be seen that the strain rate sensitivity peaks at low temperature for two different compositions, 0.01 and 0.95 at.% O, fall almost at the same temperature, around 150 K.

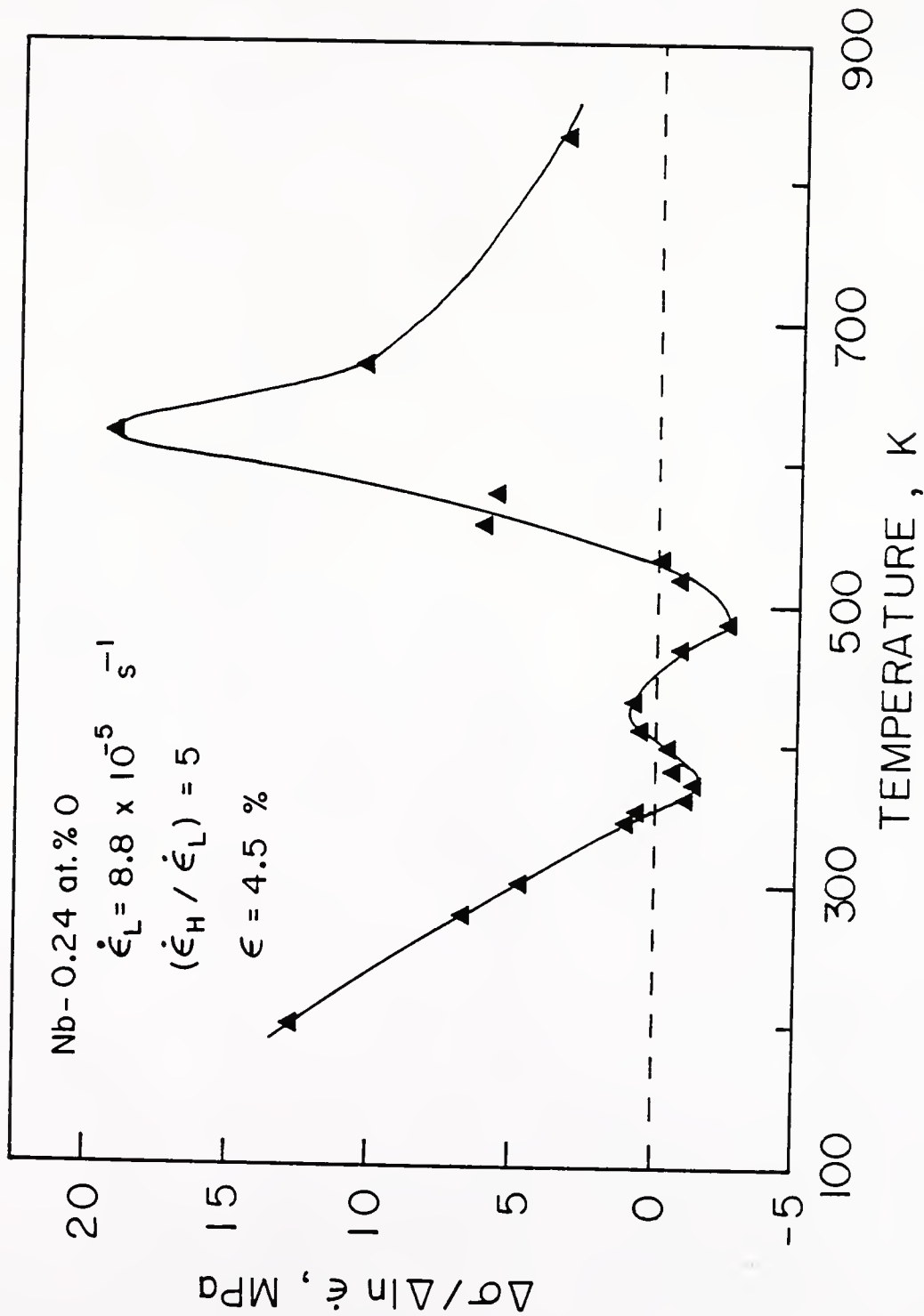


Figure 5.10 Variation of the strain rate sensitivity, $\Delta\sigma/\Delta \ln \dot{\epsilon}$, with temperature. Nb-0.24 at.% O specimens, $\dot{\epsilon}_L = 8.8 \times 10^{-5} \text{ s}^{-1}$, $(\dot{\epsilon}_H/\dot{\epsilon}_L) = 5$.

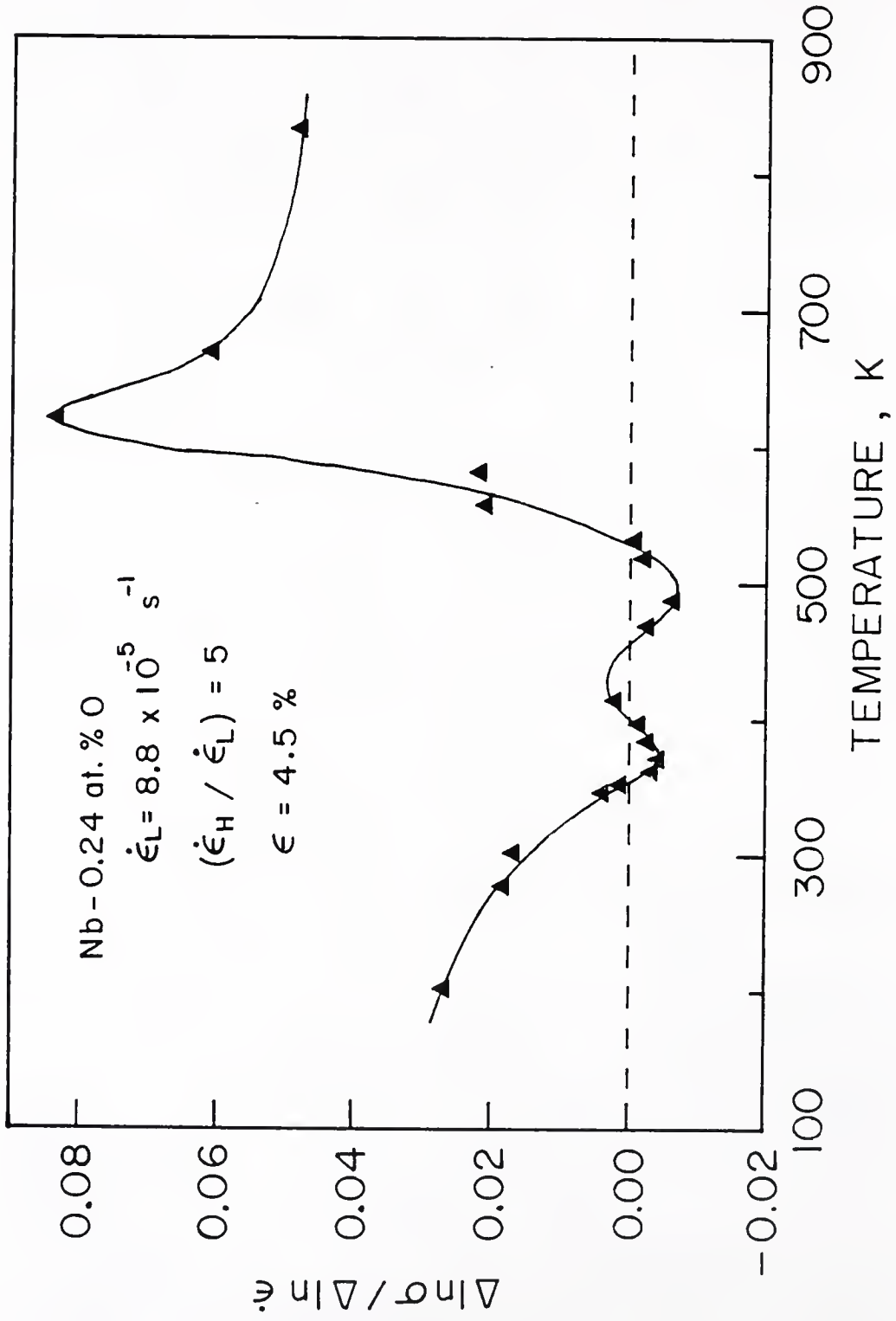


Figure 5.11 Variation of the strain rate sensitivity, $\Delta \ln \sigma / \Delta \ln \dot{\epsilon}$, with temperature. Nb-0.24 at.% O specimens, $\dot{\epsilon}_L = 8.8 \times 10^{-5} \text{ s}^{-1}$, $(\dot{\epsilon}_H / \dot{\epsilon}_L) = 5$.

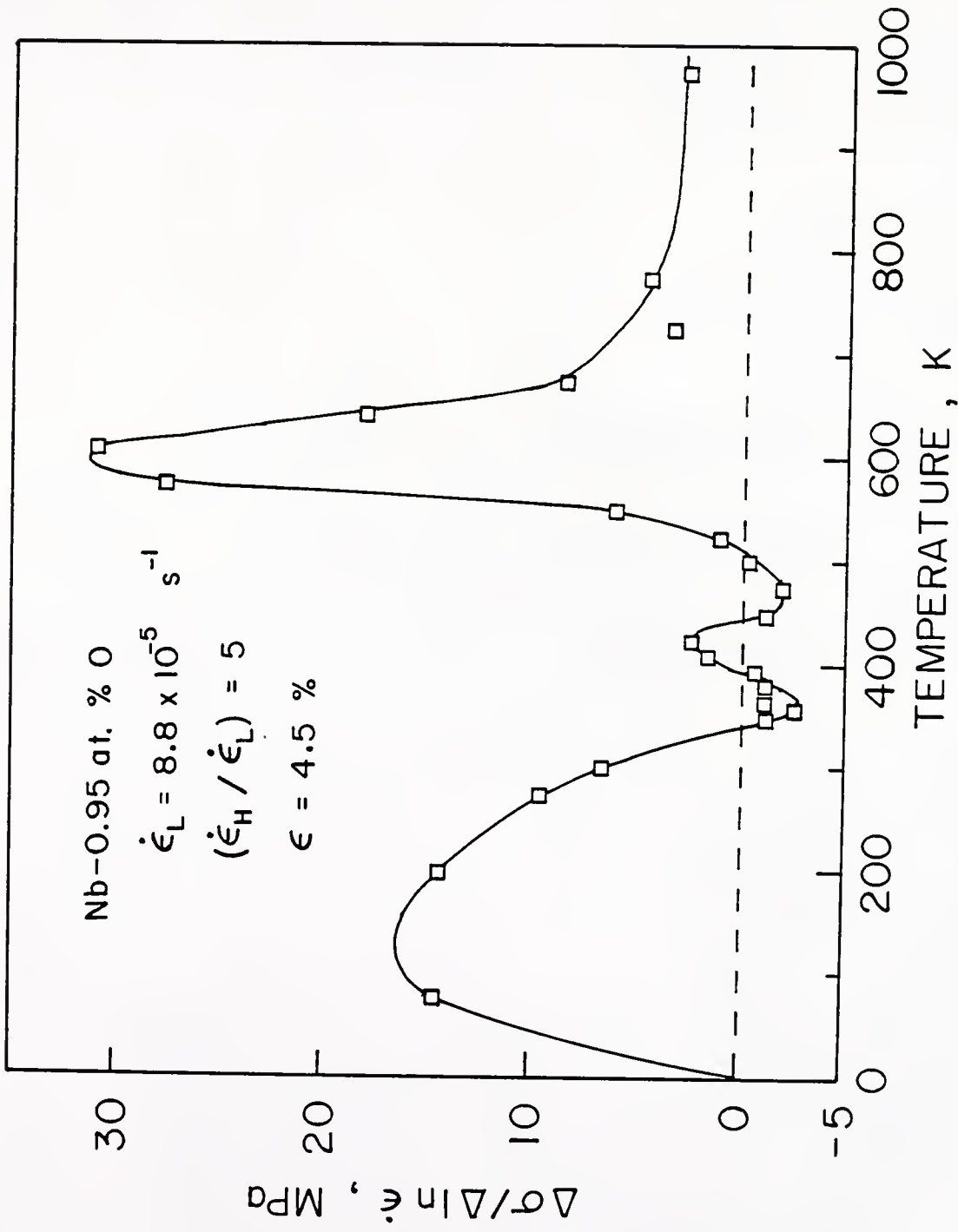


Figure 5.12 Variation of the strain rate sensitivity, $\Delta\sigma/\Delta\ln\dot{\epsilon}$, with temperature. Nb-0.95 at.% O specimens, $\dot{\epsilon}_L = 8.8 \times 10^{-5} \text{ s}^{-1}$, $(\dot{\epsilon}_H/\dot{\epsilon}_L) = 5$.

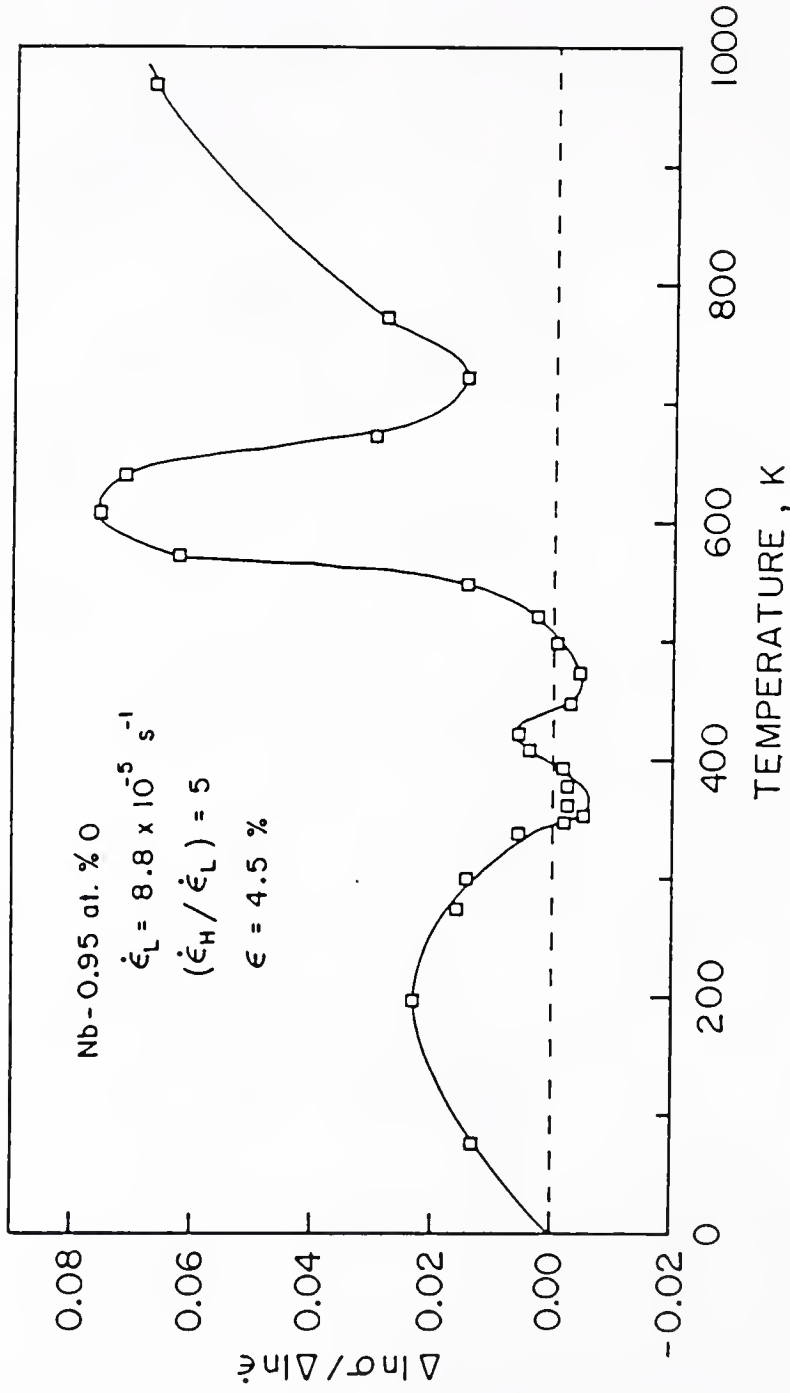


Figure 5.13 Variation of the strain rate sensitivity, $\Delta \ln \sigma / \Delta \ln \dot{\epsilon}$, with temperature. Nb-0.95 at.% O specimens, $\dot{\epsilon}_L = 8.8 \times 10^{-5} \text{ s}^{-1}$, $(\dot{\epsilon}_H / \dot{\epsilon}_L) = 5$.

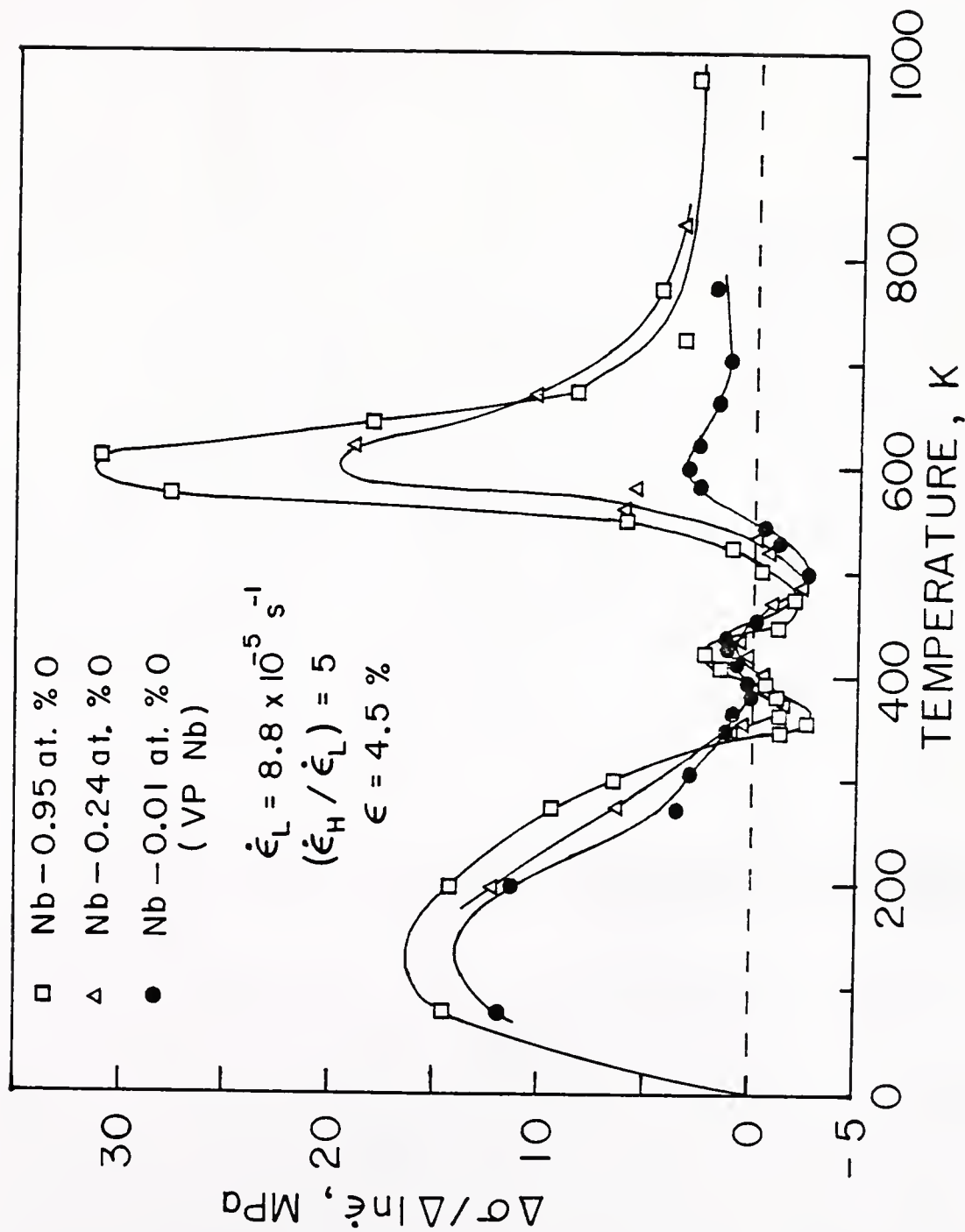


Figure 5.14 Variation of the strain rate sensitivity, $\Delta\sigma / \Delta \ln \dot{\epsilon}$, with temperature for specimens containing three levels of oxygen. $\dot{\epsilon}_L = 8.8 \times 10^{-5} \text{ s}^{-1}$ ($\dot{\epsilon}_H / \dot{\epsilon}_L$) = 5.

The peak temperature seems to be independent of the oxygen concentration. It is observed, however, that the peak height increases with oxygen concentration. The positive dependence of concentration on strain rate sensitivity continues until the temperature reaches around 335 K.

For all three different oxygen contents, there exists two temperature intervals where the strain rate sensitivity is a minimum. Note that the low temperature strain rate sensitivity minimum becomes negative as oxygen concentration increases from 0.01 to 0.24 at.% oxygen. Furthermore, the negative character of the strain rate sensitivity increases with increasing oxygen concentration. In other words, the strain rate sensitivity of higher oxygen specimens is more negative than that of lower oxygen specimens. This is not true at the higher temperature minimum. At the higher temperature minimum the strain rate sensitivity is negative to about the same degree at all three concentrations within the experimental error. The exact change of the stress with change in strain rate is not capable of being measured because deformation occurs discontinuously when serrations occur and the strain rates are not the same as the applied strain rates.

A careful examination of Figure 5.14 apparently reveals that the strain rate sensitivity minimum temperature, or the temperature at which $\Delta\sigma/\Delta\ln\dot{\epsilon} \approx 0$ is shifted to lower temperatures as the oxygen concentration increases. For instance, the temperatures where $\Delta\sigma/\Delta\ln\dot{\epsilon} \approx 0$ at the higher temperature side are 545 K, 530 K and 510 K for the specimens of 0.01, 0.24 and 0.95 at.% oxygen, respectively. A 35 K shift is observed by changing oxygen contents from 0.01 to 0.95 at.%.

Following the higher temperature minimum, the strain rate sensitivity passes a sharp peak at all oxygen concentrations. It is observed that the peak temperature is not affected by the oxygen concentrations; i.e., it is about 600 K for all specimens. However, the magnitude of the peak is a strong function of the oxygen concentration. It grows sharply with increasing oxygen concentration.

5.2.3 Effect of Base Strain ($\dot{\epsilon}_L$)

The effect of base strain rate on the plot of strain rate sensitivity versus temperature is shown in Figures 5.15 and 5.16. The VP grade Nb specimens were prestrained to 4.5% at three different base strain rates, $8.8 \times 10^{-5} \text{ s}^{-1}$, $4.4 \times 10^{-4} \text{ s}^{-1}$ and $2.2 \times 10^{-3} \text{ s}^{-1}$, and then a 5:1 rate change was made. Here again a dotted horizontal line indicates zero strain rate sensitivity.

It is seen from Figures 5.15 and 5.16 that the basic strain rate sensitivity versus temperature dependence is not changed by changing the base strain rate. For all three base strain rates, there exist two temperature ranges where strain rate sensitivity reaches a minimum and a strong peak at higher temperatures.

It is also found that, while the low temperature strain rate sensitivity minima for the first two slow base strain rates remain positive, the corresponding value at a faster base strain rate, $2.2 \times 10^{-3} \text{ s}^{-1}$ becomes negative. At the high temperature minimum the strain rate sensitivity is negative to about the same degree at all three base strain rates. It is generally seen from the figures that the curves are shifted

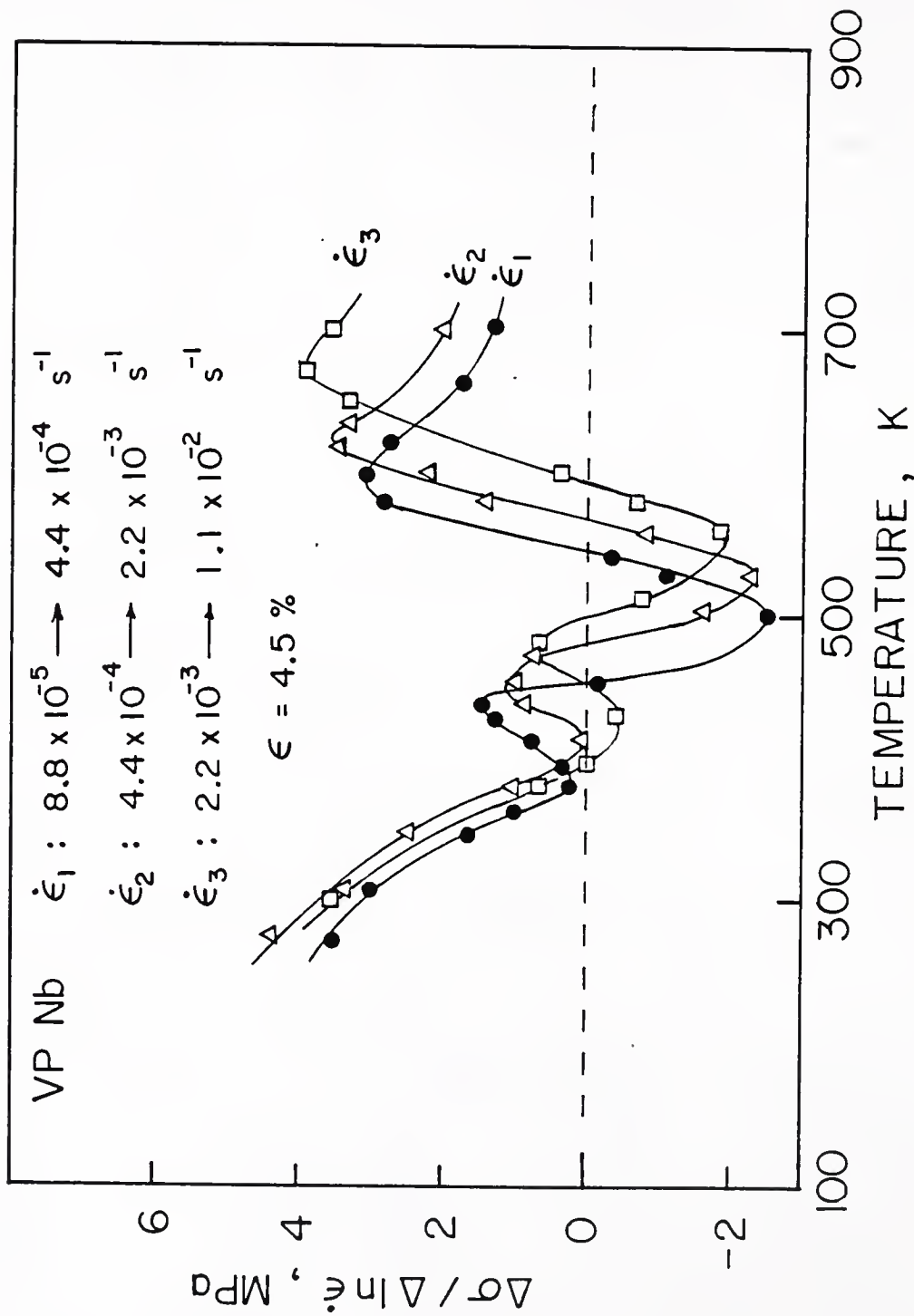


Figure 5.15 The effect of the base strain rate on a plot of $(\Delta\sigma/\Delta \ln \dot{\epsilon})$ versus temperature. VP-Nb specimen.

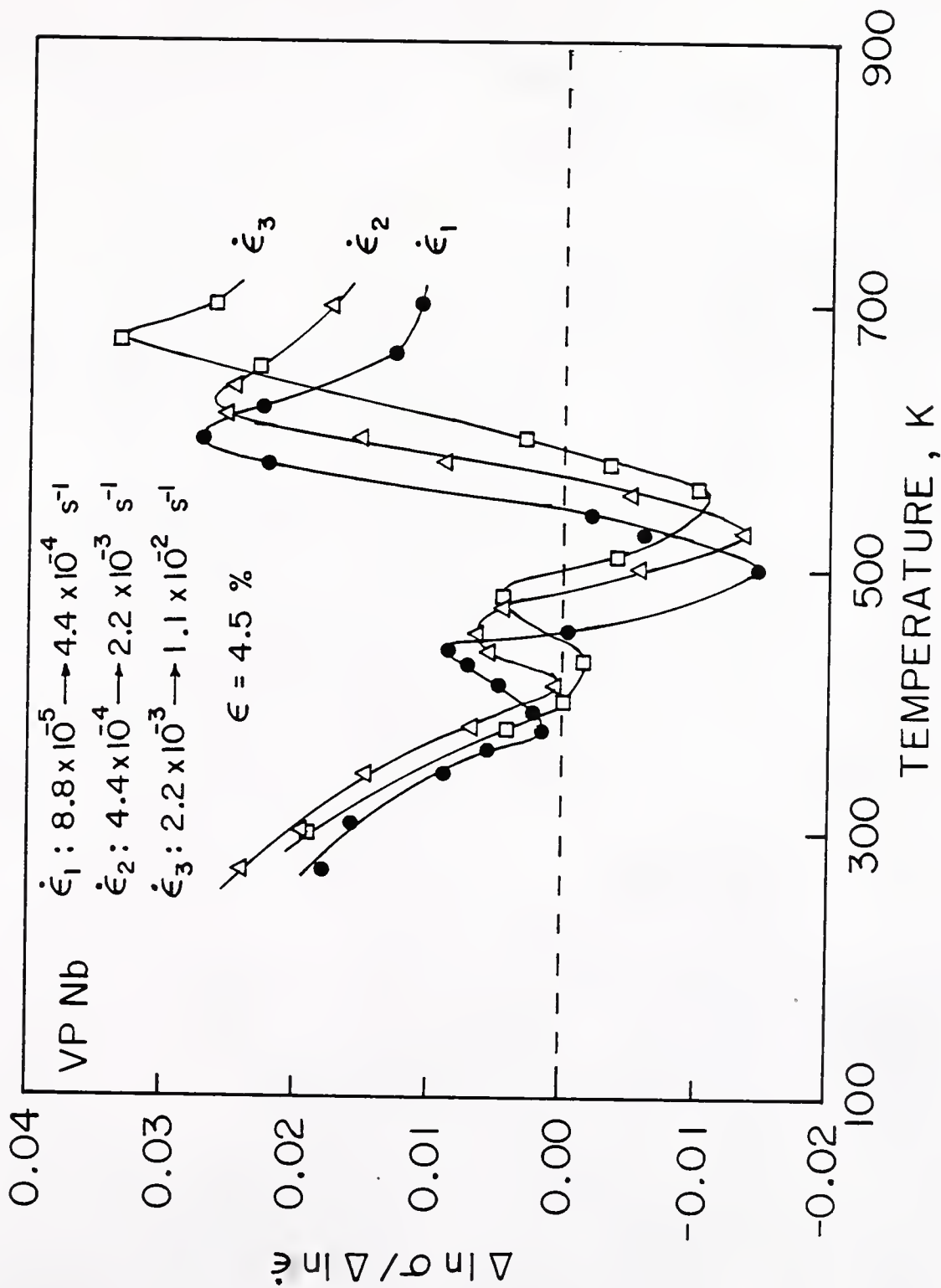


Figure 5.16 The effect of the base strain rate on a plot of $(\Delta \ln \sigma / \Delta \ln \dot{\epsilon})$ versus temperature.

to higher temperature as the base strain rate increases. Thus, for example, the temperatures where $\Delta\sigma/\Delta\ln\dot{\epsilon} \approx 0$ at the higher temperature side are 545 K, 570 K and 595 K for the base strain rates of $8.8 \times 10^{-5} \text{ s}^{-1}$, $4.4 \times 10^{-4} \text{ s}^{-1}$ and $2.2 \times 10^{-3} \text{ s}^{-1}$, respectively. Increasing the base strain rate by 25 times results in the strain rate sensitivity curve shifting by about 50 K to higher temperatures.

It might be practically necessary to know the temperature range where the plastic flow becomes unstable at a certain value of the strain rate. The temperature ranges in which the strain rate sensitivity becomes negative are measured for all base strain rates: 450 - 545 K, 480 - 570 K and 505 - 595 K for $8.8 \times 10^{-5} \text{ s}^{-1}$, $4.4 \times 10^{-4} \text{ s}^{-1}$ and $2.2 \times 10^{-3} \text{ s}^{-1}$, respectively. It appears that the temperature intervals for all three strain rates are about 95 K, regardless of the value of the base strain rate.

The peaks at temperatures above the strain rate sensitivity minimum are also observed at all three base strain rates. As the base strain increases, the peak temperature moves to the higher temperature side. The height of the high temperature SRS peak does not vary significantly with base strain rate.

5.2.4 Effect of Magnitude of Strain Rate Change

The effect of magnitude of strain rate change on the plot of strain rate sensitivity versus temperature is shown in Figure 5.17 and 5.18. VP Nb specimens were strained to 4.5% at a base strain rate of $8.8 \times 10^{-5} \text{ s}^{-1}$ and then a 25:1 strain rate change was made at each test. Data for $(\dot{\epsilon}_H/\dot{\epsilon}_L) = 5$ are also shown in the same figures.

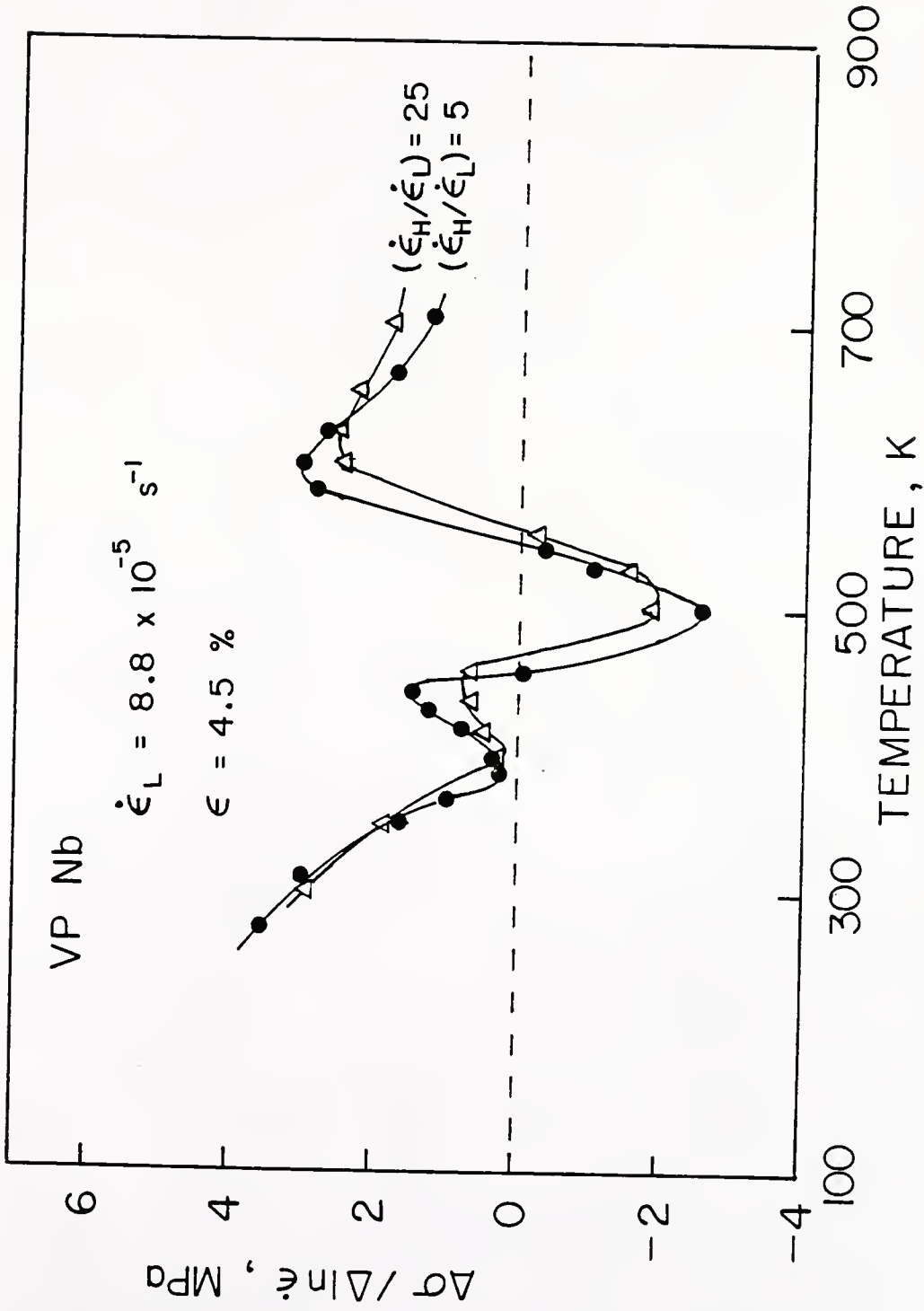


Figure 5.17 The effect of the magnitude of the strain rate change on a plot of $(\Delta\sigma/\Delta \ln \dot{\epsilon})$ versus temperature. $\dot{\epsilon}_L = 8.8 \times 10^{-5} \text{ s}^{-1}$.

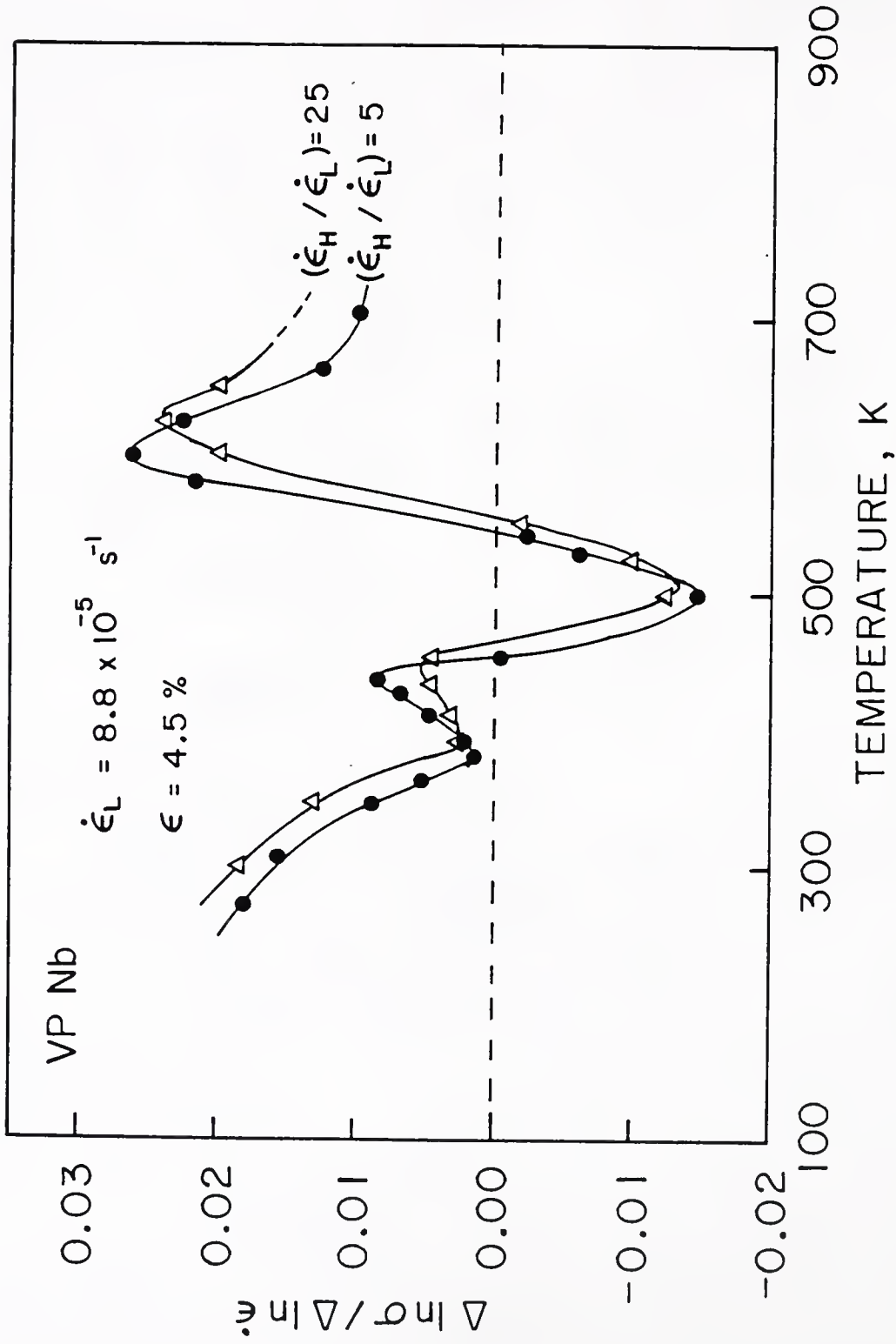


Figure 5.18 The effect of the magnitude of the strain rate change on a plot of $(\Delta \ln \sigma / \Delta \ln \dot{\epsilon})$ versus temperature. $\dot{\epsilon}_L = 8.8 \times 10^{-5} \text{ s}^{-1}$.

It may be seen that increasing the ratio five times does not affect significantly the magnitudes of both the low and high temperature minima. However, it shifts the overall curve towards higher temperatures. Thus, the two minimum temperatures and the peak temperature increase. Accordingly, the temperature at which the strain rate sensitivity becomes negative also increases with increasing magnitude of $(\dot{\epsilon}_H/\dot{\epsilon}_L)$.

5.2.5 Effect of Prestrain

In all of the previous strain rate sensitivity results prestrain was held constant at 4.5%. In Figures 5.19 and 5.20, the effect of prestrain on the strain rate sensitivity as a function of temperature is shown. Specimens were prestrained to 1% at a base strain rate of $8.8 \times 10^{-5} \text{ s}^{-1}$, and then a 25:1 rate change was made at each test. Superimposed on this curve are data for the 4.5% strain. Figures 5.19 and 5.20 reveal that decreasing prestrain from 4.5% to 1% brings the curve to the higher temperature side. However, the magnitude of both low and high temperature minima are not apparently influenced by the amount of strain imposed when the rate change is made. It is seen from Figure 5.19 that the magnitude of $\Delta\sigma/\Delta\ln\dot{\epsilon}$ at higher temperature is reduced by 40 ~ 50%. It is also observed that decreasing the strain causes the high temperature peak temperature to move to higher temperature. This is better seen in Figure 5.20.

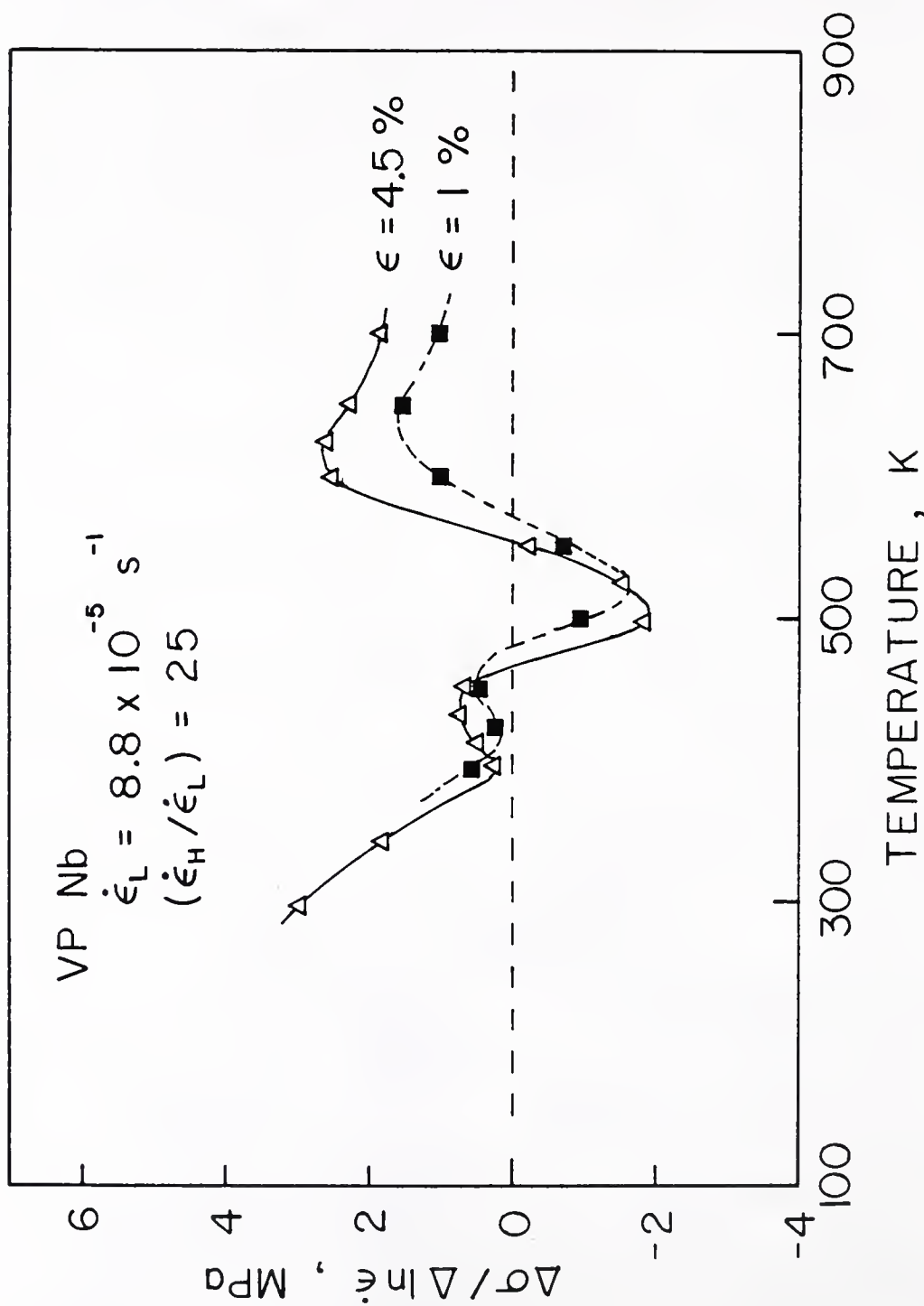


Figure 5.19 The effect of strain on a plot of $(\Delta\sigma / \Delta \ln \dot{\epsilon})$ versus temperature.
 $\dot{\epsilon}_L = 8.8 \times 10^{-5} \text{ s}^{-1}$, $(\dot{\epsilon}_H / \dot{\epsilon}_L) = 25$.

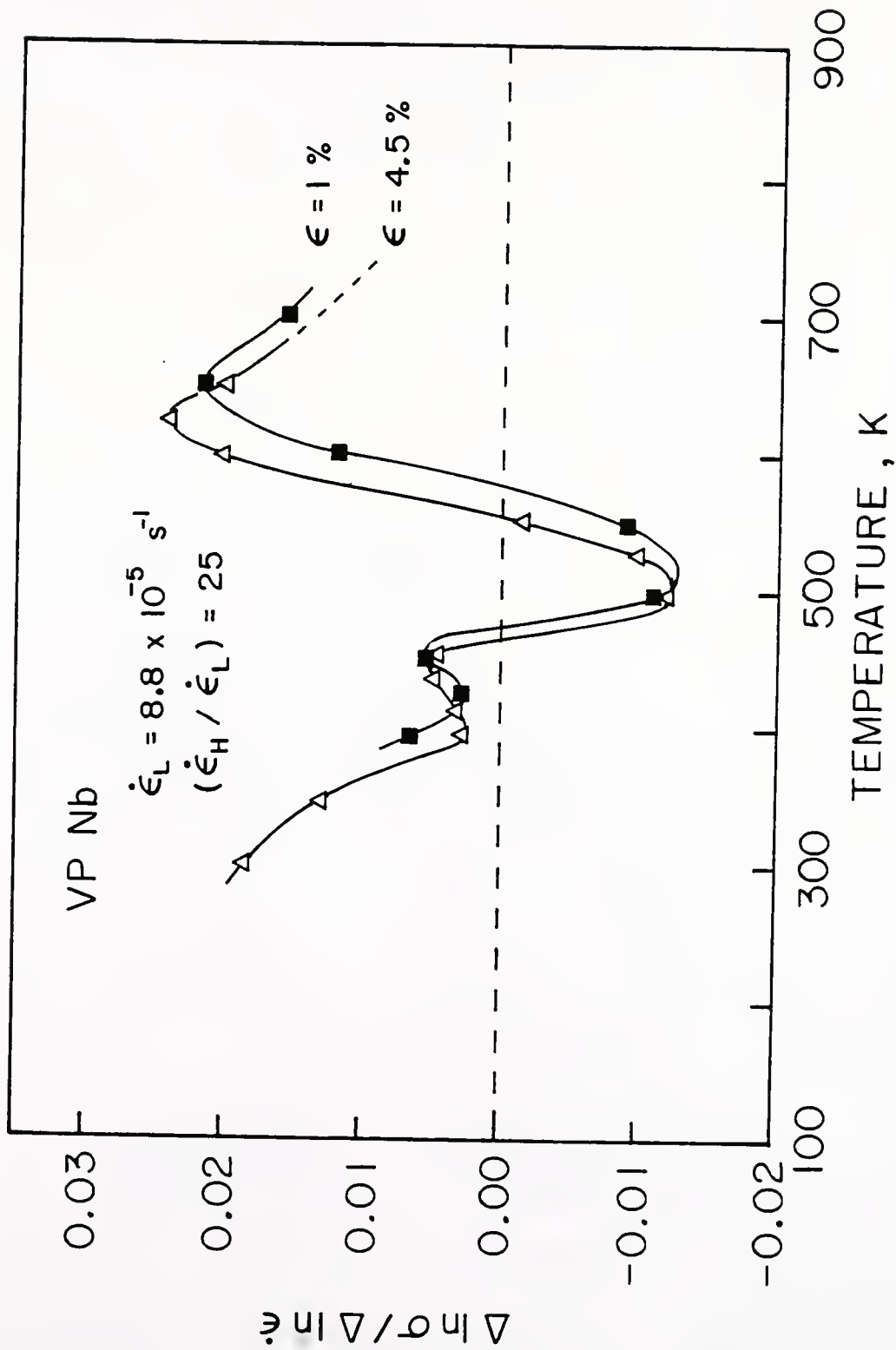


Figure 5.20 The effect of strain on a plot of $(\Delta \ln \sigma / \Delta \ln \dot{\epsilon})$ versus temperature. $\dot{\epsilon}_L = 8.8 \times 10^{-5} \text{ s}^{-1}$, $(\dot{\epsilon}_H / \dot{\epsilon}_L) = 25$.

5.3 Work Hardening Parameter

The parameter taken as a measure of the work hardening rate is the change in stress between the flow stresses at 4.5% and 4% ϵ . This quantity represents an average value of work hardening for a region near where the strain rate change was made. The results of the work hardening parameter of VP Nb specimens are plotted in Figure 5.21 as a function of temperature for three strain rates.

At each strain rate, a large work hardening peak is apparent. This figure reveals that increasing the strain rate increases the peak temperature of each maximum. The peak temperatures are approximately 510 K, 540 K and 580 K for strain rates of $8.8 \times 10^{-5} \text{ s}^{-1}$, $4.4 \times 10^{-4} \text{ s}^{-1}$ and $2.2 \times 10^{-3} \text{ s}^{-1}$, respectively. This effect can be understood by employing a relationship suggested by Cottrell [18]. He proposed that the temperature at the onset of serrated yielding, a dynamic strain aging feature, could be related to the applied strain rate by the relation

$$\dot{\epsilon} = K D \quad (5.3)$$

where K is a constant and D is diffusion coefficient of the solute atom. The above equation can be rewritten as

$$\dot{\epsilon} = K D_0 \exp\left(\frac{-\Delta H}{RT}\right) \quad (5.4)$$

and taking the natural logarithm of this equation gives

$$\ln \dot{\epsilon} = \ln(K D_0) - \frac{\Delta H}{RT} \quad (5.5)$$

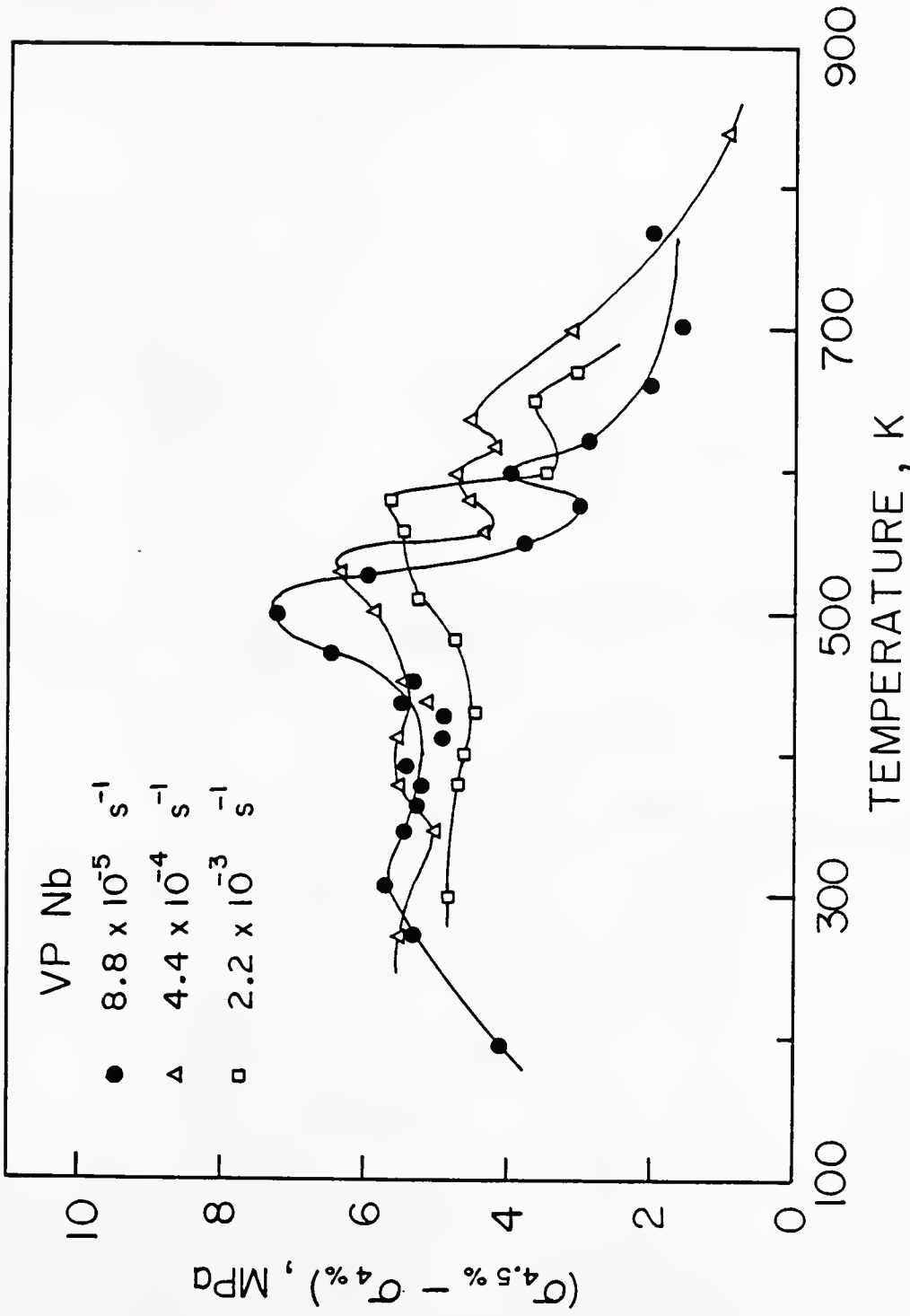


Figure 5.21 Variation of the work hardening as a function of the temperature for these different strain rates. VP-Nb specimens.

If it is assumed that the same form of equation may be applied to other dynamic strain aging phenomena, such as work hardening maxima, then the shift of these peak temperatures can be tested by plotting the inverse of the peak temperature against the logarithm of the applied strain rate. This has been done in Figure 5.22. A linear least square fit to these data gives values for ΔH of ~ 27 Kcal/mole. This value is in good agreement with the activation energy for the diffusion of oxygen in niobium. Thus, it is plausible to associate this work hardening peak with dynamic strain aging due to the presence of oxygen in niobium.

It is also apparent from Figure 5.21 that the work hardening values of VP Nb specimens essentially remain constant until the temperature reaches about 450 K. However, this is no longer true for the higher oxygen specimens. In Figure 5.23 the work hardening parameters are again plotted as a function of temperature for specimens containing higher oxygen concentrations deformed at a strain rate of $8.8 \times 10^{-5} \text{ s}^{-1}$.

The corresponding data of VP Nb specimens are superimposed in the same figure. It is observed that a general increase in the level of the work hardening for the higher oxygen specimens occurs over the entire temperature range of 196 K to 971 K. This indicates that oxygen and nitrogen are sufficient strengtheners over this temperature range. The work hardening values of the two higher oxygen specimens, 0.24 and 0.95 at.% oxygen, increase gradually as temperature increases and reach their first peaks at around 500 K. A careful examination reveals that the peak temperature decreases with increasing oxygen concentration even though the amount of the temperature shift is small.

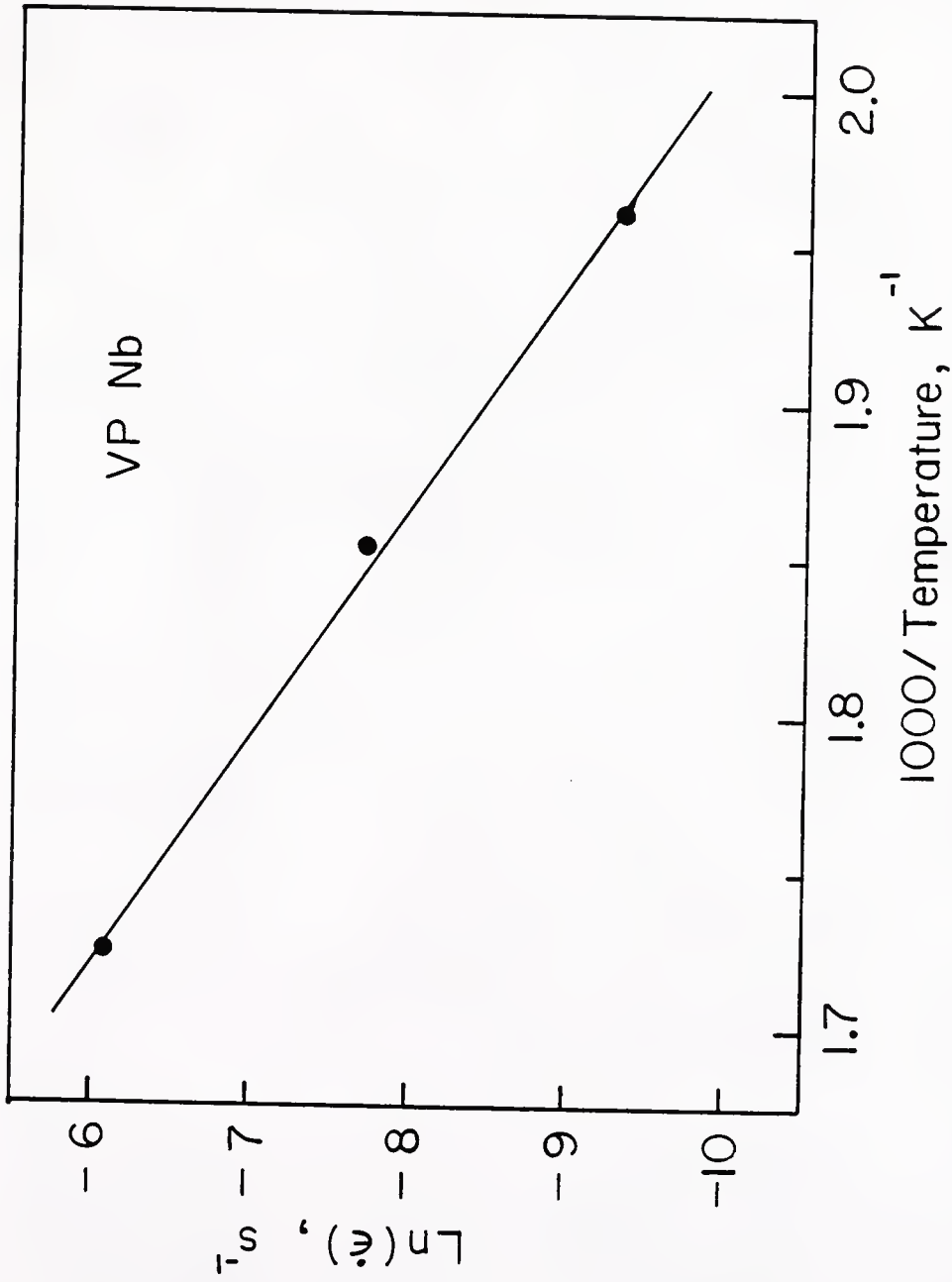


Figure 5.22 The logarithm of the strain rate as a function of the reciprocal peak temperature for each work hardening maximum. VP-Nb specimens.

It is found that the peak height is strongly dependent on the oxygen concentration; the peak grows in height with increasing level of oxygen in the specimens. The results of this are shown in Figure 5.24. A sharp increase in work hardening rate is seen as the oxygen concentration increases from 0.01 to 0.24 at.%. With a further increase in oxygen concentration, the rate of increasing work hardening parameter is reduced.

Above the temperature where oxygen peaks are observed, there is a sharp decrease in work hardening rate followed by another peak at higher temperature. This is clearly seen from Figure 5.23. These higher temperature work hardening peaks are considered to be due to the presence of nitrogen.

5.4 Strain Aging Under Stress

Some useful experimental data on the aging under stress were obtained using VP Nb specimens.

5.4.1 Effect of Aging Stress and Prestrain on the Yield Point Return

Figure 5.25 is a plot of the magnitude of the yield point return as a function of the aging stress. The aging stress is expressed as a percentage of the prestrain flow stress. VP Nb specimens were prestrained to 5% at 371 K and aged for 35 minutes at the same temperature. It is found that the magnitude of the yield point return becomes relatively constant up to 60% σ_f : no significant rise in the yield point return is observed even if the aging stress is 60% of the prestrain

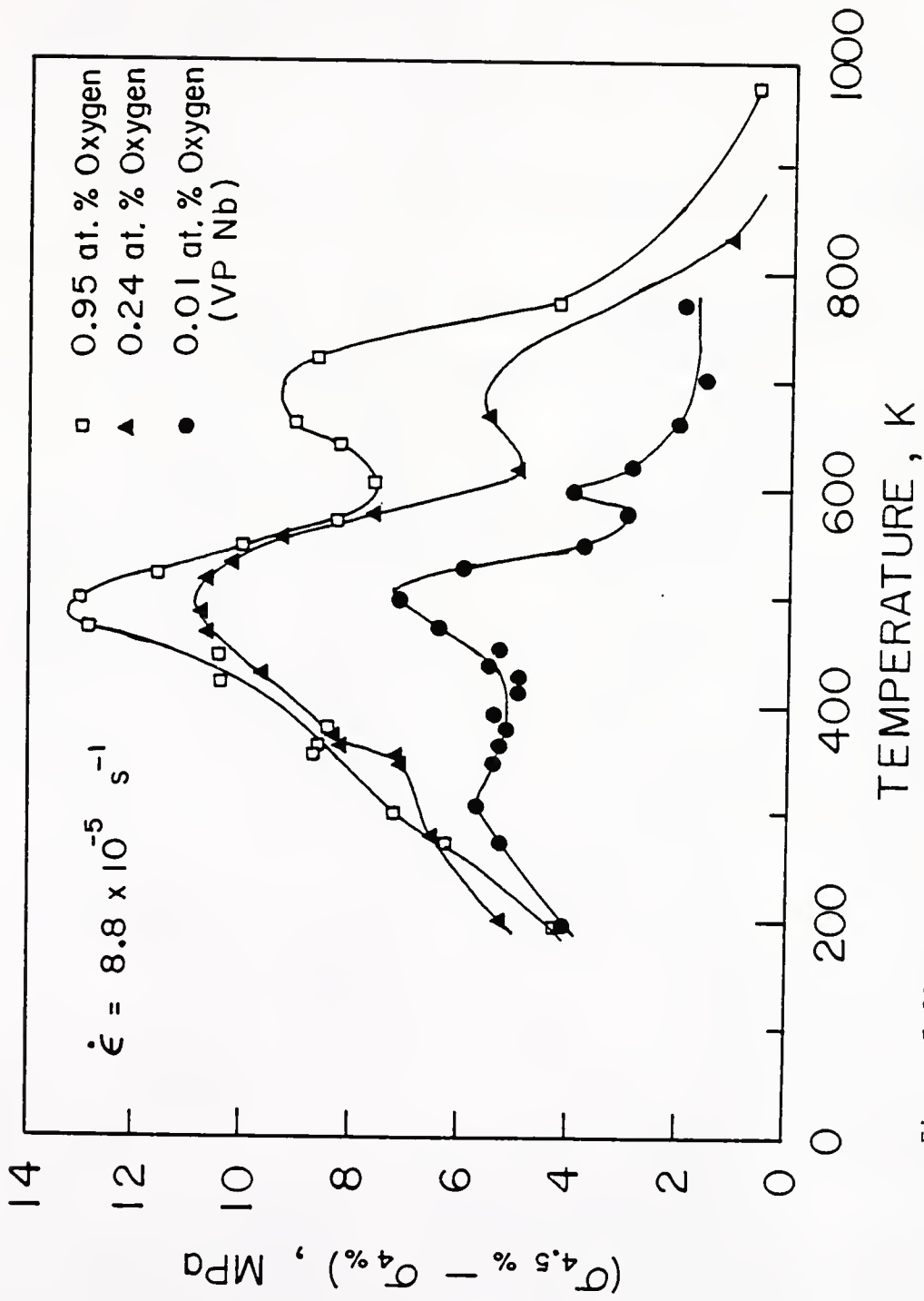


Figure 5.23 The effect of oxygen concentration on the variation of the work hardening as a function of temperature. $\dot{\epsilon} = 8.8 \times 10^{-5} \text{ s}^{-1}$.

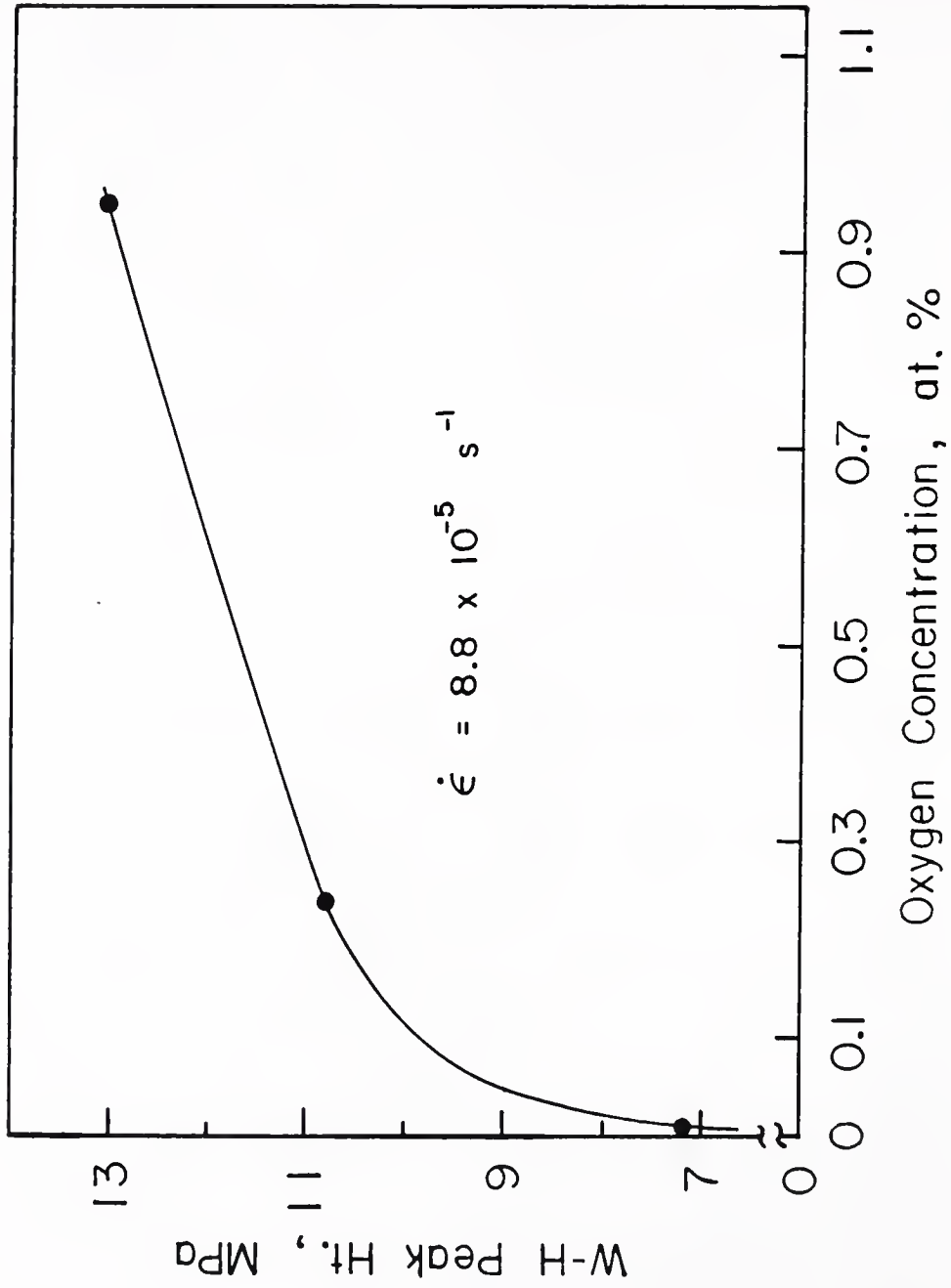


Figure 5.24 Variation of the work hardening peak as a function of the oxygen concentration. $\dot{\epsilon} = 8.8 \times 10^{-5} \text{ s}^{-1}$.

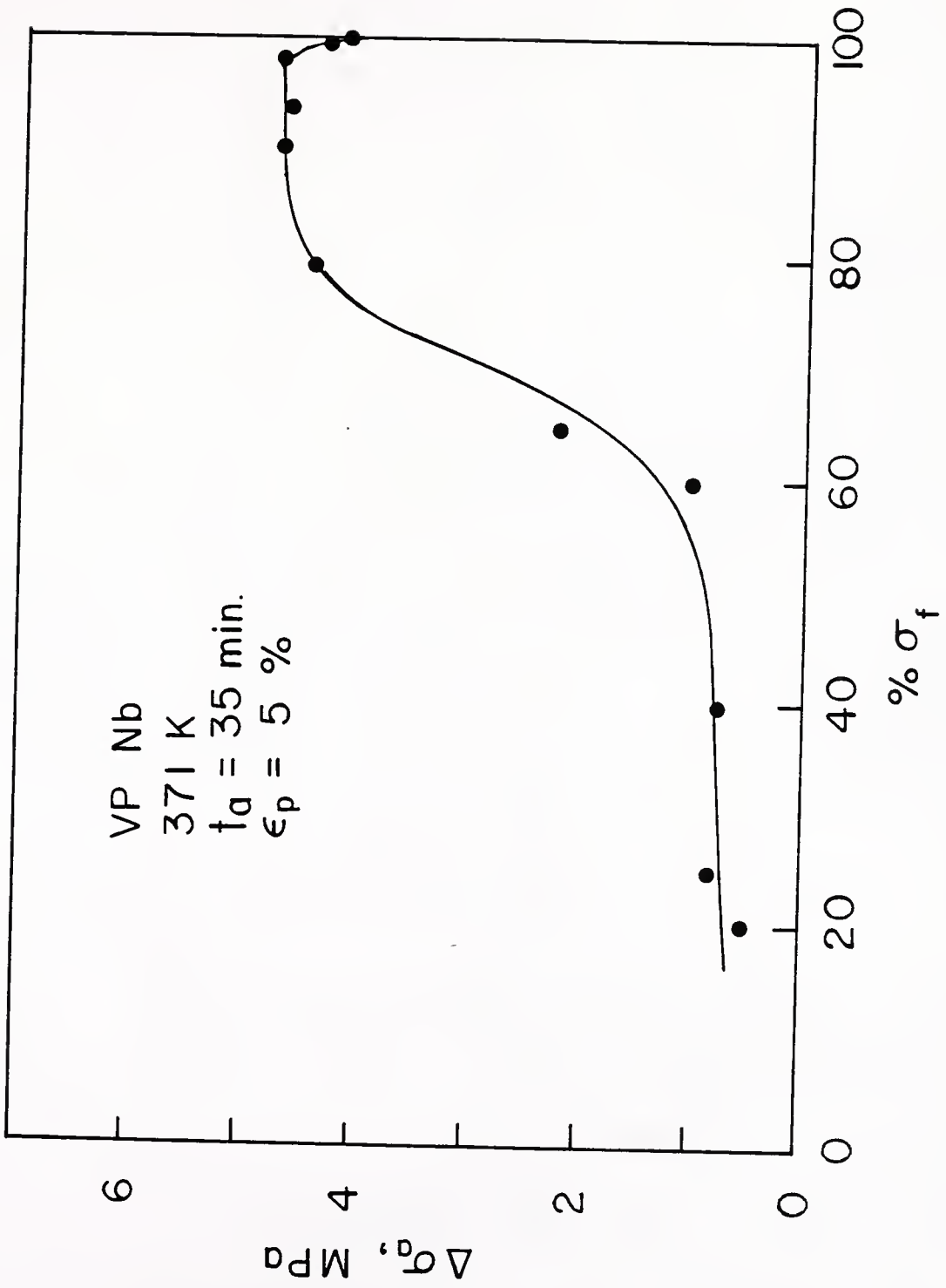


Figure 5.25 The effect of aging stress on the yield point return. VP-Nb aged at 371 K for 35 minutes. $\epsilon_p = 5\%$.

flow stress. As the aging stress increases further up to $80\% \sigma_f$, the magnitude of the yield point return increases sharply. At this aging stress level, the yield point return begins to saturate. In other words, the aging stress above $80\% \sigma_f$ does not have much effect on the magnitude of the yield point return. It stays relatively constant until the aging stress increases to $98\% \sigma_f$. Upon aging at stress levels above $98\% \sigma_f$, the magnitude of the yield point return drops slightly. In summary, increasing aging stress generally increases the size of the yield point return. However, the effect of aging stress is not significant until it reaches a value of above $60\% \sigma_f$. A sharp increase in the yield point return, $\Delta\sigma_a$, was observed when the aging stress level is between 60 and $80\% \sigma_f$. Thus, the $\Delta\sigma_a$ obtained at $80\% \sigma_f$ is approximately 3.5 times greater than that obtained at $60\% \sigma_f$.

Batches of specimens were prestrained to the various amounts of strain and aged at 371 K and $96\% \sigma_f$ for 35 minutes. The results are shown in Figure 5.26. It is found that the magnitude of the yield point return increases gradually as the prestrain increases, reaching a maximum at around $5\% \epsilon$. Further increase in prestrain reduces the size of the yield point return.

5.4.2 Average Strain Rate During Aging Under Stress

The average strain rate produced during an aging period has been measured as a function of an aging stress in a recent investigation in the vanadium-oxygen system [23,33]. They plotted the average strain rate, $\dot{\epsilon}_a$, over 35-minute aging periods as a function of the fraction of

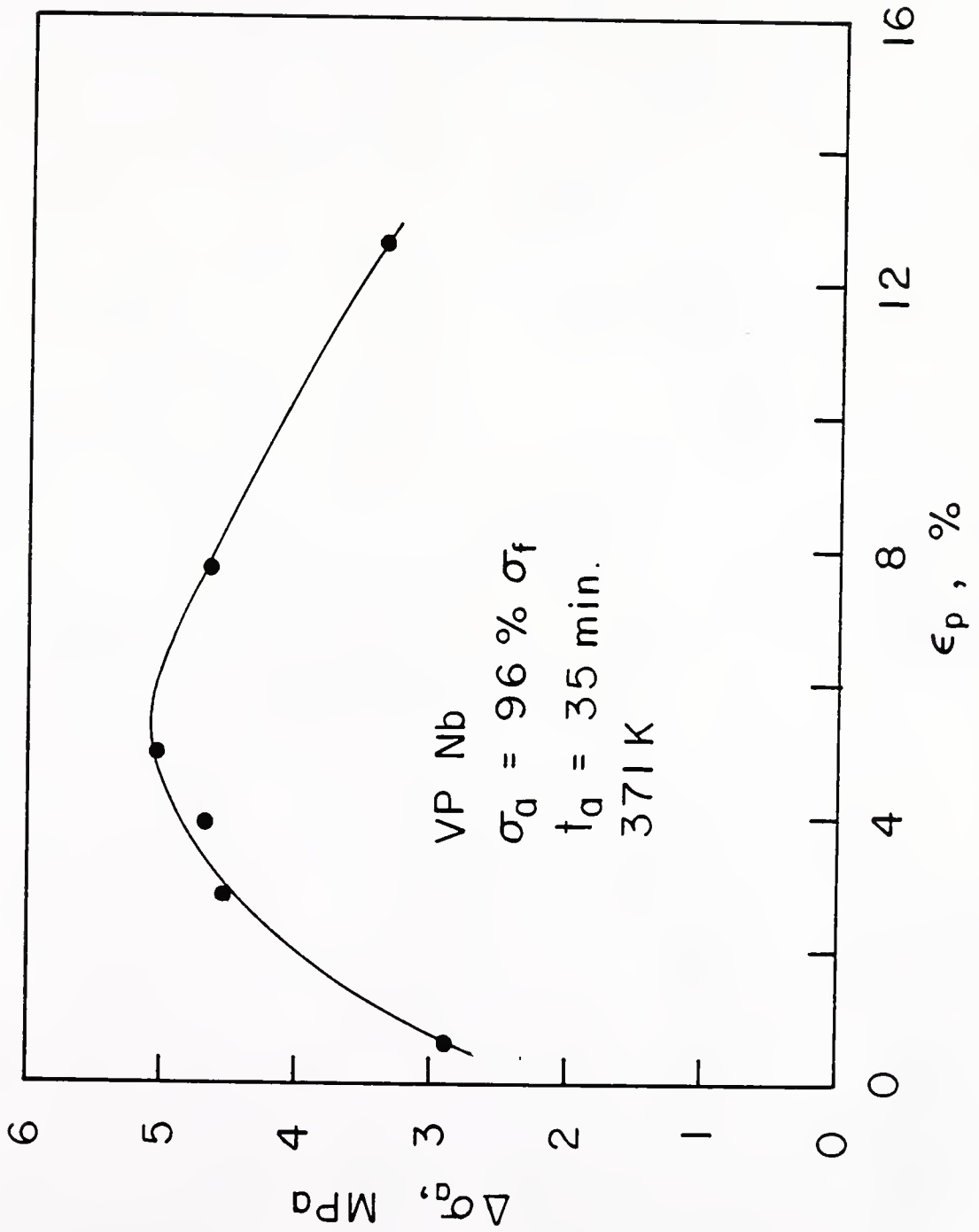


Figure 5.26 Effect of strain on the yield point return. VP-Nb aged at 371 K for 35 minutes. $\sigma_a = 96\% \sigma_f$.

the prestrain flow stress applied during aging. The results obtained at 373 K using a prestrain strain rate of $6.7 \times 10^{-5} \text{ s}^{-1}$ and a prestrain of 9% are reproduced and shown in Figure 5.27. In the same figure, the present data obtained from the VP Nb specimens prestrained to 5% at a rate of $8.8 \times 10^{-5} \text{ s}^{-1}$ at 371 K are shown. Figure 5.27 does show a strong dependence of the average strain rate during aging under stress upon the fraction of the aging stress. A good linear relationship in both V-0 and Nb-0 systems between the logarithm of the aging stress and the logarithm of the average strain rate over a 35- minute aging period is obtained. The results of Figure 5.27 reveal that the size of the average strain rate during aging of Nb-0 is approximately one order of magnitude smaller than that obtained from V-0 specimens [33] during aging under a constant stress. Thus, when the aging stress is $98\% \sigma_f$, the average strain rate over a 35-minute period for V-0 specimens is about as much as $11\% \dot{\epsilon}_p$, while only $1\% \dot{\epsilon}_p$ for Nb-0 specimens, where $\dot{\epsilon}_p$ is the prestrain strain rate.

The values of average aging strain rate considered so far were taken as an average one computed over a certain amount of the aging period. It is found, however, that the estimated strain rate varies with the aging time as can be clearly seen in Figure 5.28. In this figure, the average aging strain rate, $\dot{\epsilon}_{a,ave}$, is plotted against the aging time for two specimens aged at two different stress levels, 98% and $100\% \sigma_f$. Both specimens were strained to 5% at a prestrain rate of $8.8 \times 10^{-5} \text{ s}^{-1}$, which is marked by a solid circle in the figure.

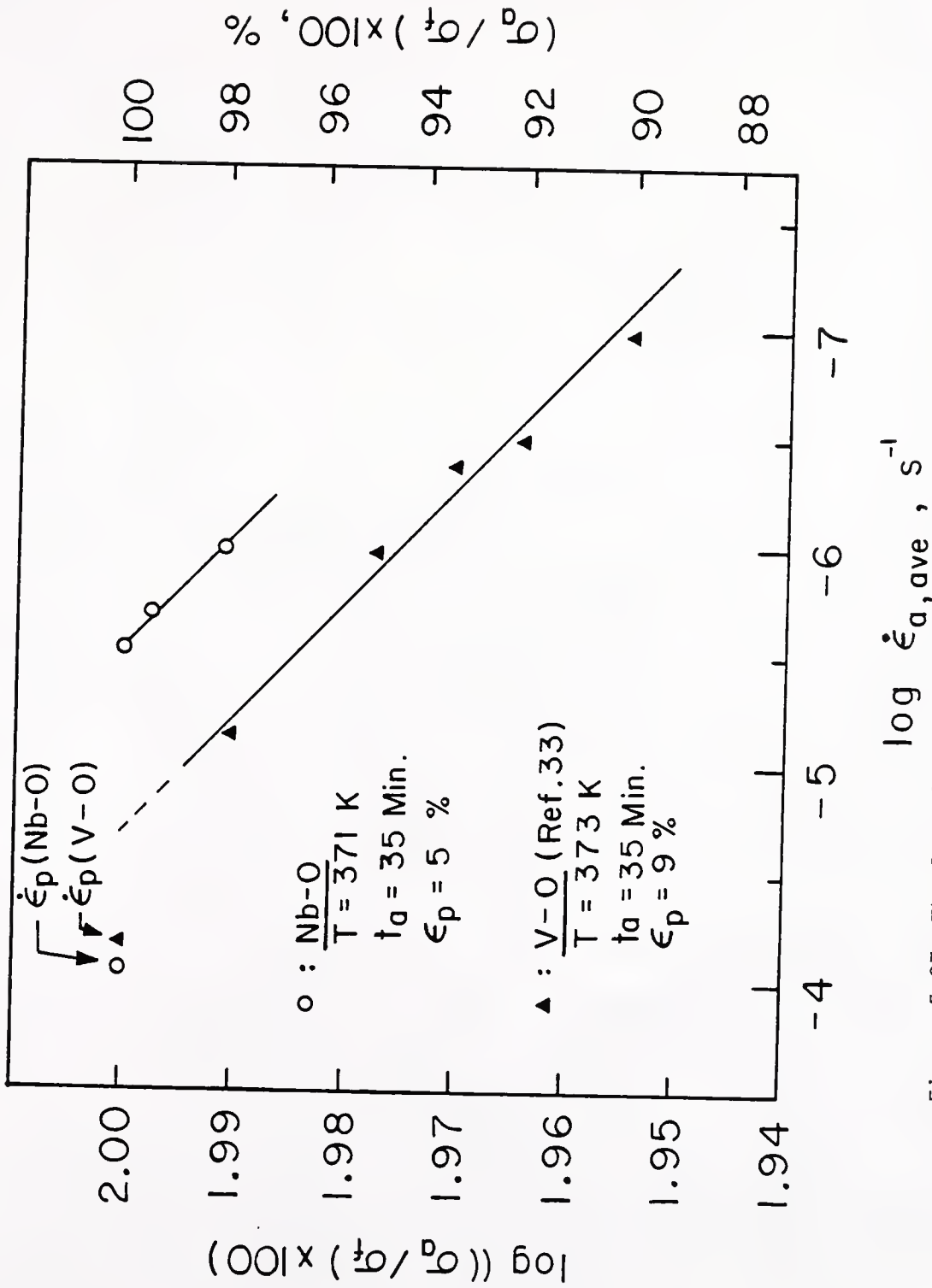


Figure 5.27 The logarithm of the aging stress versus the logarithm of the average strain rate over a 35-minute aging period. VP-Nb aged at 371 K. Data obtained from V-O [33] are also shown.

Figure 5.28 reveals that there is a sharp drop in the average aging strain rate at the very beginning of the aging process, with a larger drop for the specimen aged at 98% σ_f . It is found that the average aging strain rate decreases continuously as aging proceeds. Except for the very beginning of the aging period, the decreasing rate of the average aging strain rate is found to be almost the same for both cases. It is thus generally observed from this figure that the average aging strain rate of the specimen aged at 100% σ_f is usually 3.5 times greater than that obtained from the specimen aged at 98% σ_f . It can also be seen that, for the case of 100% σ_f aging, the average aging strain rate over the first five minutes is only about one order of magnitude slower than the prestrain strain rate.

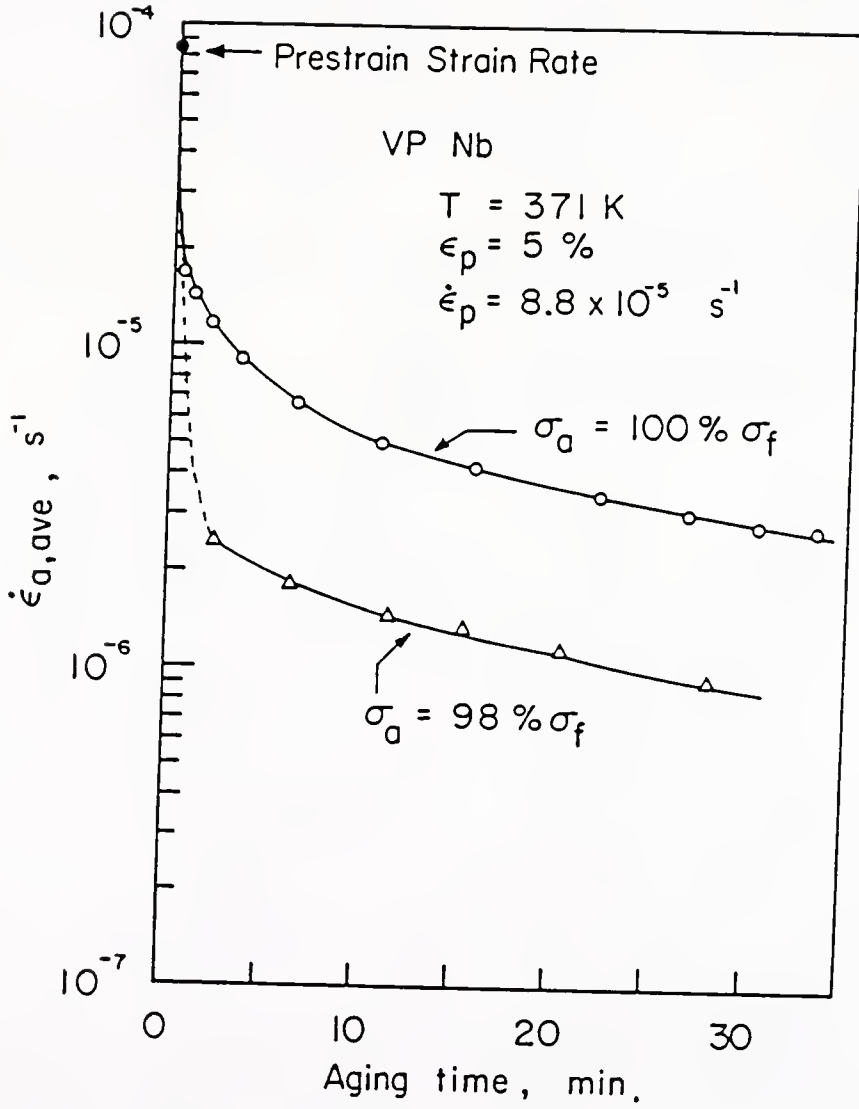


Figure 5.28 Variation of the average aging strain rate with aging time at two aging stresses, 98% and 100% σ_f . $T = 371 \text{ K}$, VP-Nb specimen.

CHAPTER VI DISCUSSION

6.1 Strain Rate Sensitivity of the Flow Stress

6.1.1 Two Strain Rate Sensitivity Minima

The variation of the strain rate sensitivity with the temperature at 4.5% strain for Nb specimens with 0.01, 0.24 and 0.95 at.% oxygen are shown in Figure 5.14. In each case there are two temperature intervals within which the strain rate sensitivity becomes a minimum.

These two SRS minima can be rationalized by the phenomenological model of dynamic strain aging [27-29]. In this model, Reed-Hill assumed that the total flow stress consists of two parts. One is a dynamic strain aging independent part and the other is due to dynamic strain aging. He used a simple power law to represent the stress that is independent of the dynamic strain aging. For the dynamic strain aging component of the flow stress, on the other hand, he used a phenomenological equation proposed by Delobelle, Oytana and Varchon [43]. In the case where dynamic strain aging is due to an interstitial solute atom in a bcc metal, the dynamic strain aging dependent flow stress is assumed to consist of two parts: one due to Snoek reordering and the other due to the formation of the Cottrell atmosphere. These two forms of aging are considered to act independently and thus their effects should be additive. Finally, he obtained an equation for the total stress.

$$\sigma_t = \sigma_E + \sigma_0^* \left(\frac{\dot{\epsilon}}{\dot{\epsilon}_0} \right)^{kT/H^0} + \{ \exp[-\alpha(T-300)] \} \\ \cdot \left\langle \sigma_{S_{\max}}^0 \{ 1 - \exp[-(\frac{t_w}{\tau_S})] \} + \sigma_{C_{\max}}^0 \{ 1 - \exp[-(\frac{t_w}{\tau_C})^{2/3}] \} \right\rangle$$

(2.35) or (6.1)

If equation (6.1) is differentiated with respect to $\ln \dot{\epsilon}$, one obtains an equation for the strain rate sensitivity, S , of the flow stress.

$$\frac{\Delta \sigma}{\Delta \ln \dot{\epsilon}} = S = \frac{\sigma_0^* kT}{H^0} \left(\frac{\dot{\epsilon}}{\dot{\epsilon}_0} \right)^{kT/H^0} - \exp[-\alpha(T-300)] \\ \cdot \{ \sigma_{S_{\max}}^0 \left(\frac{t_w}{\tau_S} \right) \exp[-(\frac{t_w}{\tau_S})] \\ + \frac{2}{3} \sigma_{C_{\max}}^0 \left(\frac{t_w}{\tau_C} \right)^{2/3} \exp[-(\frac{t_w}{\tau_C})^{2/3}] \}$$

(2.36) or (6.2)

The first term on the right hand side represents the strain rate sensitivity in the absence of dynamic strain aging. The second and the third terms represent the contributions of Snoek and Cottrell dynamic strain aging to the total strain rate sensitivity, respectively. Figure 6.1a is a computer plot of the variation of the dynamic strain aging independent part of the strain rate sensitivity as a function of temperature. Figures 6.1b and 6.1c represent the Snoek and Cottrell dynamic strain aging components, respectively. These curves were drawn with the aid of the parameters [80] listed in Table 6.1. The total strain rate sensitivity may be obtained by summing the curves in Figures 6.1a, 6.1b and 6.1c. The result is shown in Figure 6.2. Note that as equation (6.2) indicates, both Snoek and Cottrell strain aging components contribute

TABLE 6.1
VALUES OF PARAMETERS USED IN EQUATION (6.2)

A. Power Law Parameters

$$\dot{\epsilon} = 8.8 \times 10^{-5} \text{ s}^{-1}$$

$$\dot{\epsilon}_0 = 2.14 \times 10^7 \text{ s}^{-1}$$

$$H^0 = 2.48 \times 10^4 \text{ Joules/mole}$$

$$\sigma_0 = 1200 \text{ MPa}$$

$$\sigma_E = 107 \text{ MPa}$$

$$\sigma_0^* = 1093 \text{ MPa}$$

B. Dynamic Strain Aging Parameters

$$\tau_S = 0.25 \tau_\sigma$$

$$\tau_C = 5000 \tau_S = 1250 \tau_\sigma$$

where τ_σ is the jump time of an oxygen atom and where

$$\tau_\sigma = 4.14 \times 10^{-15} \exp\left(\frac{1.095 \times 10^5 \text{ Joule/mole}}{RT}\right)$$

$$\sigma_{S_{\max}}^0 = 24 \text{ MPa}$$

$$\sigma_{C_{\max}}^0 = 34 \text{ MPa}$$

$$t_w = 2.63 \text{ sec}$$

$$\alpha = 2.8 \times 10^{-3} / \text{K}$$

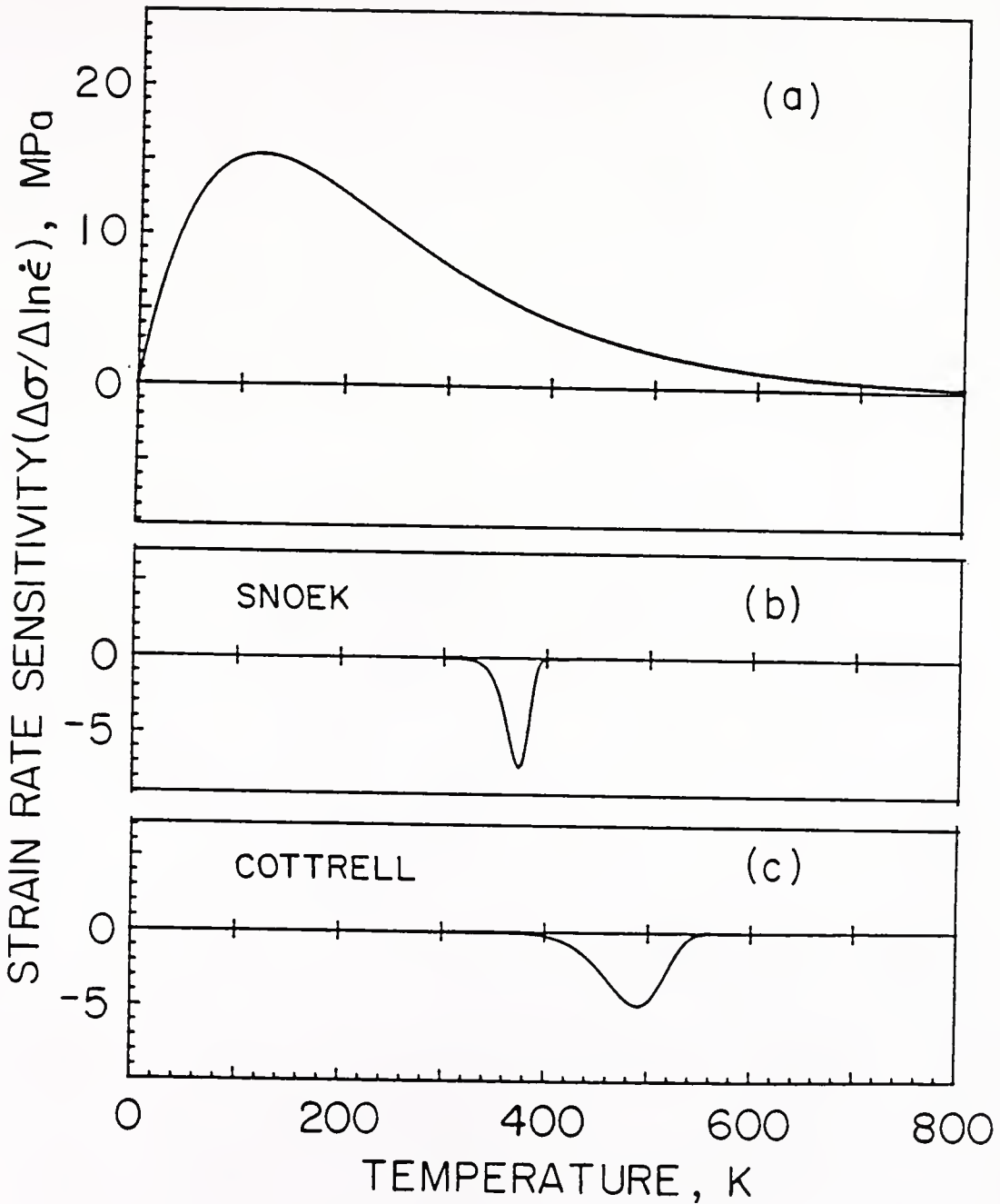


Figure 6.1 The calculated strain rate sensitivity, S , as a function of temperature. a) Curve of S for the dynamic strain aging independent part of the stress. b) Curve of S for Snoek dynamic strain aging. c) Curve of S for Cottrell dynamic strain aging.

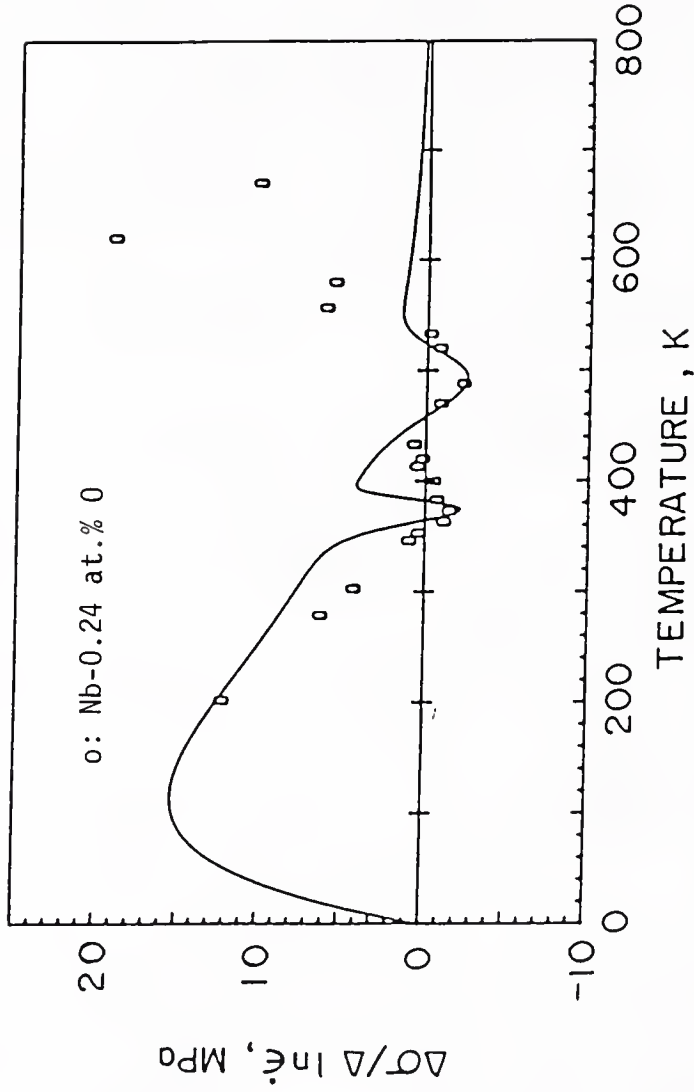


Figure 6.2 The calculated strain rate sensitivity as a function of temperature. Experimental data obtained from Nb-0.24 at.% O₅ specimens are also shown. $\dot{\epsilon}_L = 8.8 \times 10^{-5} \text{ s}^{-1}$, $\dot{\epsilon}_H = 4.4 \times 10^{-4} \text{ s}^{-1}$.

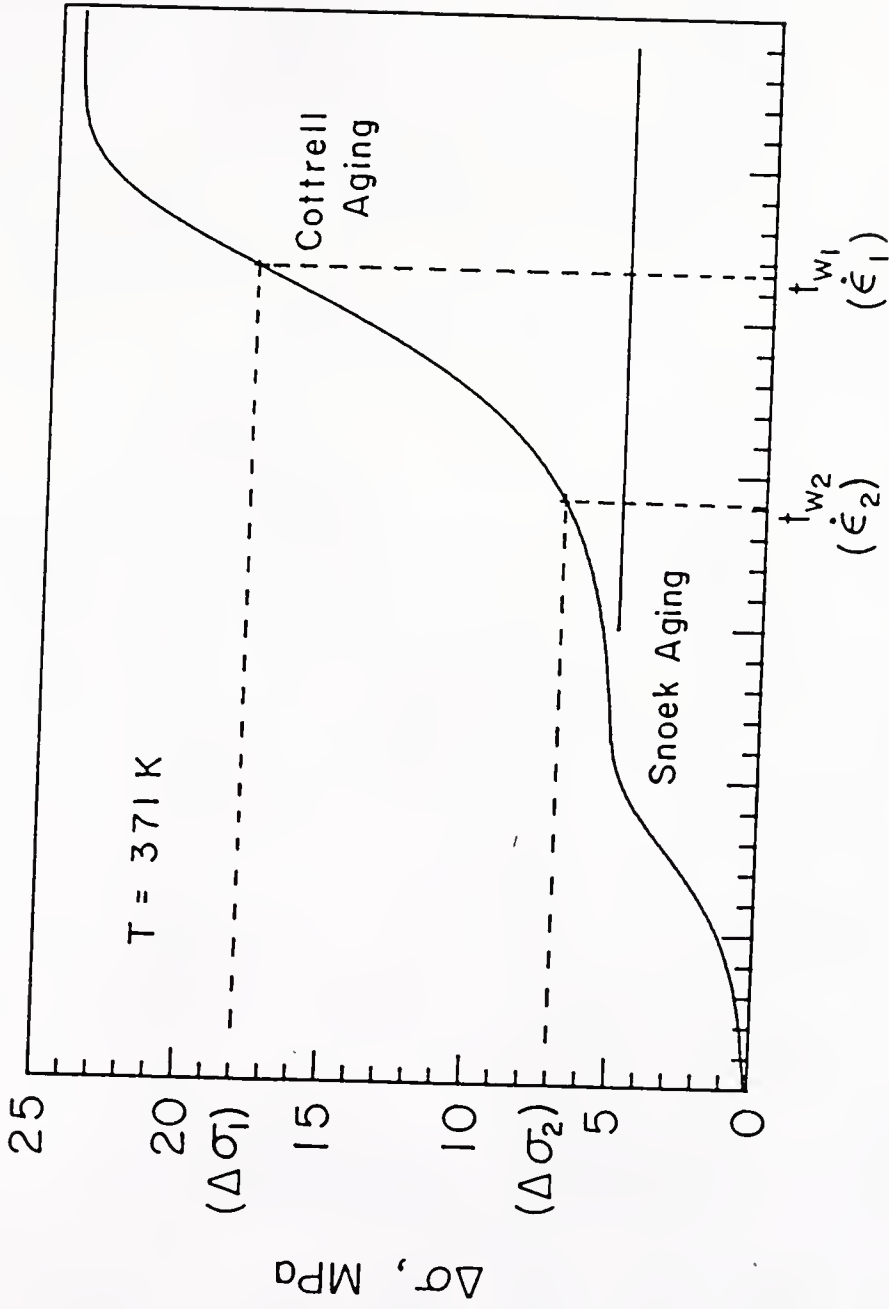
negatively to the total strain rate sensitivity. It is clearly seen from Figure 6.2 that there exist two strain rate sensitivity minima and that the minima are due to dynamic strain aging. The dynamic strain aging dependent parts and the dynamic strain aging independent part of the strain rate sensitivity are thus competitive with each other at each temperature. If the former is greater than the latter, a negative total strain rate sensitivity results. If the former is less than the latter, on the other hand, a positive strain rate sensitivity is expected at the minimum. The strain rate sensitivity data obtained with the 0.24 at.% oxygen specimens are also shown in Figure 6.2. An examination of Figure 6.2 shows that the analytical approach is able to predict the two observed regions of negative strain rate sensitivity. Above 550 K, the phenomenological theory is in serious disagreement with the observed strain rate sensitivity measurements except at very low oxygen concentration. It is now proposed that the high temperature SRS peak is associated with the motion of dislocations impeded by the dragging of solute atmospheres. This will be discussed further in section 6.1.2.

The negative contribution of strain aging to the strain rate sensitivity can be rationalized [44] by considering the magnitudes of the dynamic strain aging stress at two different strain rates. Based on Sleswyk's hypothesis [31], Reed-Hill [44] demonstrated very recently that the amount of the strain aging during the prestrain is a function of the time that dislocations wait at the obstacles, and the mobility of the solute, i.e.,

$$\Delta\sigma(t_w) = \exp[-\alpha(T-300)] \left\langle \Delta\sigma_{S_{\max}}^0 \left\{1 - \exp\left[-\left(\frac{t_w}{\tau_S}\right)\right]\right\} + \Delta\sigma_{C_{\max}}^0 \left\{1 - \exp\left[-\left(\frac{t_w}{\tau_C}\right)^{2/3}\right]\right\} \right\rangle \quad (6.3)$$

where $\Delta\sigma(t_w)$ is the amount of strain aging during the prestrain and t_w is the waiting time of the dislocations at the obstacles during the prestrain. Figure 6.3 is a computer plot for the strain aging stress component as a function of the waiting time for a bcc metal containing an interstitial in solid solution. Let us assume that t_{w1} and t_{w2} are the average waiting times corresponding to two different strain rates, $\dot{\epsilon}_1$ and $\dot{\epsilon}_2$, respectively, where $\dot{\epsilon}_2 > \dot{\epsilon}_1$. The corresponding flow stress increments due to the strain rates, $\dot{\epsilon}_1$ (or t_{w1}) and $\dot{\epsilon}_2$ (or t_{w2}) are designated as $\Delta\sigma_1$ and $\Delta\sigma_2$. It may be seen from the figure that the flow stress increment for the higher strain rate is smaller than that for the slower strain rate, i.e., $\Delta\sigma_2 < \Delta\sigma_1$. In other words, at a temperature range where dynamic strain aging is important, an increase in the strain rate yields the smaller flow stress increment, possibly resulting in a negative strain rate sensitivity.

6.1.1.1 Effect of Oxygen Concentration. As may be seen in Figure 5.14, the effect of the oxygen concentration on the strain rate sensitivity minima are twofold. First, the negative nature of the Snoek minimum becomes more pronounced as the oxygen concentration increases. The second involves the curve shifting towards lower temperature with increasing oxygen concentration. Each effect will now be briefly discussed.



WAITING TIME

Figure 6.3 A plot of the strain aging kinetics curve showing the effect of the prestrain rate (or waiting time) on the magnitude of the dynamic strain aging stress.

(i) Negativity of the Snoek Minimum. The strain rate sensitivities of the 0.95 at.% oxygen specimens exhibit large negative values in the Snoek whereas the corresponding values of the VP Nb specimens (0.01 at.% O) remain positive over this whole temperature range. It is generally observed in the present experiment that a negative strain rate sensitivity is necessary for serrated flow on a stress-strain curve. The more negative the strain rate sensitivity, the more pronounced are the serrations. In the VP Nb specimens, no detectable serrations were observed even at the minimum value of the strain rate sensitivity. With increasing oxygen concentrations the strain rate sensitivity becomes more negative and the serrations become more pronounced. This is consistent with Bradford and Carlson's observations on the V-O system in which a higher oxygen concentration is needed for the low temperature serrations. It can thus be concluded that a higher oxygen concentration is necessary to get the maximum Snoek effect: the degree of the locking of a dislocation due to the Snoek effect depends strongly on the interstitial solute atom concentration. There is evidently a critical concentration above which the dislocation locking is so effective that the strain rate sensitivity becomes sufficiently negative to cause serrations.

At the higher temperature minimum, on the other hand, the strain rate sensitivity is apparently negative to about the same degree at all three concentrations. This suggests that once a Cottrell atmosphere is formed by a certain number of interstitial solute atoms, the rest of them do not contribute significantly to this component of the stress.

(ii) The shift of the SRS versus T curve. Increasing the oxygen concentration causes the SRS curve to move to lower temperatures. The curve shift may be most clearly seen at the Cottrell minimum temperature region. The temperatures where $(\Delta\sigma/\Delta\ln\dot{\epsilon})$ becomes zero at the higher temperature region are approximately 545, 530 and 510 K for the specimens containing 0.01, 0.24 and 0.95 at.% oxygen, respectively. In other words, about a 35 K shift is observed upon increasing the oxygen from 0.01 to 0.95 atomic percent.

The question is why does an increasing oxygen concentration shift the SRS curve towards lower temperature. A qualitative explanation may be made by comparing the strain aging kinetic curves of specimens containing different concentrations of interstitials. Szkopiak [81] reported several strain aging kinetic curves obtained at a temperature of 155 C for Nb specimens containing various amounts of oxygen ranging from 200 to 700 ppm. It was found that an increasing oxygen concentration causes saturation to occur at shorter times. This implies that the effective relaxation time associated with the strain aging decreases as the oxygen concentration increases. The relaxation time for each composition was estimated from its respective curve. They were approximately 2660 s, 1472 s and 1030 s for the specimens containing 200 ppm, 400 ppm and 700 ppm, respectively. This indicates that the effective relaxation time for the aging kinetics is a strong function of oxygen concentration.

It was decided to examine the effect of the relaxation time on the strain rate sensitivity versus temperature curve using the phenomenological equation. Figure 6.4 is a computer plot of the strain rate sensitivity

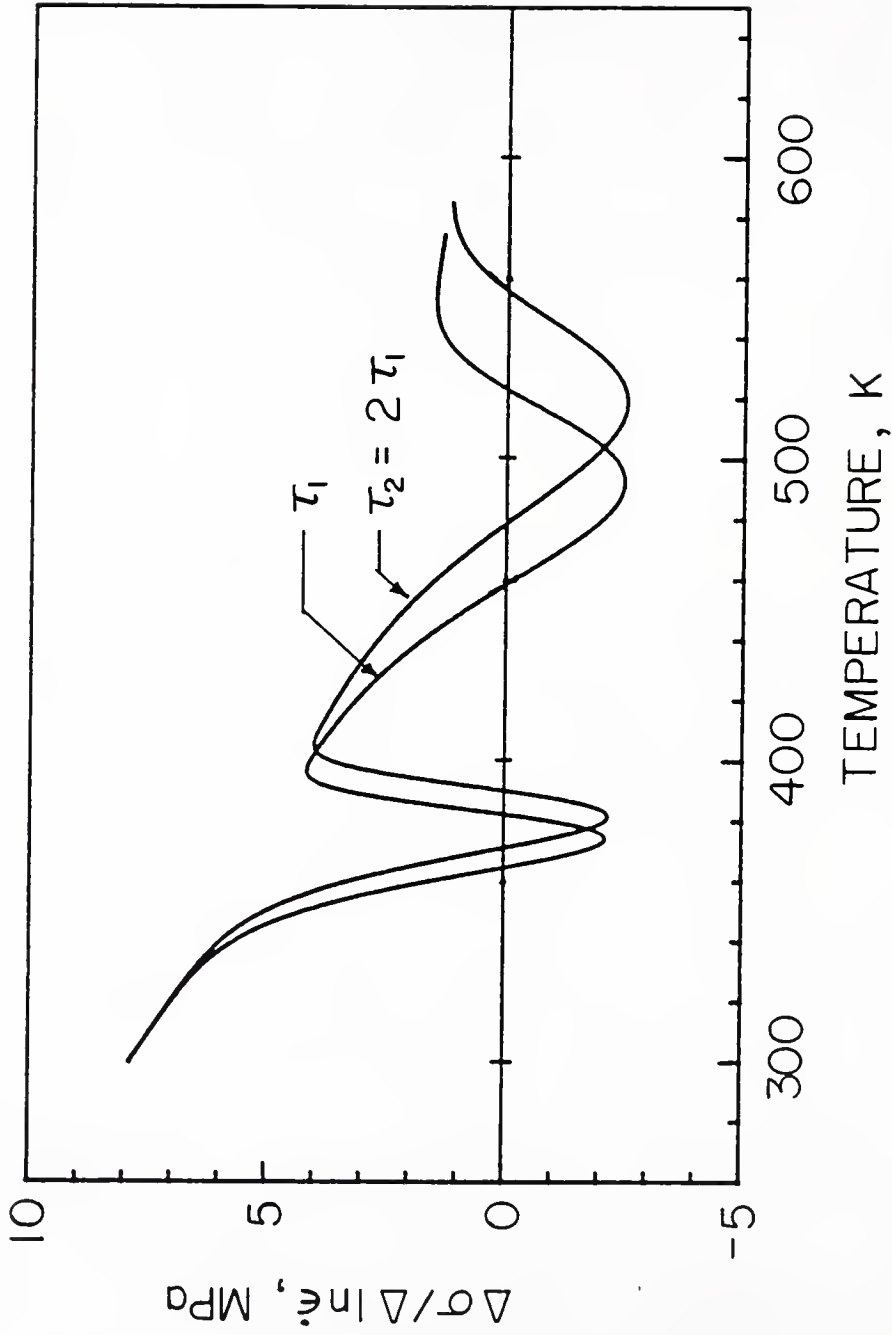


Figure 6.4 Analytical curves of strain rate sensitivity versus temperature for two relaxation times. $\tau_2 = 2\tau_1$.

versus temperature for two different relaxation times differing by a factor of two. As the figure shows, increasing the relaxation time or decreasing the oxygen concentration shifts the SRS versus T curve towards higher temperatures, which conforms to the experimental observations. It should also be noted from Figure 6.4 that the shift is larger the higher the temperature. This also agrees well with the experimental observations, as shown in Figure 5.14. From the above, it is suggested that the shifting of the entire strain rate sensitivity versus temperature curve with oxygen concentration can be explained by a difference in relaxation time. Although Figure 6.4 gives a qualitative explanation, more work is required to rationalize the dependence of the oxygen concentration on the relaxation time quantitatively. To do this, one needs to obtain aging under stress kinetic curves at several temperatures using various concentrations of interstitial solute atoms.

6.1.1.2 Effect of Base Strain Rate

The effect of the base strain rate on the plot of the strain rate sensitivity versus temperature is shown in Figures 5.15 and 5.16. It is generally seen from these figures that the curves shift to higher temperatures as the base strain rate increases. The phenomenological theory can be used to rationalize the curve shifting with base strain rate. An increase in base strain rate by five times is equivalent to a five times decrease in the waiting time using the relation, $t_w \propto \frac{1}{\dot{\epsilon}}$, if other material constants are assumed unchanged. Figure 6.5 is a computer plot showing the strain rate dependence of the SRS versus T curve. Data listed in

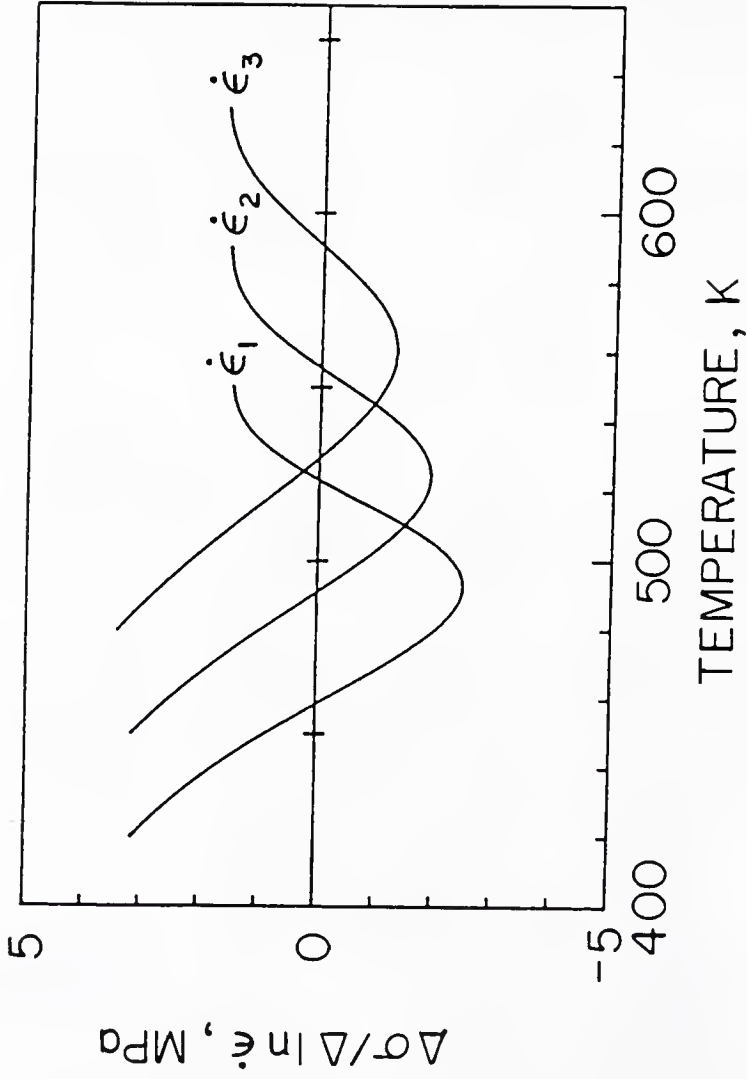


Figure 6.5 Analytical curves of strain rate sensitivity versus temperature for three base strain rates. $\dot{\epsilon}_1 = 8.8 \times 10^{-5} \text{ s}^{-1}$, $\dot{\epsilon}_2 = 5 \dot{\epsilon}_1$, $\dot{\epsilon}_3 = 25 \dot{\epsilon}_1$.

Table 6.1 were also used in this figure. The waiting time, t_w , corresponding to the curve marked by $\dot{\epsilon}_1$ was found to be 2.63 sec, which was determined by the best fit of the experimental results. The other two curves marked by $\dot{\epsilon}_2$ and $\dot{\epsilon}_3$ were obtained by decreasing the waiting time five and 25 times, respectively, corresponding to two different strain rates, $\dot{\epsilon}_2 = 5 \dot{\epsilon}_1$ and $\dot{\epsilon}_3 = 25 \dot{\epsilon}_1$. Figure 6.5 cannot be directly compared with Figure 5.15 because Figure 6.5 was drawn using the data for Nb-0.24 at.% oxygen specimens. Nevertheless, it is still possible to see the temperature shift due to a change of the base strain rate. The estimated temperature shifts from Figure 6.5 are about 30K and 65 K, which are close to those in the experimental results. It should be noted that the phenomenological theory also predicts a decreasing negativity of strain rate sensitivity with increasing base strain rate.

It is felt that, since the Snoek and Cottrell minima are due to strain aging of the interstitial solute atoms, these minima are associated with the thermal activation of the interstitial atoms. Figure 6.6 is the plot of the logarithm of the applied strain rate against $\frac{1}{T}$ for the Snoek and Cottrell minima. The apparent activation energies were estimated from the slope of each line. The estimated activation energies for the Snoek and Cottrell minima are about 26.8 Kcal/mole and 29.5 Kcal/mole, respectively. Although the values for Cottrell minima seem a little high, those two values are in reasonable agreement with the activation energy for the diffusion of oxygen in niobium.

6.1.1.3 Effect of Prestrain. The effect of the magnitude of the prestrain on the strain rate sensitivity is visible in Figure 5.19,

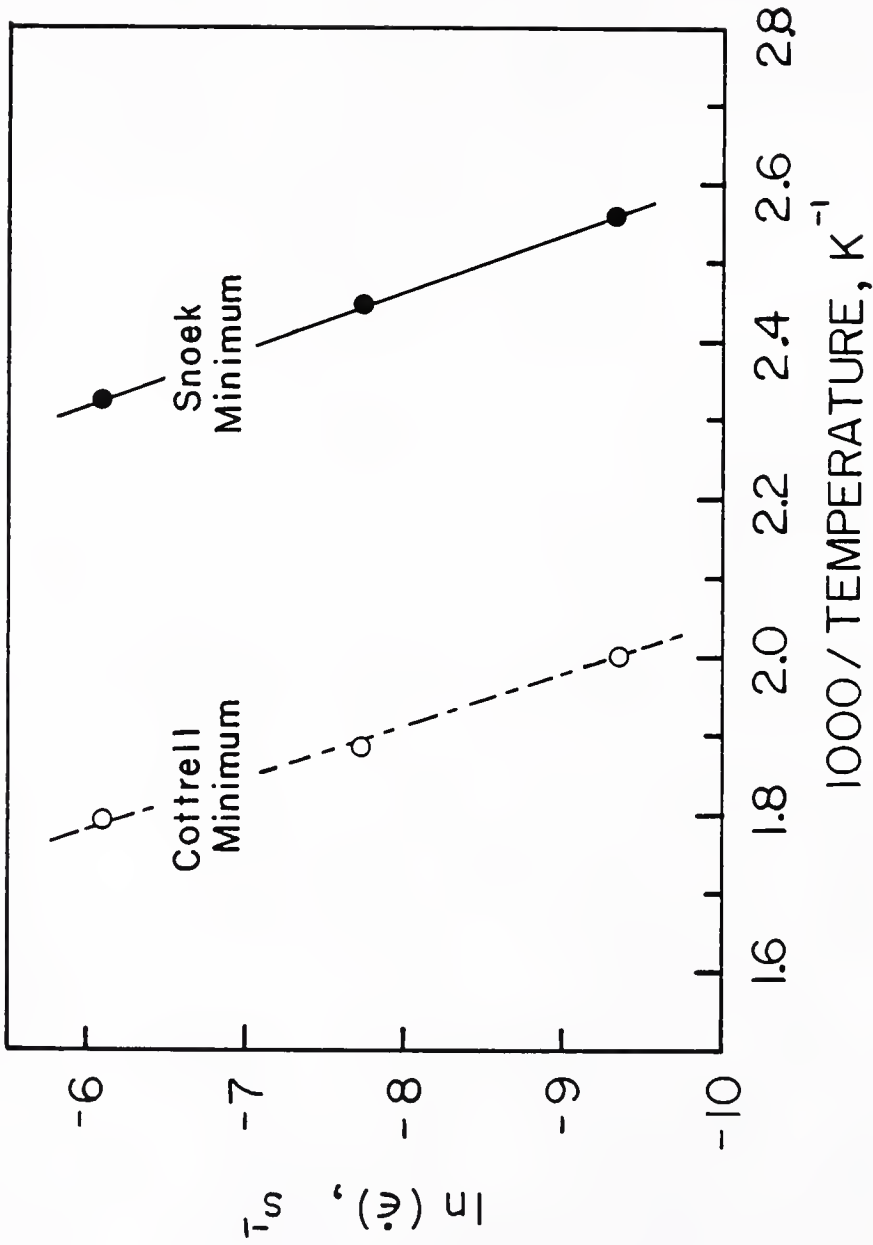


Figure 6.6 Logarithms of the strain rate as a function of the reciprocal temperature corresponding to the Snoek SRS minimum and the Cottrell SRS minimum.

which shows that the SRS versus T curve is shifted towards larger temperatures as the prestrain increases. It is believed that this strain dependence of the strain rate sensitivity comes primarily from an increase in the mobile dislocation density ρ_m with strain. This in turn affects the waiting time as follows: if it is assumed that $\rho_m = N\epsilon^\beta$, where N and β are constants, and the Orowan equation holds, then it follows [37] that

$$t_w = \frac{\phi N \epsilon^\beta b L}{\dot{\epsilon}} \quad (6.4)$$

where ϕ is a Schmid orientation factor, L is the effective obstacle spacing and b the Burgers vector. Thus, at constant strain rate, $\dot{\epsilon}$, t_w should vary directly as ϵ^β . The value of β was estimated to be 1.2 [44]. Here again the phenomenological equation for the strain rate sensitivity was used along with the parameters in Table 6.1. The waiting time was evaluated using the expression, $t_w = 2.63 (\epsilon/4.5)^\beta$. Figure 6.7 is a computer plot of the strain rate sensitivity versus temperature for three different strains, 1%, 2.5% and 4.5%. As the figure shows, an increasing strain shifts the SRS versus T curve towards lower temperature, which conforms to the experimental observation.

The effect of the strain on the appearance of the serrations is expected to be largely dependent on the temperature. At the lower temperature side of the Cottrell minimum in Figure 5.19, as an example, the strain rate sensitivity changes its sign from positive to negative as the deformation increases. This implies that the serrations should become more significant as the strain increases. However, this behavior is expected to be reversed at the high temperature side of the Cottrell minimum. Here, it is expected that the serrations will become less pronounced as deformation

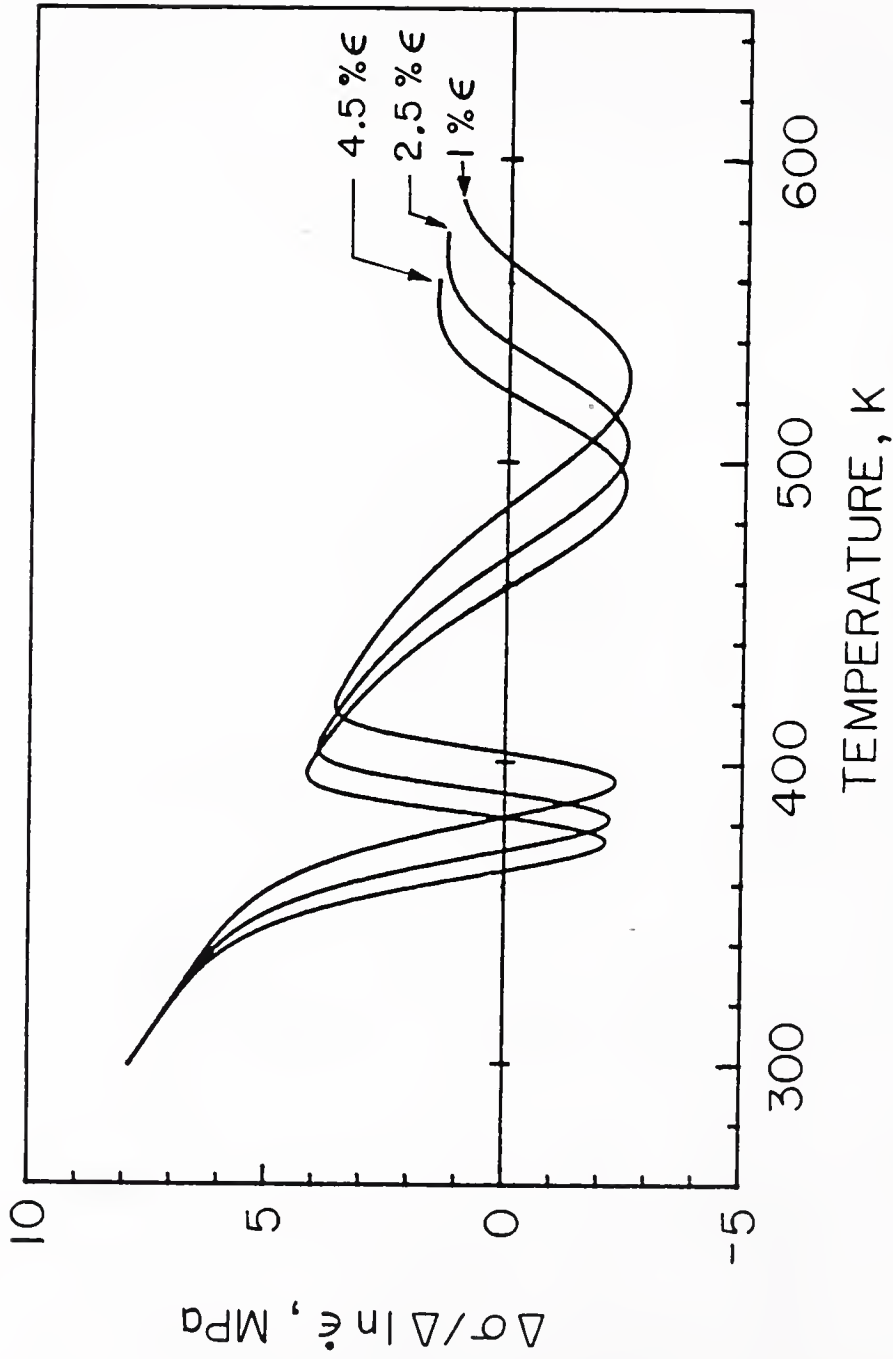


Figure 6.7 Analytical curves of strain rate sensitivity versus temperature at three prestrains between 1% and 4.5%. The values of t_w at the various strains were determined by the equation $t_w = 2.63(\epsilon/4.5)\beta$ with β equal to 1.2.

proceeds. The strain rate sensitivity was measured at three different temperatures, 395, 425 and 600 K as a function of the strain. These temperatures were selected from Figure 5.19 because the dependence of the strain rate sensitivity on the strain at 395 K and 425 K was expected to be reversed. The 600 K temperature was chosen to see if there was a big change in the strain rate sensitivity as the strain increases, as might be predicted from Figure 5.19. The results are given in Figure 6.8. As expected, at 395 K, the SRS initially decreases as the strain increases, although the change is small. The strain rate sensitivity continues to decrease until the strain reaches about 4.5 ~ 5%, beyond which it remains almost constant. On the other hand, at 425 K, the opposite dependence of the strain on the strain rate sensitivity is observed; i.e., the SRS increases initially as the deformation increases and stays constant with further deformation. Finally at 600 K, the strain rate sensitivity grows rapidly with an increasing strain, as expected from Figure 5.19. Note that the SRS becomes nearly strain independent when the strain exceeds about 5%.

6.1.1.4 Comments on the Relationship Between Serrations and SRS

It is generally agreed [24-26] that a negative strain rate sensitivity is a necessary but not a sufficient condition for the onset of serrations. The purpose of this section is to provide information on how the strain rate sensitivity data is related to the serrations. For this purpose, a concept of "quasi-single strain rate" for a SRS versus T curve will be here introduced. If a rate change is made between two strain rates which are very close to each other, one would have a SRS versus T curve like that marked $\dot{\epsilon}_1$ in Figure 6.9a. Assume that the curve $\dot{\epsilon}_1$ is obtained by

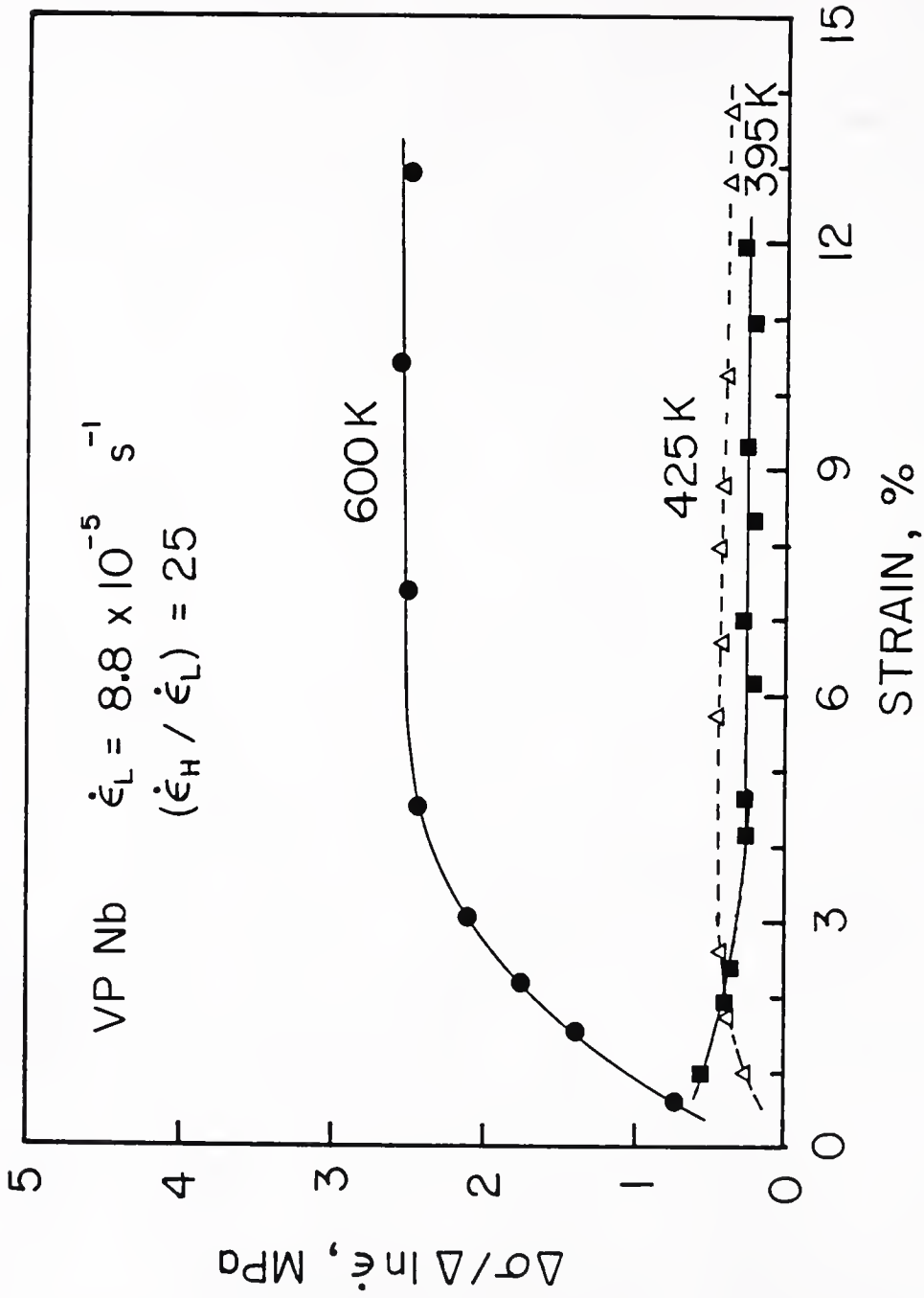


Figure 6.8 Variation of the strain rate sensitivity with strain for three temperatures, 395 K, 425 K and 600 K. $\dot{\epsilon}_L = 8.8 \times 10^{-5} \text{ s}^{-1}$, $(\dot{\epsilon}_H / \dot{\epsilon}_L) = 25$. VP-Nb specimens.

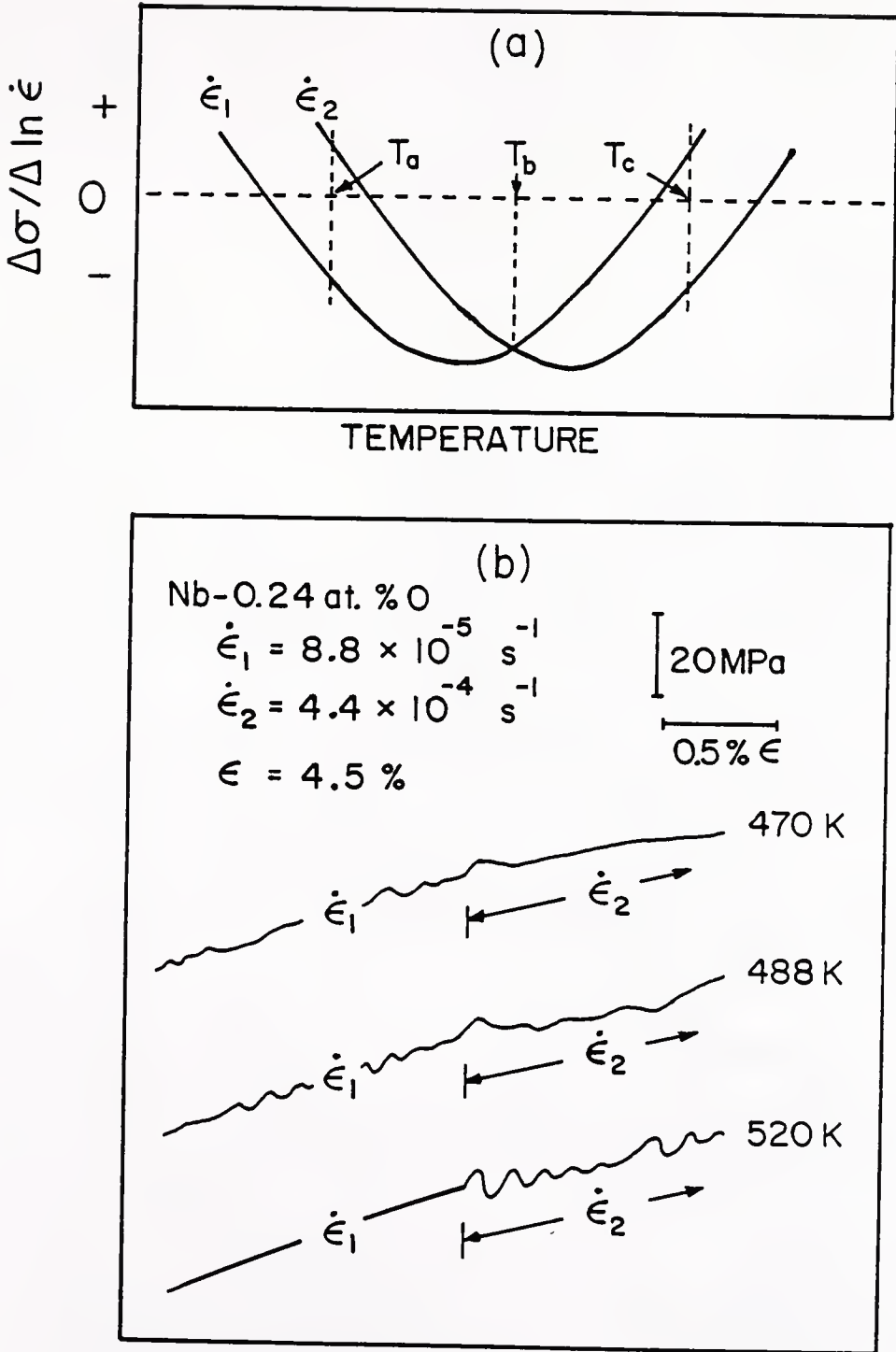


Figure 6.9 a) A schematic diagram showing the effect of two base strain rates on the SRS versus temperature relation. This diagram may predict the variation of the stress-strain curve at two strain rates. b) Variation of the stress-strain curves at two strain rates. $T = 470 \text{ K}$, 488 K and 520 K . Nb-0.24 at.% O.

changing the strain rate from $\dot{\epsilon}_1$ to $\dot{\epsilon}_{1a}$, where $\dot{\epsilon}_1 \approx \dot{\epsilon}_{1a}$. If another curve is obtained at a higher strain rate by changing $\dot{\epsilon}_2$ to $\dot{\epsilon}_{2a}$, then one should get another SRS versus T curve marked $\dot{\epsilon}_2$ in Figure 6.9a. Note that Figure 6.9a shows only the Cottrell minimum region. From the figure and the experimental observations that the negative SRS is a necessary condition for the onset of serrations, the following qualitative predictions can be made concerning the effect of a strain rate change from $\dot{\epsilon}_1$ to $\dot{\epsilon}_2$ on the occurrence of serrations.

- 1) At T_a , the serrations will disappear after increasing the strain rate,
- 2) at T_b , the serrations will occur at both strain rates, and
- 3) at T_c , the serrations will only appear after increasing the strain rate.

Although at $\dot{\epsilon}_1$ the SRS is negative at T_a , at the higher strain rate, $\dot{\epsilon}_2$, S is positive so that no serrations should appear. The reversed behavior is expected at T_c ; at $\dot{\epsilon}_1$ there should be no serrations, however, upon changing the strain rate to $\dot{\epsilon}_2$, the serrations are expected to appear.

Some results from the Nb-0.24 at.% O specimens were used in order to test the above predictions. Temperatures of 470 K, 488 K and 520 K were chosen from Figure 5.10 because they are close to T_a , T_b and T_c , respectively. The flow curves at two strain rates obtained at the three temperatures are shown in Figure 6.9b. All of these curves are in good agreement with the prediction, although in the 470K test, the flow curve at the higher strain rate is not perfectly smooth, which seems to be contrary to the prediction. However, this is considered to be due to the unstable plastic deformation that the material was experiencing before the strain rate change.

6.1.2 Strain Rate Sensitivity Peak Above the Cottrell SRS Minimum Temperature

The experimental results in Figure 5.14 show a sharp peak of the SRS above the upper limit of Cottrell dynamic strain aging. This peak cannot be explained by the phenomenological theory. This type of high temperature SRS peak has also been observed in other alloy systems, i.e., Cu-3.1% Sn [29], Ti-0 [82] and steel [83]. Thus, the high temperature SRS peak appears to be a common phenomenon that can appear in all three of the basic crystal structures; fcc, hcp and bcc.

A strong effect of oxygen concentration on the magnitude of the peak is visible in Figure 5.14. Figure 6.10 is another plot of the SRS as a function of oxygen concentration at 600 K. In this plot, results from Marz Nb (0.008 at.% O) and WC Nb (0.07 at.% O) are also included. The figure shows that the peak height increases rapidly with increasing oxygen concentration.

The peak temperature is apparently independent of the oxygen concentration. The peak appears at about 600 K when the base strain rate of $8.8 \times 10^{-5} \text{ s}^{-1}$ and the 5:1 strain rate change are used. The peak temperature, however, does move to higher temperatures with an increase in either the base strain rate or the magnitude of the strain rate change. The variation of the peak temperature with the base strain rate in VP Nb specimens is seen in Figure 5.15. The estimated peak temperatures are approximately 590 K, 625 K and 675 K for the base strain rates of $8.8 \times 10^{-5} \text{ s}^{-1}$, $4.4 \times 10^{-4} \text{ s}^{-1}$, and $2.2 \times 10^{-3} \text{ s}^{-1}$, respectively. An Arrhenius estimation of the activation energy for the peaks gave 29 Kcal/mole which is close to that for the diffusion of oxygen in niobium. This

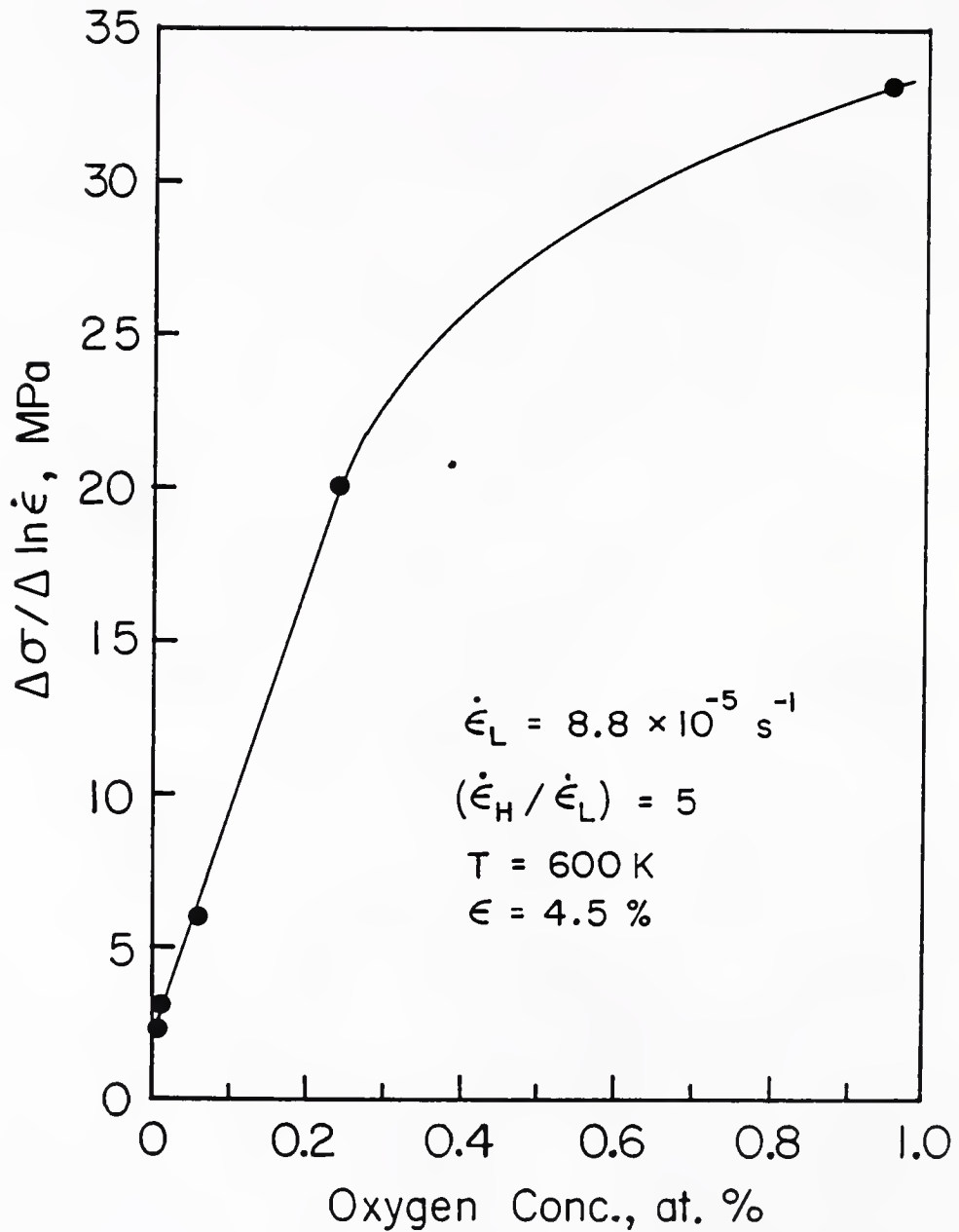


Figure 6.10 The effect of oxygen concentration on the strain rate sensitivity peak at 600 K. $\dot{\epsilon}_L = 8.8 \times 10^{-5} \text{ s}^{-1}$, $(\dot{\epsilon}_H / \dot{\epsilon}_L) = 5$.

strongly suggests that this SRS peak in Nb is associated with the presence of oxygen in solid solution.

Reed-Hill [84] proposed that the high temperature SRS peak may be associated with dislocation dragging with solute atmospheres based on the following experimental observations.

- 1) The SRS peak appears at about 100° or more above the upper limit of the Cottrell dynamic strain aging.
- 2) The apparent activation energy associated with this peak is close to that for the diffusion of the solute.
- 3) The peak height is a strong function of the solute concentration.

Basically, the phenomenological model assumes that the solute is mobile enough to pin the dislocations as they wait for thermal activation in the temperature range where dynamic strain aging is significant. However, if the temperature is high enough, then the solute is mobile enough to interfere with dislocations as they move from one obstacle to the next. In the previous theory of negative SRS behavior based on Snoek and Cottrell breakaway phenomena, the dislocation drag effects were ignored by setting $t_w \gg t_f$, where t_w is the waiting time of the dislocation at an obstacle and t_f is the flight time between subsequent obstacles. However, if the temperature is high enough, then the dislocations may be dragged with solute atmospheres, and the assumption that $t_w \gg t_f$ may no longer hold. Under these circumstances, a stress due to dragging becomes important. Thus, it is suggested [84] that the effect of drag has to be considered in computing the total flow stress. It is also believed [85] that the temperature where DSA is rate controlling is lower than that where dislocation drag is rate controlling. Actually the two mechanisms are

believed to be essentially two different aspects of a common phenomenon; namely the interaction of dislocation and mobile solute atoms. It is possible that these two effects can be treated together. However, for the present it is perhaps better to treat them as separate phenomena and consider that DSA controls at lower temperatures. The effect of the drag stress on the strain rate sensitivity, assuming that above the Cottrell SRS minimum drag becomes rate controlling, will now be briefly discussed. The original theory of dislocation drag is due to Cottrell and Jaswon [36]. They showed that there is a critical velocity of the dislocation where the dragging stress becomes a maximum. The critical velocity and strain rate are given approximately by

$$v_C = \frac{4kTD}{A} \quad (6.6)$$

or

$$\dot{\epsilon}_C = \frac{1}{2} \rho_m b v_C = 2\rho_m b kTD/A \quad (6.7)$$

where A is a parameter that depends on the elastic constants, the volume change caused by the solute atom, and the strength of the dislocation. As equation (6.7) indicates, the critical tensile strain rate increases as the temperature increases.

In Figure 6.11, a schematic plot of the drag stress as a function of the dislocation velocity is shown [86,87]. Note that the drag stress increases almost proportionally to the strain rate up to $\dot{\epsilon}_C$ [86,87]. The critical strain rate is calculated using equation 6.7, assuming $A = 2.47 \times 10^{-20}$ dyne cm, $\rho_m = 5 \times 10^8$ cm/cm³ and $b = 2.86 \times 10^{-8}$ cm. Since $D = 2.11 \times 10^{-12}$ cm²/sec at 600 K, the calculated critical strain rate becomes 2.02×10^{-4} s⁻¹. This is indicated in Figure 6.11. Note that the strain

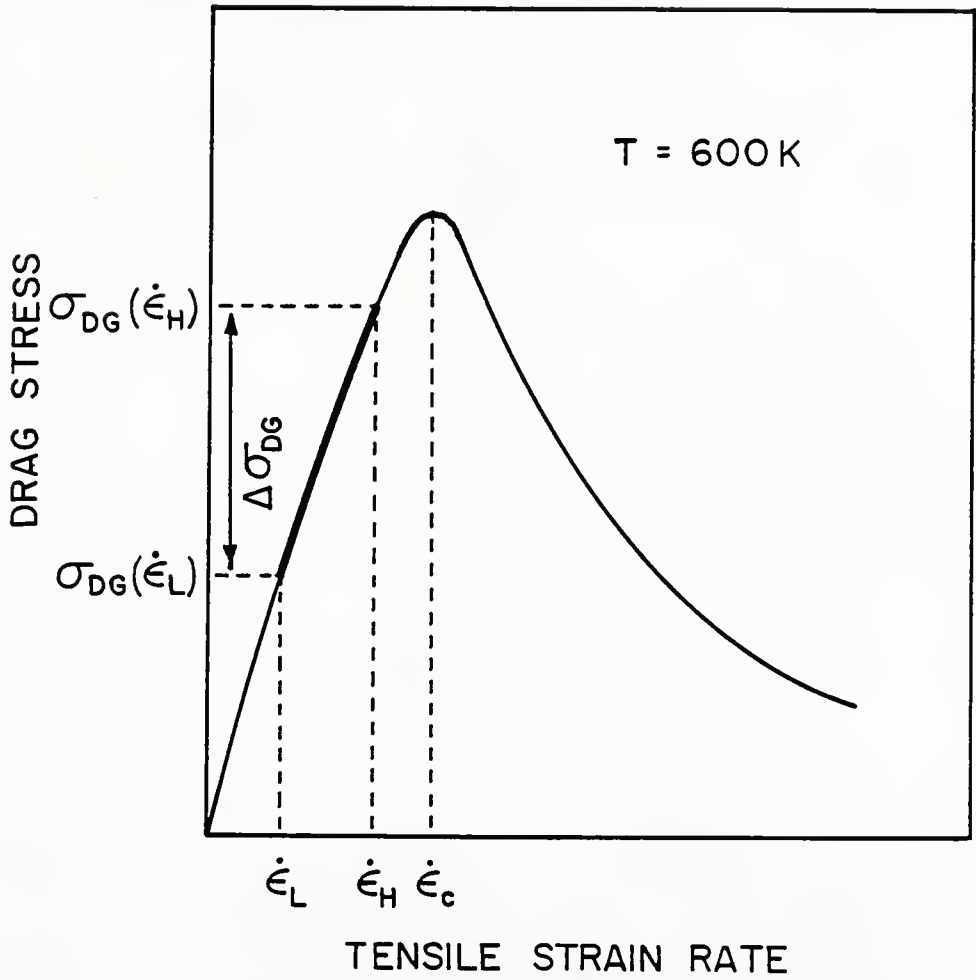


Figure 6.11 A schematic diagram of the drag stress as a function of tensile strain rate. The calculated value of critical strain rate at T = 600 K is $2.02 \times 10^{-4} \text{ s}^{-1}$.

rates, $\dot{\epsilon}_L = 8.8 \times 10^{-5} \text{ s}^{-1}$ and $\dot{\epsilon}_H = 4.4 \times 10^{-4} \text{ s}^{-1}$, that are used for the SRS measurements are still slower than that of the critical strain rate. The drag stresses associated with the strain rates, $\dot{\epsilon}_L$ and $\dot{\epsilon}_H$ are designated as $\sigma_{DG}(\dot{\epsilon}_L)$ and $\sigma_{DG}(\dot{\epsilon}_H)$, respectively. Thus, the drag stress difference due to the rate change from $\dot{\epsilon}_L$ to $\dot{\epsilon}_H$ is designated as $\Delta\sigma_{DG}$, which seems to determine the SRS peak. From Figure 6.11, it is believed that, if the rate change is made at a strain rate below $\dot{\epsilon}_C$, the resulting SRS will be positive.

Further, the peak dragging stress at $\dot{\epsilon}_C$ was again given by Cottrell and Jaswon [36] as

$$\tau_C = 17 AC_0N/b \quad (6.8)$$

where C_0 is the mean solute concentration and N is the total number of atoms in a unit volume. According to equation (6.8), the peak dragging stress is linearly proportional to the solute concentration. The effect of solute concentration on the dragging stress is schematically shown in Figure 6.12. It is assumed in this figure that an increase in concentration does not affect the critical strain rate, $\dot{\epsilon}_C$. An increase in the dragging stress with increasing concentration is believed to be associated with an increasing SRS peak height. An almost linear relationship between the SRS peak and the oxygen concentration may be seen in Figure 6.10 for oxygen concentrations below 0.24 at.%.

Another piece of evidence that the SRS peak at around 600 K is related to the dragging of solute may be seen in Figure 6.13. In this figure, a series of stress-strain curves of the Nb-0.95 at.% O specimens

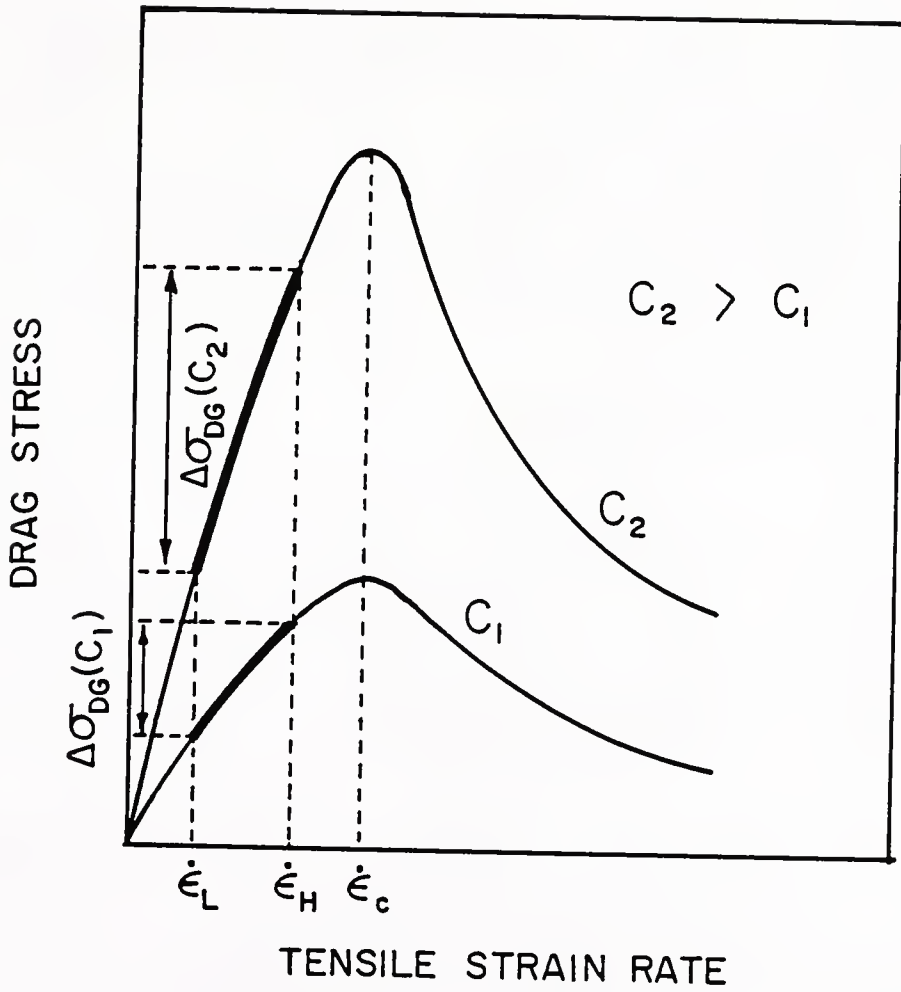


Figure 6.12 A schematic diagram showing the effect of concentration on a plot of the drag stress versus tensile strain rate.

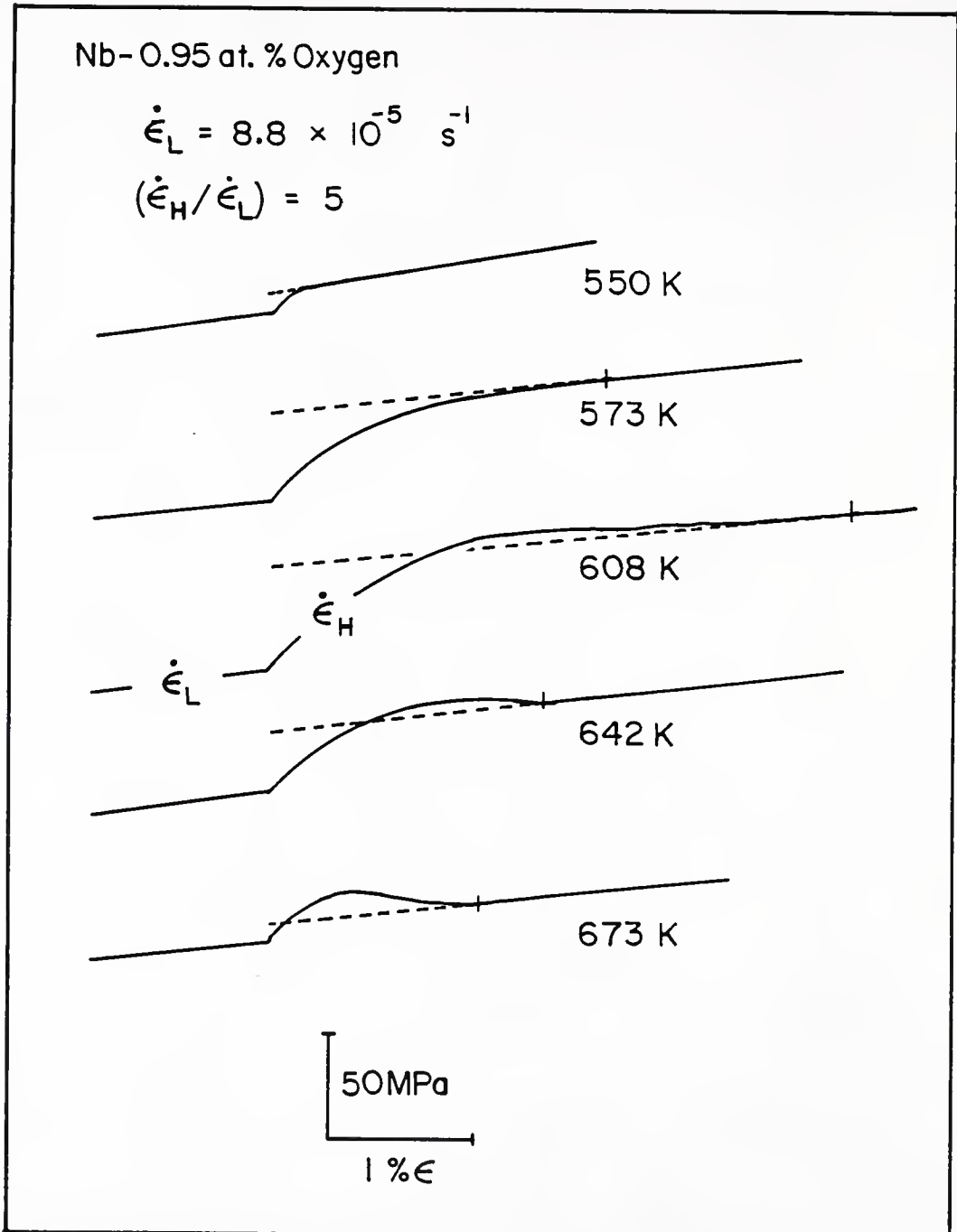


Figure 6.13 Variation of the stress-strain curves upon increasing the strain rate from $\dot{\epsilon}_L = 8.8 \times 10^{-5} \text{ s}^{-1}$ to $\dot{\epsilon}_H = 4.4 \times 10^{-4} \text{ s}^{-1}$ at several temperatures. Nb-0.95 at.% oxygen.

before and after changing the strain rate at five different temperatures, 550, 573, 608, 642 and 673 K are shown. These five temperatures were chosen because the first two and the last two are below and after the SRS peak temperature, respectively. At 550 K, a small ($\Delta\sigma$) is observed. The value of ($\Delta\sigma$) increases as the temperature increases, being a maximum at 608 K. With further increase in temperature ($\Delta\sigma$) again becomes smaller. A careful examination of the flow curves upon increasing the strain rate reveals that, as the temperature reaches the SRS peak temperature, a longer time (or a larger strain) is required to reach a steady state condition. The strain which is needed at 573 K was estimated to be about 2.4%. The corresponding value at 608 K was 4.1%. This value decreases if the temperature is increased further. The large values of the strain seem to be related to the SRS peak. This strongly indicates that in this temperature range an unusual deformation mechanism is operating. It is felt that a longer time to obtain a steady state is due to something like a viscous flow (or dragging) of the dislocations. This might imply that, at this point, the flight time, t_f , becomes significant.

Since Yoshinaga and Morozumi [88] indicate that the peak in a plot of flow stress versus temperature corresponds to the drag stress peak, it was decided to examine directly how the flow stress versus temperature curve is related to the SRS. In this study, WC Nb specimens were used. Figure 6.14a is a plot of the flow stress as a function of the temperature between 450 and 700 K for two strain rates, $\dot{\epsilon}_L = 8.8 \times 10^{-5} \text{ s}^{-1}$ and $\dot{\epsilon}_H = 4.4 \times 10^{-4} \text{ s}^{-1}$. The flow stresses were taken at a strain of 4.5%. On each curve, a flow stress maximum can be observed. The temperature where the flow stress becomes a maximum shift towards higher temperatures

as the strain rate increases. The flow stress peak temperatures are 520 and 560 K for the strain rates 8.8×10^{-5} and $4.4 \times 10^{-4} \text{ s}^{-1}$, respectively. It can be seen in Figure 6.14a that, below about 545 K, the flow stress at the slower strain rate is higher than that of the faster one, indicating a negative flow stress difference. This may yield a negative SRS; it should be noted that since the flow stress difference of two individual curves at two different strain rates, $\dot{\epsilon}_L$ and $\dot{\epsilon}_H$ are not necessarily the same as the flow stress difference upon changing the strain rate from $\dot{\epsilon}_L$ to $\dot{\epsilon}_H$, one-to-one comparison cannot be made. However, it still provides a qualitative result. At 545 K, the two flow stress curves cross each other, possibly implying the zero strain rate sensitivity. Note that this temperature is above the flow stress peak temperature at $\dot{\epsilon}_L$ and below that at $\dot{\epsilon}_H$. The difference in flow stress ($\Delta\sigma$) at two strain rates were taken and plotted in Figure 6.14b together with the calculated value of the strain rate sensitivity ($\Delta\sigma/\Delta\ln\dot{\epsilon}$). A ($\Delta\sigma$) peak or a ($\Delta\sigma/\Delta\ln\dot{\epsilon}$) peak is observed close to 590 K. It should be noted that this peak temperature is higher than the flow stress peak temperature at the faster strain rate. In the same figure, results of the SRS measured at 4.5% ϵ by changing strain rate from $\dot{\epsilon}_L$ to $\dot{\epsilon}_H$ are superimposed. The experimentally measured strain rate sensitivity has a peak at around 590 K. This temperature is in excellent agreement with that estimated from the flow stress difference at two strain rates. Although a direct comparison cannot be made, it may be suggested that this high temperature SRS peak basically represents the flow stress difference at two strain rates.

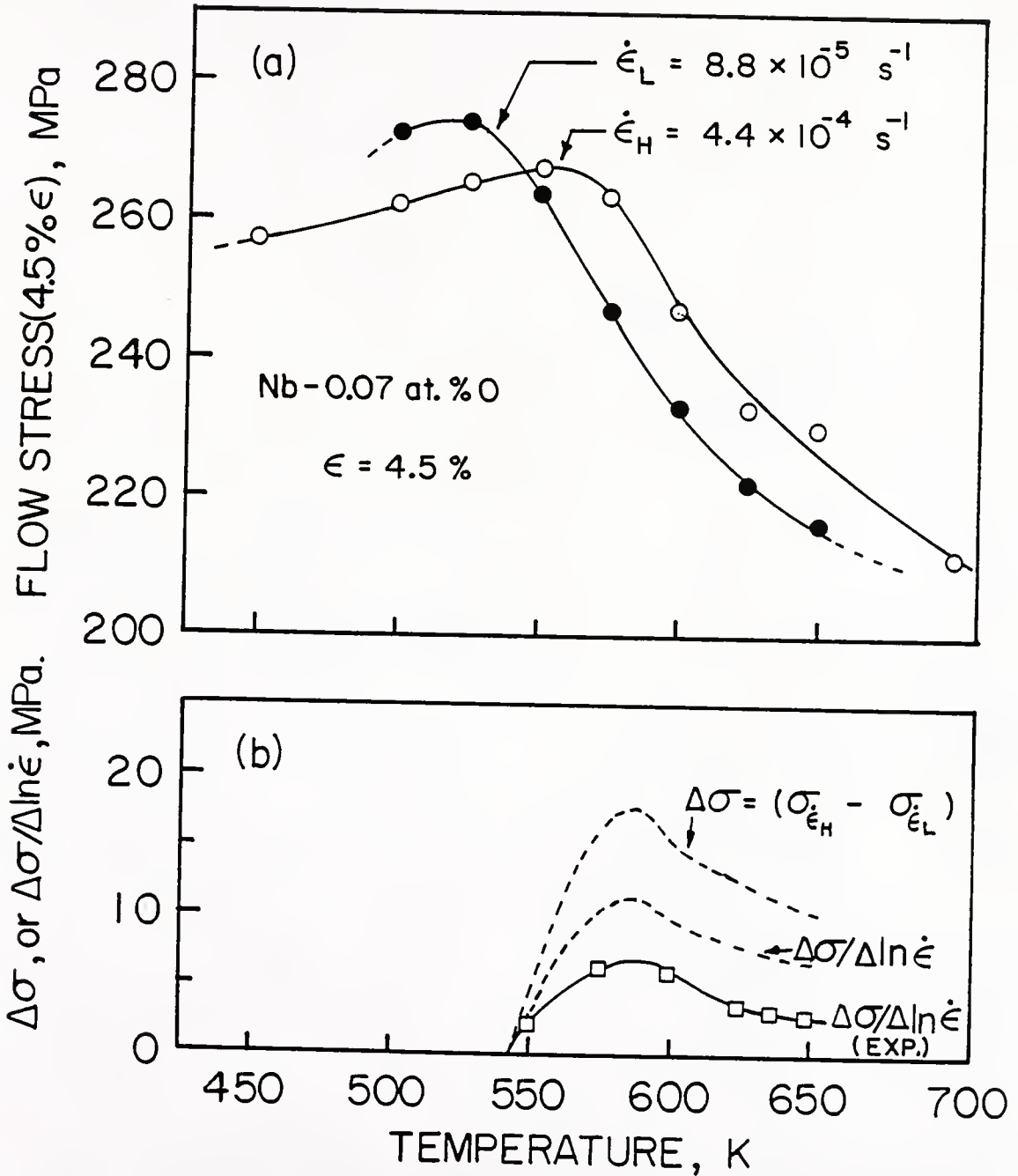


Figure 6.14 a) Variation of the flow stresses with temperature at two strain rates, $\dot{\epsilon}_L = 8.8 \times 10^{-5} \text{ s}^{-1}$ and $\dot{\epsilon}_H = 4.4 \times 10^{-4} \text{ s}^{-1}$. Nb-0.07 at.% O. $\epsilon = 4.5\%$. b) Variations of $(\Delta\sigma)$ and $(\Delta\sigma/\Delta\ln\dot{\epsilon})$ with temperature. Experimental strain rate sensitivity data, $(\Delta\sigma/\Delta\ln\dot{\epsilon})$, are also shown.

Since an increase in the base strain rate (assuming that $(\dot{\epsilon}_H/\dot{\epsilon}_L) = \text{constant}$) will increase the critical strain rate, $\dot{\epsilon}_c$, and in turn increase the temperature where the drag stress is assumed to be a maximum, it is now obvious that the SRS peak temperature should depend on the base strain rate and the ratio of the strain rate change. Increasing both the base strain rate and the magnitude of the strain rate change should result in an increase in the SRS peak temperature. This is due to the shift of the drag stress peak temperature to higher temperatures. These effects are shown in Figures 5.15 through 5.18.

In conclusion, it is reasonable to assume that the strain rate sensitivity peak is associated with the dragging stress and its height is very sensitive to solute concentration. On the other hand, the peak temperature is a function of the

- 1) base strain rate,
- 2) magnitude of the strain rate change, and
- 3) strain where the strain rate change is made.

The first two will increase the peak temperature, whereas the third has an opposite effect.

6.2 Work Hardening

The VP Nb work hardening parameter is shown in Figure 5.21 as a function of temperature for three strain rates. At each strain rate, a large work hardening peak is apparent. The peak temperature shifts towards higher temperature as the strain rate increases. As mentioned

in section 5.3, these work hardening peaks are associated with dynamic strain aging due to the presence of oxygen in niobium. The higher work hardening rates in the vicinity of the peak have been generally shown [1,6,89-91] to be associated with increased rates of dislocation accumulation. This increase may be rationalized in terms of an increase in the dislocation density caused by the discontinuous plastic deformation associated with serrated flow. In this regard, an attempt was made to relate the work hardening parameter to the strain rate sensitivity data. This may be seen in Figure 6.15. The work hardening parameter for a strain rate, $\dot{\epsilon}_L = 8.8 \times 10^{-5} \text{ s}^{-1}$ and the SRS data for this same base strain rate are plotted here as functions of the temperature. Below the work hardening peak, an arrow points to the temperature range over which serrations were observed. Note that the work hardening peak is closely related to the serrations. Wilcox and Rosenfield [91] reported a higher work hardening rate was found to be consistent with the greater frequency of serrations. Figure 6.15 shows that the work hardening rate at $\dot{\epsilon}_L$ begins to increase when the SRS becomes negative. As the temperature increases further, the work hardening rate increases while the SRS decreases. Note that the work hardening peak temperature is very close to the SRS minimum temperature in this particular case.

The effect of oxygen concentration on the average work hardening rate may be seen in Figure 5.23. It is apparent that the effect of oxygen on the work hardening rate is small for temperatures below about 250 K. As the temperature increases, however, the work hardening difference between VP Nb (0.01 at.% O) and 0.95 at.% O specimens becomes bigger

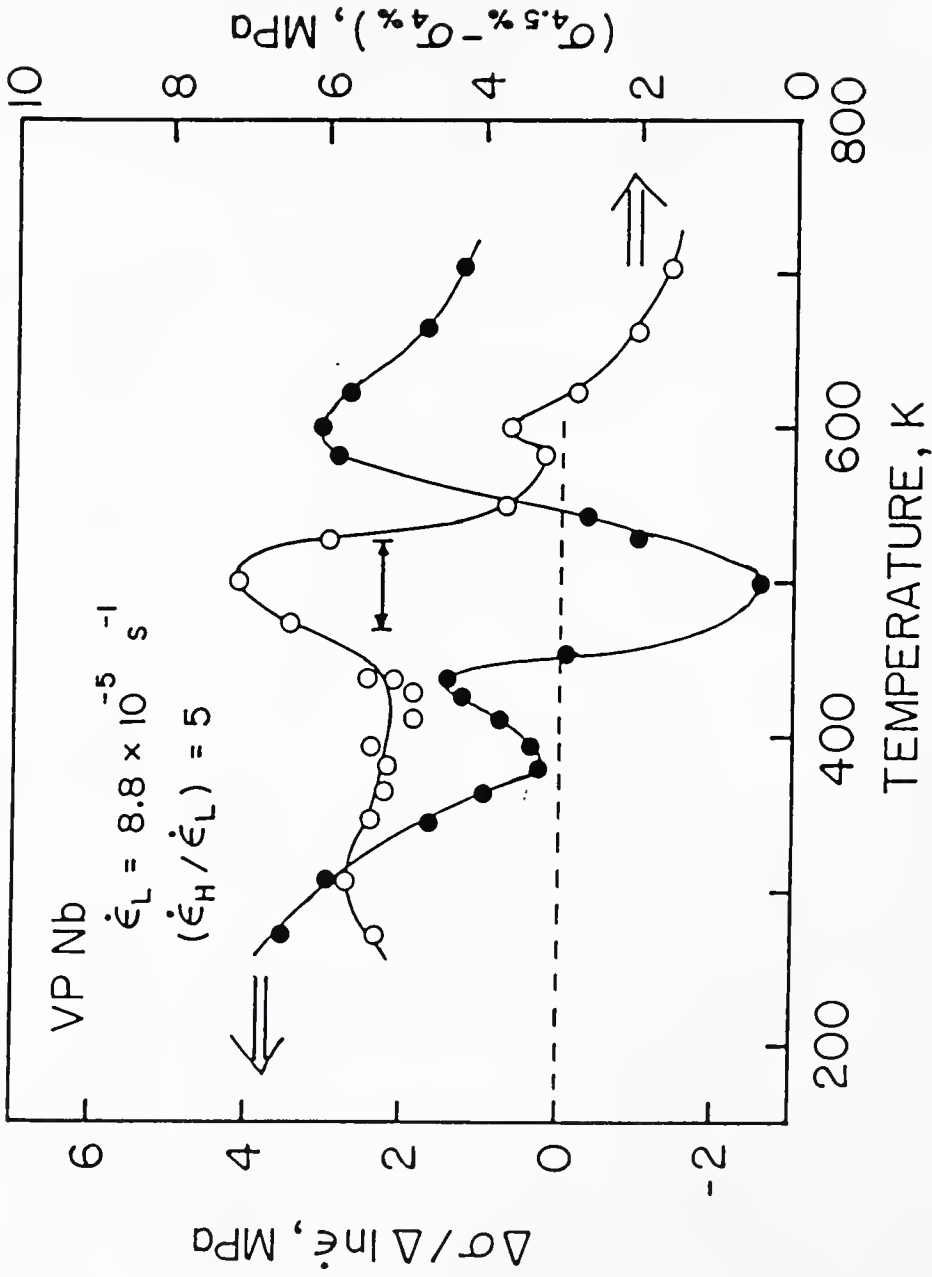


Figure 6.15 Superimposed are the variations of work hardening and strain rate sensitivity with temperature. An arrow shown below the work hardening peak points to the temperature range over which serrations were observed. $\dot{\epsilon}_L = 8.8 \times 10^{-5} \text{ s}^{-1}$, $(\dot{\epsilon}_H / \dot{\epsilon}_L) = 5$. VP-Nb Specimens.

and bigger and it reaches a maximum at the work hardening peak around 500 K. At this temperature, the peak value for the 0.95 at.% O specimen was about twice that for the VP Nb specimen. A careful examination of Figure 5.23 suggests that the peak temperature may shift towards lower temperatures with increasing oxygen concentration. The peak temperatures of 0.95 at.% O and the VP Nb specimen appear to be at about 490 K and 510 K, respectively; this suggests a 20 K shift. Since the work hardening peak is a result of dynamic strain aging it is interesting to compare this temperature shift with that of the SRS minimum (see Figure 5.14). (The shift of the SRS curve with oxygen concentration has been discussed in detail in section 6.1.1.1.). It is clearly seen from Figure 5.14 that the Cottrell minimum temperature moves from about 500 K to 475 on increasing the oxygen concentration from 0.01 to 0.95 at.% oxygen; a 25 K shift is estimated. This is consistent with the value observed for the work hardening peak. From this, it may be concluded that the work hardening peak temperature is closely related to the SRS minimum temperature.

6.3 Strain Aging Under Stress

One of the most striking accomplishments in the strain aging under stress experiment [23,33] was the measurement of the average strain rate during the aging under stress period. Beckerman and Reed-Hill [23,33] reported the average strain rate, $\dot{\epsilon}_{a,ave}$, over a 35-minute aging period as a function of the fraction of prestrain flow stress, σ_f . The result is shown in Figure 5.27, in which the present data obtained from the VP Nb specimens are also included.

Linear relationships between logarithms of the aging stress and the average strain rate during aging indicate that a power law is obeyed in both the Nb-0 and the V-0 system. Figure 5.27 reveals that the magnitudes of the average strain rate during aging of the VP Nb specimens are approximately one order of magnitude smaller than those for the V-0 specimens. Thus, when the aging stress is 98% σ_f , $\dot{\epsilon}_{a,ave}$ over a 35-minute period for V-0 specimens is about 11% $\dot{\epsilon}_p$, while only 1% $\dot{\epsilon}_p$ is observed in the Nb-0 specimen. This is clearly seen in Figure 6.16, where the average strain rate is expressed as a fraction of the prestrain strain rate, $(\dot{\epsilon}_a/\dot{\epsilon}_p)$ and is plotted as a function of prestrain flow stress (σ_a/σ_f) . This figure shows that as the aging stress increases the average value of the aging strain rate increases. Although the aging is made at a stress level of 99.5% σ_f , the average strain rate during aging is only 2.34% of the prestrain strain rate in the Nb-0 alloy. The corresponding value in V-0 alloy was estimated to be about as much as 21.1% $\dot{\epsilon}_p$.

Thus, the magnitude of the $\dot{\epsilon}_{a,ave}$ is considered to be functions of a number of factors, such as the Young's modulus, the aging temperature, aging stress level, aging period, prestrain, the prestrain strain rate, solute concentration, etc.

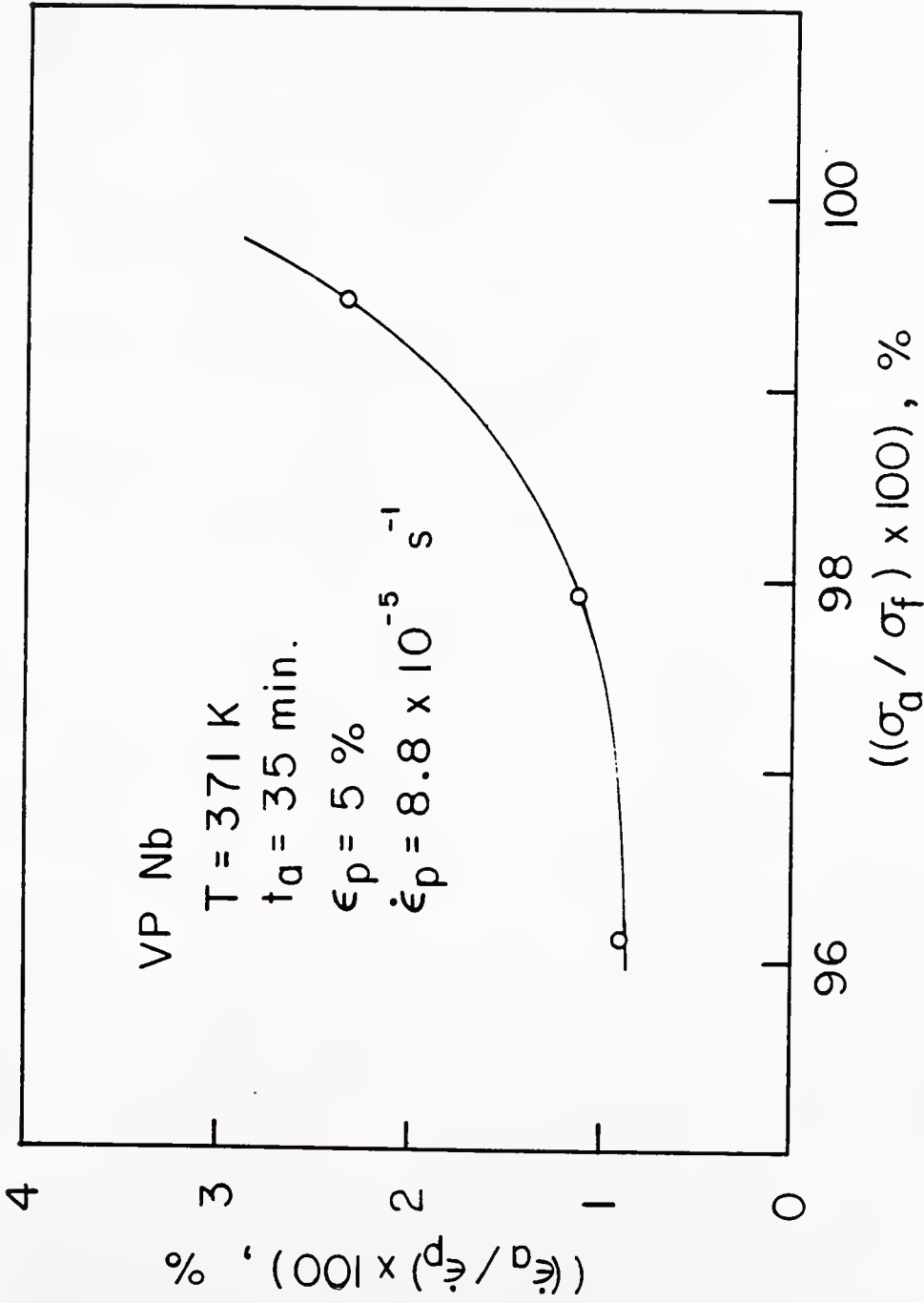


Figure 6.16 Variation of $(\dot{\epsilon}_a / \dot{\epsilon}_p)$ with (σ_a / σ_f) . $T = 371 \text{ K}$, $\dot{\epsilon}_p = 8.8 \times 10^{-5} \text{ s}^{-1}$, $t_a = 35 \text{ minutes}$, VP-Nb specimens.

CHAPTER VII CONCLUSIONS

1. There are two temperature intervals within which the strain rate sensitivity becomes a minimum. That at lower temperatures is believed to be due to Snoek and that at higher temperatures to Cottrell dynamic strain aging.
2. The following observations support the belief that the low temperature serrations are associated with Snoek dynamic strain aging.
 - a) Between 346 and 381 K, where relatively periodic Type A serrations appear, the experimentally determined average time between serrations agrees well with the jump time of an oxygen atom.
 - b) The values of the $\dot{\epsilon}/D$ ratio for the low temperature serrations lie between 10^{11} and 10^{15} with the largest serrations appearing at an $\dot{\epsilon}/D$ equal to 10^{14} . These values are much larger than the 10^9 value normally associated with Cottrell dynamic strain aging.
3. At the lower temperature or Snoek minimum, the negative character of the strain rate sensitivity increases with concentration. This would account for the fact that the Snoek serrations become more pronounced at higher oxygen concentrations.
4. The strain rate sensitivity versus temperature curve shifts towards higher temperature as the base strain rate increases. Measurements of the apparent activation energy associated with the Snoek and Cottrell strain rate sensitivity minima, using data obtained at three base strain rates, indicate that both minima are probably associated with the diffusion of oxygen in niobium.

5. An increasing magnitude of the strain rate change causes the SRS versus T curve to shift towards higher temperature whereas increasing oxygen concentration and prestrain result in the reversed behavior.
6. The Cottrell strain rate sensitivity minimum appears to be closely related to the work hardening peak for Nb-0.01 at.% oxygen specimens.
7. An abnormally high SRS peak was observed at high temperature and showed the following characteristics.
 - a) It appears about 100 or more degrees above the Cottrell SRS minimum temperature.
 - b) The peak height increases sharply as the oxygen concentration increases.
 - c) The peak shifts towards higher temperatures with increasing base strain rate and magnitude of the strain rate change.
 - d) The apparent activation energy for the peak is close to that for the diffusion of oxygen in niobium.
 - e) The stress-strain curve, upon increasing the strain rate in this temperature range, reveals that a long period of time is required to reach a steady state at the new strain rate.
 - f) Based upon the above experimental observations, it is proposed that this SRS peak is associated with the dragging of the solute atoms by the dislocations.

REFERENCES

1. R. E. Reed-Hill, Reviews on High Temp. Materials, Vol. II, No. 3, 217 (1974).
2. S. A. Bradford and O. N. Carlson, Trans. TMS-AIME, 224, 738 (1962).
3. E. Pink and A. Grinberg, Mat. Sci. Engr., 51, 1 (1981).
4. H. Takehashi and T. Takeyama, Trans. Jap. Inst. of Metals, 15, 357 (1974).
5. A. S. Keh, Y. Nakada and W. C. Leslie, Dislocation Dynamics, edited by A. R. Rosenfield, G. T. Hahn, A. L. Bement, Jr. and R. I. Jaffee, McGraw-Hill, NY, 381 (1968).
6. B. J. Brindley and J. T. Barnby, Acta Met., 14, 1765 (1966).
7. A. W. Sleeswyk, Acta Met., 8, 130 (1960).
8. P. G. McCormick, Acta Met., 19, 463 (1971).
9. A. J. R. Soler-Gomez and W. J. McG. Tegart, Phil. Mag., 20, 495 (1969).
10. B. Russell, Phil. Mag., 8, 615 (1963).
11. S. R. MacEwen and B. Ramaswami, Phil. Mag., 22, 1025 (1970).
12. P. R. Cetlin, A. S. Güler and R. E. Reed-Hill, Met. Trans., 4, 513 (1973).
13. A. W. Cochardt, G. Schoeck and H. Widersich, Acta Met., 3, 533 (1955).
14. G. Schoeck and A. Seeger, Acta Met., 7, 419 (1959).
15. J. T. Evans and R. M. Douthwaite, Acta Met., 21, 49 (1973).
16. R. E. Reed-Hill, Dislocation Modelling of Physical Systems, edited by M. F. Ashby, R. Bullough, C. S. Hartley and J. P. Hirth, Pergamon Press, Elmsford, NY, 163 (1981).
17. A. H. Cottrell and B. A. Bilby, Proc. Phys. Soc. A, 62A, 49 (1949).
18. A. H. Cottrell, Phil. Mag., 44, 829 (1953).
19. M. J. Manjoine, Trans. Amer. Soc. Mech. Engrs., 66, A211 (1944).
20. J. D. Baird, Met. Rev., 16, 1 (1971).

21. Y. Nakada and A. S. Keh, *Acta Met.*, 15, 879 (1967).
22. W. S. Owen and M. J. Roberts, *Dislocation Dynamics*, edited by A. R. Rosenfield, G. T. Hahn, A. L. Bement, Jr. and R. I. Jaffee, McGraw-Hill, NY, 357 (1968).
23. L. P. Beckerman, Ph.D. Dissertation, Gainesville, Florida (1980).
24. R. A. Mulford and U. F. Kocks, *Acta Met.*, 27, 1125 (1979).
25. P. G. McCormick, *Scripta Met.*, 12, 197 (1978).
26. S. H. van den Brink, A. van den Beukel and P. G. McCormick, *Phys. Stat. Sol. (a)*, 30, 469 (1975).
27. R. E. Reed-Hill, *Proc. Intl. Conf., "Thermodynamics and Kinetics of Metallurgical Process,"* Bangalore, India, July, 1981.
28. K. W. Qian and R. E. Reed-Hill, *Scripta Met.*, 16, 807 (1982).
29. K. W. Qian and R. E. Reed-Hill, *Acta Met.*, 31, 87 (1981).
30. A. Taylor and N. J. Doyle, *J. Less-Common Metals*, 13, 313 (1967).
31. A. W. Sleeswyk, *Acta Met.*, 6, 598 (1958).
32. G. F. Bolling, *Phil. Mag.*, 4, 537 (1959).
33. L. P. Beckerman and R. E. Reed-Hill, *Proc. 5th Intl. Conf. Strength of Materials and Alloys*, edited by P. Haasen, V. Gerold and G. Kostorz, Pergamon Press, Oxford, p. 535 (1979).
34. J. Snoek, *Physica*, 8, 711 (1941).
35. A. H. Cottrell, *Dislocations and Plastic Flow in Crystals*, Oxford University Press (1953).
36. A. H. Cottrell and M. A. Jaswon, *Proc. Roy. Soc. A*, 199, 104 (1949).
37. P. G. McCormick, *Acta Met.*, 20, 351 (1972).
38. P. G. McCormick, *Acta Met.*, 21, 873 (1973).
39. P. G. McCormick, *Acta Met.*, 22, 489 (1974).
40. A. van den Beukel, *Phys. Stat. Sol. (a)*, 30, 197 (1975).
41. J. Friedel, *Dislocations*, Pergamon Press, Oxford, p. 405 (1964).
42. H. Conrad and H. Wiedersich, *Acta met.*, 8, 128 (1960).
43. P. Delobelle, C. Oytana and D. Varchon, *Mat. Sci. Engr.*, 29, 261 (1977).

44. R. E. Reed-Hill, S. C. Park and L. P. Beckerman, *Acta Met.*, in press (1983).
45. A. Portevin and F. Le Chatelier, *Trans. Amer. Soc. for Steel Treating*, May, 457 (1924).
46. R. W. Thompson and O. N. Carlson, *J. Less-Common Metals*, 7, 321 (1964).
47. Y. Nakada and A. S. Keh, *Acta Met.*, 18, 437 (1970).
48. J. R. Donoso, P. G. Watson and R. E. Reed-Hill, *Met. Trans.*, 10A, 1165 (1979).
49. S. Kinoshita, P. J. Wray and G. T. Horne, *Trans. Met. Soc. AIME*, 233, 1902 (1965).
50. P. Dadras, *Trans. JIM*, 19, 230 (1978).
51. M. Jovanovic, B. Djuric and Dj. Drobnjak, *Scripta Met.*, 15, 469 (1981).
52. M. J. Roberts and W. S. Owen, *Met. Trans.*, 1, 3203 (1970).
53. E. Pink, *Trans. Met. Soc. AIME*, 245, 2597 (1969).
54. K. S. B. Rose and S. G. Glover, *Acta Met.* 14, 1505 (1966).
55. J. D. Baird and A. Jamieson, *J. Iron Steel Inst.*, 204, 793 (1966).
56. W. J. Bratina, J. T. McGrath and D. Mills, *Trans. JIM*, 9, supplement, 436 (1968).
57. H. Conrad and W. Hayes, *Trans. ASM*, 56, 249 (1963).
58. J. W. Christian and B. C. Masters, *Proc. Roy. Soc. A*, 281, 240 (1964).
59. A. H. Cottrell and R. J. Stokes, *Proc. Roy. Soc. A*, 233, 17 (1955).
60. W. G. Johnston and J. J. Gilman, *J. Appl. Phys.*, 30, 129 (1959).
61. K. V. Ravi and R. G. Gibala, *Acta Met.* 18, 623 (1970).
62. H. Conrad and S. Frederick, *Acta Met.*, 10, 1013 (1962).
63. E. S. Tankins and R. Maddin, *Columbium Metallurgy*, Interscience Publishers, Ltd., p. 343-363 (1961).
64. D. Tseng and K. Tangri, *Scripta Met.*, 11, 719 (1977).
65. J. T. Michalak, *Acta Met.*, 13, 213 (1965).

66. A. van den Beukel and U. F. Kocks, *Acta Met.*, 30, 1027 (1982).
67. U. F. Kocks and M. Mecking, *Dislocation Modelling of Physical Systems*, edited by M. F. Ashby, R. Bullough, C. S. Hartley and J. P. Hirth, Pergamon Press, Elmsford, NY, 173 (1981).
68. U. F. Kocks, *Prog. Mat. Sci.*, Chalmers Anniversary Volume, 185 (1981).
69. P. Penning, *Acta Met.*, 20, 1169 (1972).
70. D. V. Wilson and B. Russell, *Acta Met.*, 7, 628 (1959).
71. T. Mura and J. D. Brittain, *Acta Met.*, 8, 767 (1960).
72. E. A. Almond and D. Hull, *Phil. Mag.*, 14, 515 (1966).
73. M. Duval and J. I. Dickson, *Metal Science*, Sept. 523 (1979).
74. Z. C. Szkopiak and L. W. Derby, *J. Nucl. Mat.*, 13, 130 (1964).
75. H. E. Rosinger, G. B. Craig and W. J. Bratina, *Mat. Sci. Engr.*, 5, 163 (1969/1970)
76. S. H. Carpenter and G. S. Baker, *J. Appl. Phys.*, 36, 1733 (1965).
77. E. Gebhardt and R. Rothenbacker, *Z. Metall.*, 54, 443 (1963).
78. F. J. M. Boratto and R. E. Reed-Hill, *Met. Trans.*, 8A, 1125 (1977).
79. R. E. Reed-Hill, *Physical Metallurgy Principles*, 2nd Edition, D. Van Nostrand Company, New York, p. 441 (1973).
80. S. C. Park, L. P. Beckerman and R. E. Reed-Hill, *Met. Trans.*, 14A, 463 (1983).
81. Z. C. Szkopiak, *Acta Met.*, 16, 381 (1968).
82. C. Yin, M. Doner and H. Conrad, *Met. Trans.*, 6A, 1901 (1975).
83. R. E. Reed-Hill, unpublished research (1983).
84. R. E. Reed-Hill and B. L. Adams, a proposal submitted to NSF (1983).
85. R. E. Reed-Hill, Private Communication (1983).
86. H. Yoshinaga and S. Morozumi, *Phil. Mag.*, 23, 1367 (1971).
87. S. Takeuchi and A. S. Argon, *Phil. Mag.*, 40, 65 (1979).
88. H. Yoshinaga and S. Morozumi, *Phil. Mag.*, 23, 1351 (1971).

89. D. J. Dingley and D. McLean, *Acta Met.*, 15, 885 (1967).
90. J. W. Edington, T. C. Lindley and R. E. Smallman, *Acta Met.*, 12, 1025 (1964).
91. B. A. Wilcox and A. R. Rosenfield, *Mat. Sci. and Engr.*, 1, 201 (1966).

BIOGRAPHICAL SKETCH


Soon Chun Park was born on October 28, 1946 in Seoul, Korea. He attended the Han-yang University, Seoul, Korea, where he received a Bachelor of Science degree in materials science and engineering in February, 1973. Then he entered the Korea Advanced Institute of Science (KAIS). He received a Master of Science degree in materials science and engineering from KAIS in August, 1975.

For approximately three and a half years thereafter he worked at the Korea Atomic Energy Research Institute (KAERI) as a research engineer.

In 1975 he was awarded a Colombo Plan Scholarship from Great Britain with which he was able to complete a diploma in metallurgy at the Imperial College of Science and Technology, London, Great Britain, in 1977.

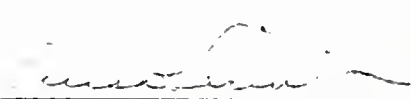
In 1979, he attended the University of Florida to continue graduate work towards acquisition of a degree of Doctor of Philosophy in the field of materials science and engineering.

I certify that I have read this study and that in my opinion it conforms to acceptable standards of scholarly presentation and is fully adequate, in scope and quality, as a dissertation for the degree of Doctor of Philosophy.




R. E. Reed-Hill, Chairman
Professor of Materials Science
and Engineering

I certify that I have read this study and that in my opinion it conforms to acceptable standards of scholarly presentation and is fully adequate, in scope and quality, as a dissertation for the degree of Doctor of Philosophy.



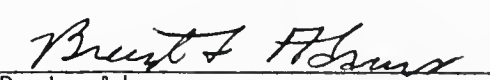
E. D. Verink, Jr.
Professor of Materials Science
and Engineering

I certify that I have read this study and that in my opinion it conforms to acceptable standards of scholarly presentation and is fully adequate, in scope and quality, as a dissertation for the degree of Doctor of Philosophy.



R. T. DeHoff
Professor of Materials Science
and Engineering

I certify that I have read this study and that in my opinion it conforms to acceptable standards of scholarly presentation and is fully adequate, in scope and quality, as a dissertation for the degree of Doctor of Philosophy.



B. L. Adams
Assistant Professor of Materials
Science and Engineering

I certify that I have read this study and that in my opinion it conforms to acceptable standards of scholarly presentation and is fully adequate, in scope and quality, as a dissertation for the degree of Doctor of Philosophy.

LE Malvern

L. E. Malvern
Professor of Engineering Science
and Mechanics

This dissertation was submitted to the Graduate Faculty of the Department of Materials Science and Engineering in the College of Engineering and to the Graduate School, and was accepted as partial fulfillment of the requirements for the degree of Doctor of Philosophy.

December, 1983

Hubert A. Bewis
Dean, College of Engineering

Dean for Graduate Studies and Research

